International Journal of Bifurcation and Chaos, Vol. 19, No. 10 (2009) 3235–3282

FROM THE BOX-WITHIN-A-BOX BIFURCATION STRUCTURE TO THE JULIA SET. PART II: BIFURCATION ROUTES TO DIFFERENT JULIA SETS FROM AN INDIRECT EMBEDDING OF A QUADRATIC COMPLEX MAP

CHRISTIAN MIRA
19 rue d'Occitanie, Fonsegrives, 31130 QUINT,
and Department of Economics and Quantitative Methods,
University of Urbino, Italy
c.mira@free.fr

ANNA AGLIARI
Catholic University of Milan, Italy
anna.agliari@unicatt.it

LAURA GARDINI
Department of Economics and Quantitative Methods,
University of Urbino, Italy
laura.gardini@uniurb.it

Received January 27, 2008; Revised March 24, 2009

Part I of this paper has been devoted to properties of the different Julia set configurations, generated by the complex map T_Z: $z' = z^2 - c$, c being a real parameter, $-1/4 < c < 2$. These properties were revisited from a detailed knowledge of the fractal organization (called "*box-within-a-box*"), generated by the map $x' = x^2 - c$ with x a real variable. Here, the second part deals with an embedding of T_Z into the two-dimensional noninvertible map $\overline{T} : x' = x^2 + y - c$; $y' = \gamma y + 4x^2 y$, $\gamma \geq 0$. For $\gamma = 0$, $\overline{T}$ is semiconjugate to T_Z in the invariant half plane ($y \leq 0$). With a given value of c, and with γ decreasing, the identification of the global bifurcations sequence when $\gamma \to 0$, permits to explain a route toward the Julia sets, from a study of the basin boundary of the attractor located on $y = 0$.

Keywords: Noninvertible map; Julia set; fractal set; embedding; stability; basin; global bifurcation.

1. Introduction

The paper [Mira & Gardini, 2009], henceforth denoted as Part I of the present work, has been devoted to different configurations of the Julia sets J generated by the map T_Z: $z' = z^2 - c$, when the parameter c is restricted to the real axis: $-1/4 < c < 2$, $z = x + jy$, $j^2 = -1$. This first part permitted the definition of parameter intervals inside which J belongs to well-defined types. The two-dimensional real form of the complex map is:

$$T_Z : \begin{cases} x' = x^2 - y^2 - c \\ y' = 2xy \end{cases} \tag{1}$$

From the knowledge of the fractal bifurcation organization called "*box-within-a-box*", generated by the one-dimensional real Myrberg's noninvertible map $x' = x^2 - c$ [Myrberg, 1963], five different principal types of Julia sets have been defined,

corresponding to c-interval and their boundaries. Now the purpose is to explain bifurcation routes leading to these different types. This is achieved by an "indirect" embedding of T_Z into a two-dimensional family of noninvertible maps $\overline{T}$:

$$\overline{T} : \begin{cases} x' = x^2 + y - c \\ y' = \gamma y + 4x^2 y \end{cases} \tag{2}$$

with $-1/4 \leq c \leq 2$, $\gamma \geq 0$. The embedding is not a "direct" one because its link with T_Z is not obtained by equating the parameter γ to zero. Indeed the maps family is characterized by the fact that $\overline{T}_{\gamma=0}$ is semiconjugate to T_Z in the invariant half plane ($y \leq 0$) (cf. [Agliari *et al.*, 2003, 2004]), i.e. $\overline{T}_{\gamma=0} \circ h_1 = h_1 \circ T_Z$, where $h_1(x, y) = (x, -y^2)$ (this is easily proved noticing that $\overline{T} \circ h(x, y) = \overline{T}(x, -y^2) = (x^2 - y^2 - c, -4x^2y^2)$ and $h \circ T_Z(x, y) = h(x^2 - y^2 - c, 2xy) = (x^2 - y^2 - c, -4x^2y^2)$). This property leads to the following remarks:

Then the properties of the different Julia set configurations, obtained for fixed values of parameter c, are revealed from a bifurcation study when γ decreases from 1 to 0, i.e. a route toward Julia sets. For $\gamma = 0$ the basin boundary structure (in the sense defined in Sec. 1 of Part I) generated by $\overline{T}$ in (2) is particular in the invariant half plane ($y \leq 0$), $\overline{T}_{\gamma=0}$ being equivalent to the two-dimensional map T_Z in this half plane. This means that this basin boundary in $y < 0$ is a fractal set nowhere smooth, except for the particular value of $c = 0$.

The study framework is founded on the following elements. The line $y = 0$ is invariant by $\overline{T}$. The restriction of $\overline{T}$ to $y = 0$ is the Myrberg's noninvertible map T, $x' = x^2 - c$, characterized inside the interval $-1/4 \leq c \leq 2$ by the fractal bifurcation organization "*box-within-a-box*" described in Sec. 2 of Part I, with bibliographic references. The fractal bifurcation organization of T plays a basic role in the study of the two-dimensional map $\overline{T}$. Indeed let D be the basin of the attractor (in the simplest cases, a period k cycle or a period k chaotic attractor) located in the half plane ($y \leq 0$) (either on $y = 0$, or in $y < 0$), and a given c value of the above interval with $\gamma > 0$ decreasing. Our investigations will show that the map restricted to the boundary arc ∂D_- of $D_- = D \cap (y \leq 0)$ generates the box-within-a-box structure, with respect to parameter γ, c having a fixed value, either completely, or in a perturbed form. Moreover, in the parameter plane (c, γ) a basic organization of a well-defined set of bifurcation curves is reproduced according to this fractal structure. Then, from these considerations, the route to the different configurations of the Julia set (as described in Part I and quoting Julia [1918] and Fatou [1919, 1920]) can be also explained, from the qualitative changes of ∂D_- when $\gamma > 0$ decreases and tends toward zero. In this framework, the paper also constitutes a more complete study of the two-dimensional noninvertible map $\overline{T}$ with respect to previous publications [Agliari *et al.*, 2003, 2004], from the presentation of several global bifurcations generated by $\overline{T}$.

The plane (x, y) of the noninvertible map $\overline{T}$ is divided into three unbounded open areas Z_r, $r = 0, 2, 4$, each one generating r real distinct rank-one preimages. The boundaries of the regions Z_r are made up of branches of the rank-one critical curve LC, locus of points having two determinations of the inverse map T^{-1} merging on the set LC_{-1}, obtained by equating to zero the Jacobian determinant of $\overline{T}$, $\overline{T}(LC_{-1}) = LC$ [Mira *et al.*, 1994; Mira *et al.*, 1996a; Mira *et al.*, 1996b; Agliari *et al.*, 2003]. The map T_Z does not have the same property. Its critical set is only a critical point: $C = (-c, 0)$ and $C_{-1} = (0, 0)$ ($z = -c$ and $z = 0$, respectively, for the complex map), while C ($x = -c$) is the rank-one critical point of the one-dimensional map restriction of $\overline{T}$ to $y = 0$, i.e. $x' = x^2 - c$.

Following the route toward different Julia sets from the above indirect embedding (2) some nonclassical phase plane behaviors are met. It is the case of:

(a) *direct transition nonconnected multiply-connected basin* (Sec. 4.3),
(b) for $\gamma = 0$ bifurcation destroying a chaotic attractor in the presence of a Julia set containing a dendrite (cf. Part I, Sec. 5.5).

It is worth noting that the map $\overline{T}$ given by (2) is not generic in a classical sense. Indeed the absence of generality is related to the structure of the critical curve made up of two arcs one of them being double, as noted in [Agliari *et al.*, 2003]. This appears considering the map $\overline{T}$ as resulting from $\varepsilon = 0$, when it is embedded into the map

$$T_\varepsilon : \begin{cases} x' = x^2 + y - c \\ y' = \gamma y + 4x^2 y + \varepsilon x \end{cases}$$

which is of so-called type $Z_0 - Z_2 < Z_4$ (following the notation used in [Mira *et al.*, 1996a; Mira *et al.*, 1996b]), the symbol "<" denoting the existence of a *cusp point* on the critical curve corresponding to a cape of Z_4 "penetrating" into Z_2. The nonclassical

nongenerality of the map T_ε in the case $\varepsilon = 0$ corresponds to a bifurcation value for the critical set LC, which exhibits a "double" arc L^b, resulting from the merging of two arcs of the critical set $LC_{\varepsilon\neq 0}$, as shown in the qualitative situations of Fig. 2 of [Agliari *et al.*, 2003].

Such a situation gives rise to very singular dynamic properties of the phase plane (x, y), when c-values correspond in the half plane $y \leq 0$ to a basin D which is a domain of convergence toward a semi-stable (or neutral) cycle located on its boundary ∂D, or correspond to a *dendrite* (see details in Part I). In the two cases, the behavior in the half plane $y > 0$ is not affected by this singular behavior, and remains classical.

After this introduction local and global bifurcations of a two-dimensional noninvertible map, with their related symbolism, are defined in Sec. 2, from a general point of view. Section 3 considers more specifically the case of map $\overline{T}$ with the definitions of its critical set, and some basic bifurcations. The investigation of the bifurcation structure as a function of the parameter γ is developed in Secs. 4 and 5, with an analysis of the bifurcation curves issued from the period doubling cascade, and the definition of c intervals having the same qualitative behavior for decreasing γ values. From the results of the previous sections, Secs. 6–8 explain the features of the different types of Julia sets defined in Part I, by studying the qualitative changes of the boundary ∂D_- when $\gamma > 0$ decreases and tends toward zero. The case of a dendrite as Julia set is considered in Sec. 9. Some conclusions are drown in the last section.

2. Bifurcations of the Map $\overline{T}$

2.1. *Local bifurcations*

Consider the map (2), $X' = \overline{T}(X, \Lambda)$, $X = (x, y)$, and the parameter plane $\Lambda = (c, \gamma)$. The multipliers S_1 and S_2 of a $(k; j)$-cycle are the eigenvalues of the linearization of the map $\overline{T}^k$ in one of the k points of this cycle. A cycle with multipliers $|S_i| < 1$, $i = 1, 2$, will be called (understood "asymptotically") stable, or attracting. A cycle with one of the multipliers $|S_i| > 1$, $i = 1, 2$, will be called unstable, or repelling.

The bifurcations considered here are related to the map $\overline{T}$ in the half plane $y \leq 0$, which for this map implies defined signs of the multipliers. In the parameter plane (c, γ) a *fold bifurcation curve* F_k^j is such that only one of the multipliers associated with a $(k; j)$ cycle is $S_1 = +1$. This curve corresponds to the merging of a (k, j) saddle cycle ($0 < S_1 < 1$, $S_2 > 1$) with a stable (or unstable) (k, j) node cycle ($0 < S_1 < 1$, $0 < S_2 < 1$). A *flip curve* f_k^j is such that one of the two multipliers is $S_1 = -1$, which gives rise to the classical period doubling from the $(k; j)$ cycle. In the simplest cases (as the map (2)), this curve corresponds to a stable (k, j) node cycle ($-1 < S_1 < 0$, $S_2 < 1$) which turns into a (k, j) saddle k-cycle ($S_1 < -1$, $0 < S_2 < 1$ in the half plane $y \leq 0$), giving rise to a stable $(2k, j')$-node cycle ($0 < S_1 < 1$, $0 < S_2 < 1$, in the half plane $y \leq 0$). A *transcritical bifurcation* curve Tc_k^j, corresponds to an exchange of stability between two (k, j) cycles merging at the bifurcation, for which one of their two multipliers is $S_1 = +1$.

The case $S_i(X, \Lambda_b) = e^{\pm j\varphi}$, $i = 1, 2$, $j^2 = -1$, corresponds to a *Neimark bifurcation*. In the simplest cases (as the map (2)), when Λ crosses through Λ_b a stable (resp. unstable) focus point of a $(k; j)$ cycle becomes unstable (resp. stable) and gives rise to a stable (resp. unstable) invariant closed curve (γ) for a supercritical (resp. subcritical) Neimark bifurcation of map $\overline{T}^k$. The corresponding bifurcation curve (N_k^j) in the parameter plane is called a *Neimark curve*.

Fold, flip and Neimark bifurcation curves are given in a parametric form (the vector X being the parameter of the parametric form, $S_i(X, \Lambda)$ being one of the two multipliers of the cycle (k, j) here considered) by the relations:

$$X = T^k(X, \Lambda), \quad X \neq T^r(X, \Lambda), \quad \text{for } r < k, \ \dim X = 2$$

$$S_i(X, \Lambda) = +1, \ i = 1, 2, \quad \text{for } F_k^j \text{ and } Tc_k^j;$$

$$S_i(X, \Lambda) = -1, \quad i = 1, 2, \quad \text{for } f_k^j$$

$$S_i(X, \Lambda) = e^{\pm j\varphi}, \quad i = 1, 2, \ j^2 = -1, \quad \text{for Neimark curves.}$$

The Neimark bifurcation may give rise to many situations, when φ is commensurable with 2π. The simplest one corresponds to a closed curve (γ) made up of the unstable (resp. stable) manifold of a period k saddle associated with a stable (resp. unstable) period k node (or a period k focus). More complex cases, depending on the nonlinear terms, occur when certain values of φ, commensurable with 2π, $\varphi = 2p\pi/q$, are related to *exceptional critical cases* requiring special *normal forms* for their study [Mira, 1987, pp. 215–239].

A set of bifurcation curves in a parameter plane $\Lambda = (c, \gamma)$ is not enough to account for the complete bifurcation properties. Indeed it does not permit to identify the merging cycles. For this reason, the parameter plane must be considered as made up of sheets, each one being associated with a given cycle $(k; j)$, in a three-dimensional auxiliary qualitative space having a "*foliated structure*", the third dimension being an adequate "qualitative" norm related to the (k, j) cycle. The identification of the sheets "geometry" allows to show how to pass continuously from one sheet to another following a continuous path of the parameter plane, i.e. to know the possible communications between sheets. In the simplest case, a *fold bifurcation curve* is the junction of two sheets, one related to a saddle $(k; j)$ cycle, the other to a $(k; j)$ cycle having the modulus of each of the two multipliers less than one (stable node, or stable focus far from the bifurcation curve), or having the modulus of its two multipliers greater than one (unstable node, or unstable focus far from the bifurcation curve). A *flip bifurcation curve* is the junction of three sheets, one associated with a $(k; j)$ cycle having the modulus of its two multipliers less (resp. greater) than one, the second sheet corresponding to a saddle $(k; j)$ cycle having one of its two multipliers less than -1, the third being related to a $(2k; j')$ cycle having the modulus of its two multipliers less (resp. greater) than one.

The sheets of the auxiliary three-dimensional space present folds along fold curves, and have junctions with branching along flip, or transcritical, curves. The association of several bifurcation curves with their corresponding sheets, and communications through codimension $s \geq 2$ singularities, constitutes a *bifurcation structure*. Codimension-2 points correspond to complex communications between the sheets [Mira, 1987].

2.2. *Global bifurcations*

Let D be the basin of an attracting set, ∂D its boundary, L the critical curve separating an open region Z_0 (each point of which has no real preimage) from an open region Z_2 (each point of which has two real rank one preimages), L_{-1} the curve of rank-one merging preimages. Figure 1 shows the bifurcation giving rise to a multiply-connected basin [Fig. 1(c)] from a simply-connected basin [Fig. 1(a)]. The bifurcation occurs when the number of intersection points $\partial D \cap L$ changes [two points a and b merge in Fig. 1(b)]. In the case of Fig. 1(c) H_0

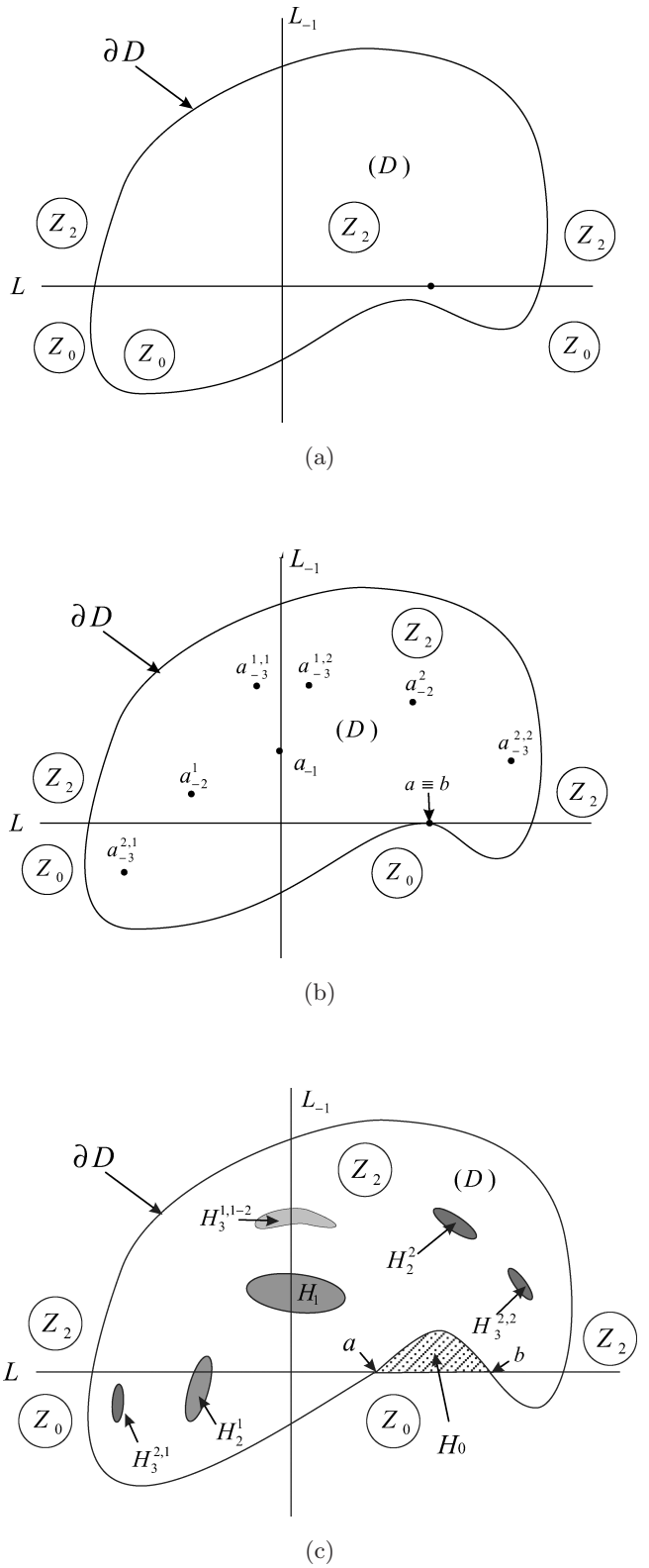

Fig. 1. Global bifurcation simply-multiply connected basin. Out of the basin (D) and its boundary, the orbits are diverging. Z_0 (no preimage) and Z_2 (two rank-one preimages) are separated by L (critical curve), locus of points having two coincident rank-one preimages located on L_{-1}. The increasing rank preimages of $H_0 \subset Z_2$ create holes inside (D), here limited to rank three.

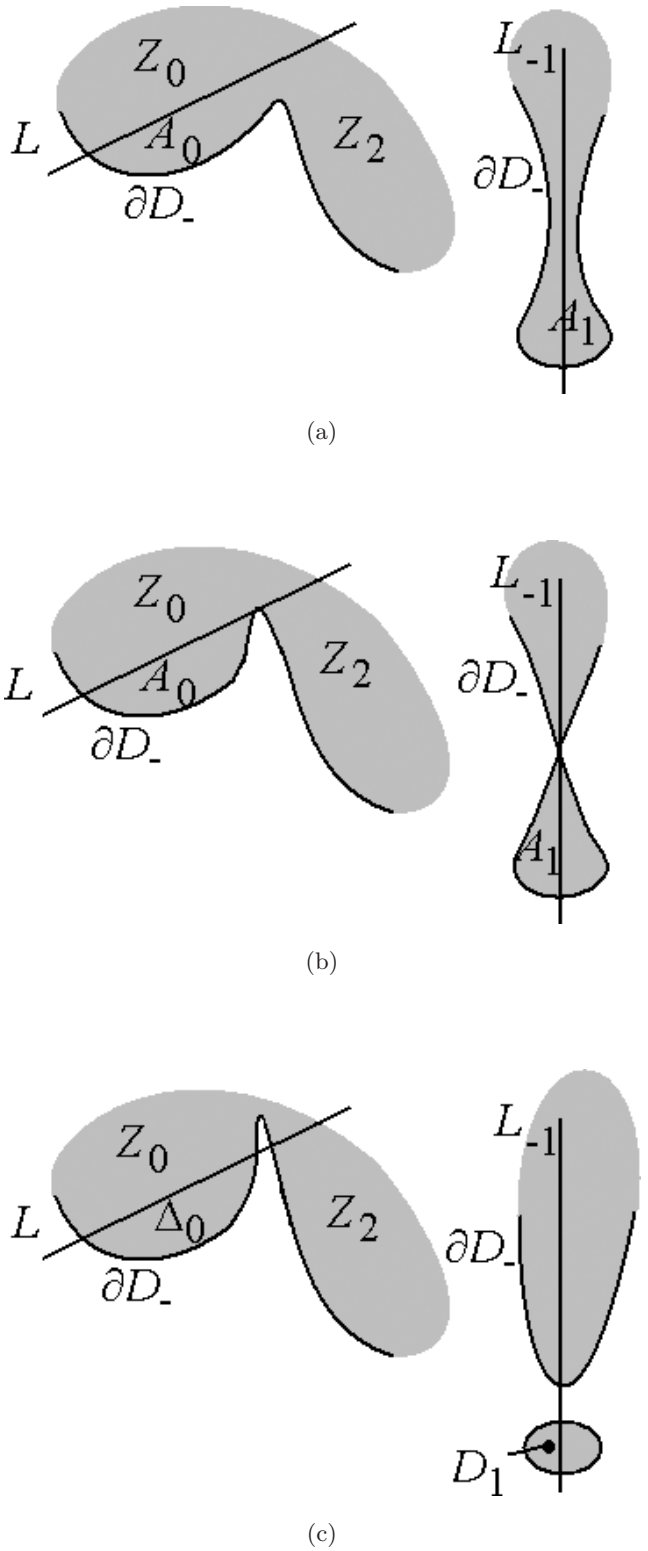

Fig. 2. Bifurcation giving rise to a nonconnected basin [Fig. 2(c)] from a simply connected basin [Fig. 2(a)]. The bifurcation occurs when the number of intersection points $\partial D \cap L$ changes [Fig. 2(b)]. In the case of Fig. 2(c), Δ_0 is called a *headland*, its increasing rank preimages create nonconnected parts of the basin (called *islands*). The "main" island $D_1 = T^{-1}(\Delta_0)$ intersects L_{-1}.

is called a *bay*, its increasing rank preimages create holes (called *lakes*) inside the basin, $H_1 = T^{-1}(H_0)$, $H_2^1 \bigcup H_2^2 = T^{-1}(H_1)$, etc.

Figure 2 shows the bifurcation giving rise to a nonconnected basin [Fig. 2(c)] from a simply-connected basin [Fig. 2(a)]. The bifurcation occurs when the number of intersection points $\partial D \cap L$ changes. In the case of Fig. 2(c), Δ_0 is called a *headland*, its increasing rank preimages create nonconnected parts of the basin (called *islands*), $D_1 = T^{-1}(\Delta_0)$, $D_2^1 \bigcup D_2^2 = T^{-1}(D_1)$, etc ... From a parameter variation a new set of islands is also created when an isolated island initially belonging to Z_0 crosses through the critical curve L, one of its part belonging to Z_2. The bifurcation corresponds to the contact of the island boundary with L. More details about such bifurcations are given in [Mira *et al.*, 1994, Mira *et al.*, 1996a].

3. Some Basic Properties of the Map $\overline{T}$

3.1. *Critical set and properties of the inverse map*

The map $\overline{T}$ is noninvertible. Indeed the Jacobian determinant of $\overline{T}$, $|J(x, y)| = 2x\gamma + 8x^3 - 8xy$, vanishes on LC_{-1}, made up of two branches, $LC_{-1} = L_{-1}^a \bigcup L_{-1}^b$:

$$L_{-1}^a\colon x = 0, \quad L_{-1}^b\colon y = \frac{\gamma}{4} + x^2 \tag{3}$$

The rank-one image of LC_{-1} gives the critical curve $LC = \overline{T}(LC_{-1})$, also made up of two branches, $LC = L^a \bigcup L^b$:

$$L^a : y = \gamma(x + c), \quad L^b : \begin{cases} y = \left(x + c + \dfrac{\gamma}{4}\right)^2 \\ x \geq \dfrac{\gamma}{4} - c \end{cases} \tag{4}$$

In the phase plane the critical curve LC separates regions Z_i each point of which has i rank-one preimages, $i = 0, 2, 4$. For $\gamma \geq 0$ (the case studied in this paper) these regions are bounded by the following arcs of LC:

- a straight line L^a with positive slope if $\gamma > 0$ intersecting the x-axis at the point $(-c, 0)$ ($x = -c$ is the rank one critical point of the Myrberg's map, restriction of $\overline{T}$ on the x-axis),
- a branch of parabola L^b, tangent to L^a at the point $C = (-c + \gamma/4, \gamma^2/4)$.

In the particular case $\gamma = 0$, L^a reduces to the x-axis and is tangent to L^b at the point $(-c, 0)$.

The region Z_0 always exists, and Z_4 becomes wider and wider as the parameter γ decreases. The region Z_4 is a subset of the half plane $y > 0$ if $\gamma \geq 0$. The papers [Agliari *et al.*, 2003, 2004] provide the figures related to the regions Z_i.

For $\gamma > 0$ the half plane $(y < 0)$ includes the areas Z_0, Z_2 and a portion of critical curve L^a. The inverses of a point $p = (u, v) \in (y < 0)$ are obtained by solving with respect to (x, y) the system $u = x^2 + y - c$, $v = \gamma y + 4x^2 y$. Any point $p = (u, v) \in Z_2$ has the following inverses:

$$\overline{T}_1^{-1}(u, v) = (\sqrt{\xi},\ u + c - \xi),$$
$$\overline{T}_2^{-1}(u, v) = (-\sqrt{\xi},\ u + c - \xi)$$
$$\text{where}\ \ \xi = \frac{1}{2}\left(u + c - \frac{\gamma}{4} - \sqrt{\left(u + c + \frac{\gamma}{4}\right)^2 - v}\right) \tag{5}$$

3.2. *Some basic bifurcations*

The restriction of the map $\overline{T}$ to the x-axis is the one-dimensional Myrberg's map $x' = x^2 - c$. Thus, at $c = c_{(1)0} = -1/4$ a saddle-node bifurcation occurs, and for $c > -1/4$ $\overline{T}$ admits two fixed points on the x-axis denoted P^* and Q^*. The points P^* and Q^* are respectively the points q_2 and q_1 for the map reduced to the x-axis (cf. Part I, Sec. 2):

$$P^* = \left[\frac{1 - \sqrt{1 + 4c}}{2},\ 0\right],$$
$$Q^* = \left[\frac{1 + \sqrt{1 + 4c}}{2},\ 0\right].$$

The eigenvalues of the fixed point Q^* are $S_1(Q^*) = 1 + \sqrt{1 + 4c}$ with eigendirection $r_1 = (1, 0)$ (i.e. it is the eigenvalue of the restriction of $\overline{T}$ to the x-axis), and $S_2(Q^*) = \gamma + (1 + \sqrt{1 + 4c})^2$ with eigendirection $r_2 = (-1, 1 + \sqrt{1 + 4c})$. As $S_1 > 1$, it is always unstable for the map $\overline{T}$, as saddle or repelling node. Its rank-one preimage Q^*_{-1} on $y = 0$, different from Q^*, is such that $x(Q^*_{-1}) = -x(Q^*)$. The eigenvalues of the fixed point P^* are $S_1(P^*) = 1 - \sqrt{1 + 4c}$ with eigendirection $r_1 = (1, 0)$ (i.e. on the x-axis), and $S_2(P^*) = \gamma + (1 - \sqrt{1 + 4c})^2$ with eigendirection $r_2 = (1, \sqrt{1 + 4c} - 1)$.

From the relations (5) defining the inverses $\overline{T}_1^{-1}(u, v)$ and $\overline{T}_2^{-1}(u, v)$, with $\gamma = 0$ and $v = 0$, it appears that the inverse of the segment $x(Q^*_{-1}) \leq x \leq -c$ on the x-axis, in the half plane $y \leq 0$, is the segment $-(1 + \sqrt{1 + 4c})/2 + c \leq y \leq 0$ of the y-axis. So the ordinate of the lowest point of the Julia set, obtained for $\gamma = 0$, is $y = -(1 + \sqrt{1 + 4c})/2 + c$.

The bifurcations organization generated by the restriction of the map $\overline{T}$ to the x-axis is that of the Myrberg's map described in Sec. 2 of Part I, with $\lambda \equiv c$. It is the box-within-a-box one with $c_{(1)_0} = \lambda_{(1)_0} = -1/4$, $c_1^* = \lambda_1^* = 2$.

Moreover, at $\gamma = 1$ another saddle-node bifurcation occurs, so that for $\gamma < 1$, the map $\overline{T}$ admits two more fixed points:

$$R^* = \left(-\frac{\sqrt{1 - \gamma}}{2},\ c - \frac{1 - \gamma}{4} - \frac{\sqrt{1 - \gamma}}{2}\right),$$
$$S^* = \left(\frac{\sqrt{1 - \gamma}}{2},\ c - \frac{1 - \gamma}{4} + \frac{\sqrt{1 - \gamma}}{2}\right)$$

At the bifurcation value $\gamma = 1$ the two fixed points $R^* = S^* = (0, c)$ have the multipliers (eigenvalues) $S_1 = 1$ and $S_2 = 0$, and belong to the curve LC_{-1} defined above. Let us define, for $\gamma \leq 1$, $H_+(c, \gamma) = c - (1 - \gamma/4) - (\sqrt{1 - \gamma})/2$ and $H_-(c, \gamma) = c - (1 - \gamma/4) + (\sqrt{1 - \gamma}/2)$ the functions giving the second coordinate of these two more fixed points of $\overline{T}$. Then the two arcs: $H_- = 0$ for $c \leq 0$, and $H_+ = 0$ for $c \geq 0$ define a *transcritical bifurcation* Tc_{2^0}, where R^* and S^* exchange their stability with the fixed point P^* (on $y = 0$). For $H_- = 0$ we have $S^* \equiv P^*$, $S_2(P^*) = S_2(S^*) = +1$, while for $H_+ = 0$ and we have $R^* \equiv P^*$, $S_2(P^*) = S_2(R^*) = +1$. In the interval $-1/4 < c < 0$, S^* is locally stable, with $y(S^*) < 0$, if $H_- < 0$, and it is a saddle if $H_- > 0$ while the fixed point R^* $(y(R^*) < 0)$ is a saddle in a sufficiently small neighborhood of H_-. For $c > 0$ and $H_+ > 0$ R^* is locally stable, with $y(R^*) > 0$. If $H_+ < 0$ R^* is a saddle in a sufficiently small neighborhood of H_+. The fixed point S^* is a saddle in a sufficiently small neighborhood of H_+. By crossing through Tc_{2^0}, with decreasing values of γ, P^* become a stable node for $\overline{T}$, while S^* and R^* become saddles, with $y(S^*) > 0$ and $y(R^*) < 0$. See the qualitative picture on such bifurcations in Fig. 3(a) for $c < 0$ and in Fig. 3(b) for $c > 0$.

P^* now represents the fixed point q_2 of the Myrberg's map. The flip bifurcation points of the box ω_1 denoted c_{bi} in Part I, here will be denoted c_{2^i}, $i = 1, 2, 3, \ldots$, with $c_{2^1} = 3/4$ (i.e. c_{b1}) and $c_{2^2} = 5/4$ (i.e. c_{b2}). The index $i = 0$ corresponds to the fold bifurcation $c_{(1)0}$, the limit point is $c_{2^\infty} = c_{1s} \simeq 1.401155189$.

The map $\overline{T}$ is symmetric with respect to the axis $x = 0$, i.e. $\overline{T}(-x, y) = \overline{T}(x, y)$. This means that the basins are symmetric sets.

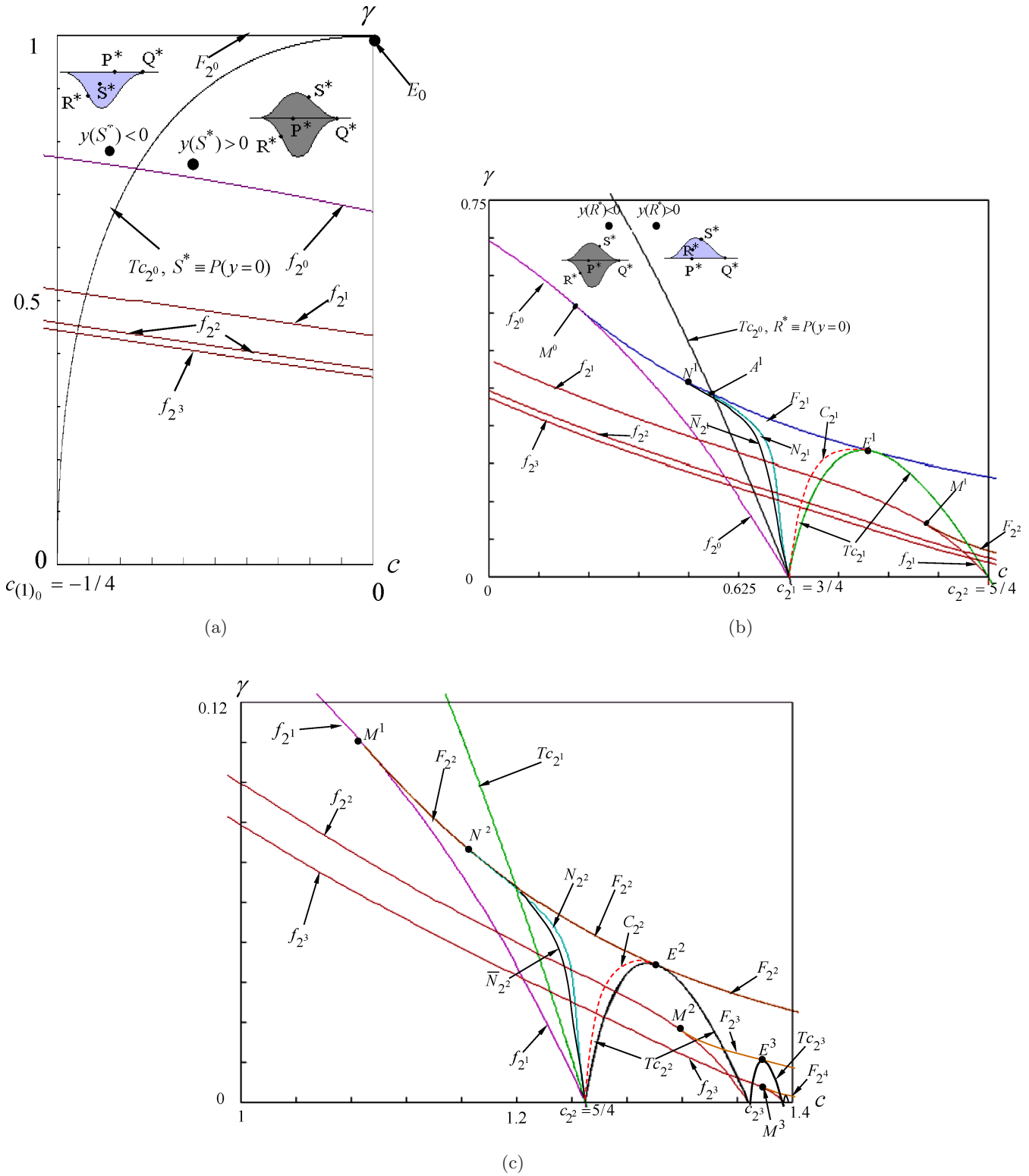

Fig. 3. Basic bifurcation curves of the interval $-1/4 = c_{2^0} = c_{(1)0} \le c \le c_{1s}$. Related to a period 2^i cycle, F_{2^i}, f_{2^i}, Tc_{2^i}, N_{2^i}, $i = 0, 1, 2, \ldots$, respectively correspond to fold, flip, transcritical, and Neïmark bifurcations.

3.3. *First set of bifurcation curves*

The bifurcation curves considered here [Figs. 3(a) and 3(b)] are viewed in the interval $-1/4 = c_{2^0} = c_{(1)0} \leq c \leq c_{2^1} = 3/4$ (i.e. c_{b1}) the boundaries being respectively the fold point and the first flip one for the Myrberg's map $x' = x^2 - c$, restriction of $\overline{T}$ to the x-axis. We are essentially interested in cycle points, and in the basin boundaries in the half plane ($y \leq 0$), and their bifurcations. The case $c < -1/4$ is out of the field of this study. It corresponds to the boundary of the domain of bounded orbits (when it exists, i.e. c not too small) entirely located in the half plane ($y < 0$).

Note that the half plane ($y < 0$), with $\gamma \geq 0$, is invariant by application of $\overline{T}$. The "germinal" situation is the bifurcation value $\gamma = 1$, for which the two fixed points $R^* = S^* = (0, c)$ belong to LC_{-1} with multipliers (eigenvalues) $S_1 = 1$ and $S_2 = 0$. In the parameter plane (c, γ) the line $\gamma = 1$ is a fold curve, now denoted F_{2^0}, joining two sheets of the foliated dim3 space: one related to the fixed point R^* (a stable node for $\gamma = 1 - \varepsilon$, $\varepsilon > 0$ being sufficiently small), the other associated with the unstable fixed point S^* (a saddle near $\gamma = 1$). For $\gamma > 1$ the whole phase plane has no singularity except those on the x-axis, and for $y \neq 0$ the points have divergent trajectories.

Consider the behavior of the fixed point R^* (i.e. a period 2^0 cycle). The curve Tc_{2^0} (Figs. 3(a), 3(b) and Fig. 5 with $i = 1$) is tangent to the fold curve F_{2^0} at the point E^0 ($c = 0$, $\gamma = 1$). Not too far from F_{2^0} ($c > 0$) for $H_+ > 0$ R^* is a stable node ($y(R^*) > 0$), while P^* (on $y = 0$) is a saddle ($-1 < S_1 < 1$, $S_2 > +1$) if $c \leq 3/4$, and an unstable node ($S_1 < -1$, $S_2 > +1$) if $c > 3/4$. The segment ($-x(Q^*) \leq x \leq x(Q^*)$; $y = 0$) belongs to the basin boundary $\partial D(R^*)$ of R^*, and the half plane $y < 0$ has no singularity if the point $(c; \gamma)$ remains not too far from F_{2^0}. For $H_+ < 0$, below the transcritical bifurcation Tc_{2^0} R^* becomes a saddle ($S_1 > 1$; $-1 < S_2 < 1$), and the fixed point P^* becomes a stable node. Close to this bifurcation its basin is simply connected and has a part $D_-(P^*)$ in the region $y < 0$, $R^* \in \partial D_-(P^*)$. If $c > 0$ the region $H_+ < 0$ contains the arc of flip curve f_{2^0}, ending at ($c = c_{2^1} = 3/4$, $\gamma = 0$) [Fig. 3(b)]. The flip curve f_{2^0} is related to a period doubling from R^*. Crossing through f_{2^0}, R^* turns into an unstable node ($S_1 > 1$; $S_2 < -1$) and gives rise to a period two saddle also belonging to the basin boundary arc $\partial D_-(P^*)$. The curve f_{2^0} contains a flip codimension two point M^0 ($c \simeq 0.2049$, $\gamma \simeq 0.5482$) which is a tangential contact with a fold arc F_{2^1}. With decreasing values of γ crossing through this F_{2^1} arc, the map generates a period two node (attracting or repelling) and a period two saddle ($S_1 > 1$; $0 < S_2 < 1$).

The basin part $D_-(R^*)$ does not exist in the region (R_1^1) of Fig. 4 with $i = 1$, because the stable fixed point R^* is in the positive half plane ($y > 0$) and other invariant sets do not exist in the half plane ($y < 0$). The region R_1^1 is bounded by an arc F_{2^1}, the point $A^1 = Tc_{2^0} \cap F_{2^1}$ ($c(A^1) \simeq 0.5662$, $\gamma(A^1) \simeq 0.35988$) and an arc Tc_{2^0}, while the upper boundary is the first fold bifurcation curve F_{2^0} ($\gamma = 1$). From the flip bifurcation arc f_{2^0} with $c < c(M^0)$ a decrease of γ leads to successive period doubling of a period 2^i saddle, which gives rise to a cascade of flip curves (the first Myrberg' spectrum) f_{2^i}, $i = 1, 2, \ldots$, with the limit f_s when $i \to \infty$.

The fold arc F_{2^1} [Fig. 3(b)] is tangent to the arc N_{2^1} of Neimark bifurcation ($S_{1,2} = e^{\pm j\varphi}$, $j^2 = -1$) at the point N^1 ($\varphi = 0$, i.e. $S_1 = S_2 = 1$). For $c(M^0) < c < c(N^1)$, decreasing γ and crossing through the fold curve F_{2^1} gives rise to the above period 2^1 saddle and the corresponding period 2^1 node is unstable, and the two cycles belong to $y < 0$. For $c(N^1) < c < c(E^1)$ crossing through F_{2^1}, a period 2^1 saddle always appears, but now associated with a period 2^1 stable node (belonging to $y < 0$), which turns into a stable period 2^1 focus when γ decreases. With a further decrease of γ, the stable period 2^1 focus becomes unstable, and crossing through the Neimark curve N_{2^1} it gives rise to a period 2^1 invariant closed curve (γ_{2^1}) [path $\widehat{bgh}$ of Fig. 6(a)]. On the path $\widehat{bd}$ of Fig. 6(b), the period 2^1 saddle may undergo a period doubling followed by the inverse process. With a new γ decrease, moving away the curve N_{2^1} the invariant closed curve turns into another period 2^1 attractor (weakly chaotic ring, or chaotic area [Mira *et al.*, 1996a; Frouzakis *et al.*, 1997]). Then the stable period 2^1 invariant closed curve, or the period 2^1 attractor, is destroyed with its basin at points of the bifurcation arc $\overline{N}_{2^i}$ after contact of the attractor with its corresponding basin boundary.

The fold arc F_{2^1} is also tangent to a transcritical bifurcation curve Tc_{2^1} at a point E^1, $c \simeq 0.9658$, $\gamma \simeq 0.247$ [Fig. 3(b)]. For $c > c(E^1)$, crossing through F_{2^1} always gives rise to a period 2^1 saddle and a stable node, which now belong to the half plane ($y > 0$). The curve Tc_{2^1} intersects $\gamma = 0$ at

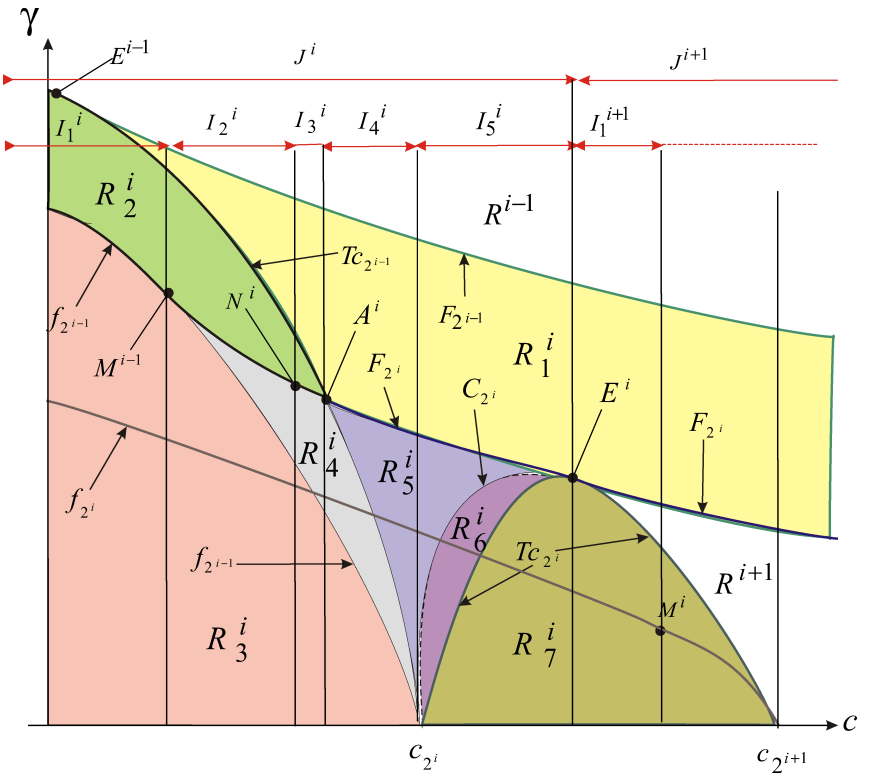

Fig. 4. Partition of the parameter plane in regions giving a similar qualitative behavior in the phase plane.

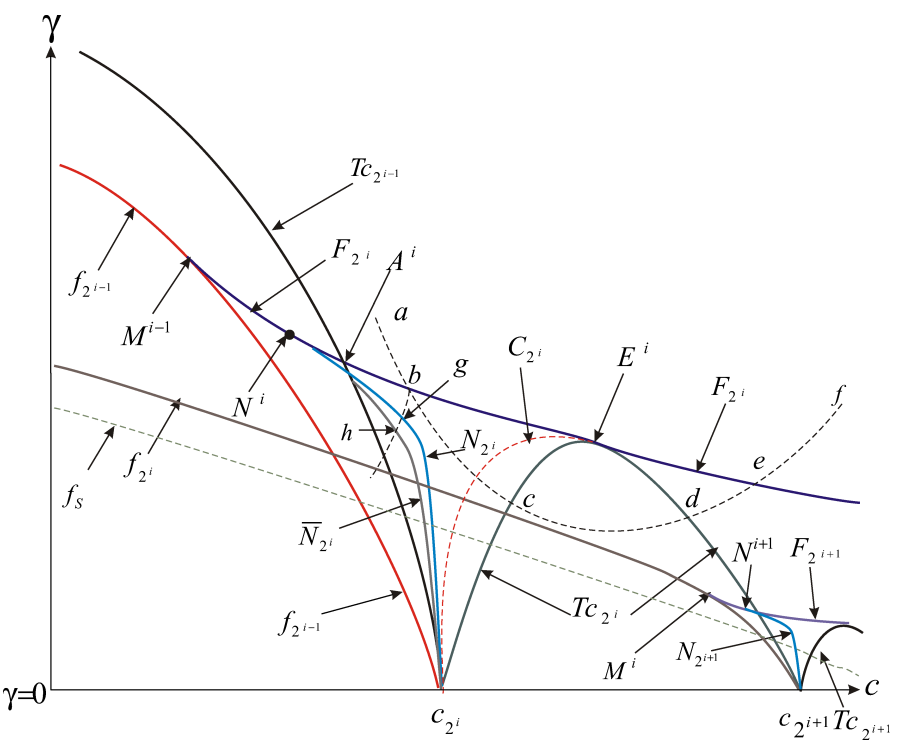

(a)

Fig. 5. Qualitative changes in the phase plane by following the path (*abcdef*) in the parameter plane. $Sad2^i$, $SN2^i$, denote a period 2^i saddle cycle, and a stable period 2^i node, respectively.

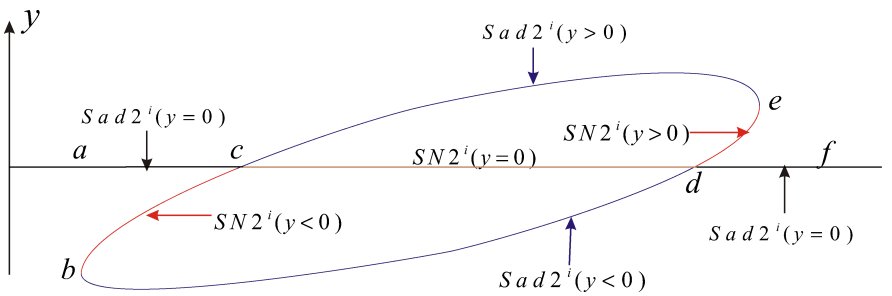

(b)

Fig. 5. (*Continued*)

the points $c = c_{2^1} = 3/4$ (i.e. c_{b1}) and $c = c_{2^2} = 5/4$ (i.e. c_{b2}) flip points of the Myrberg's map $x' = x^2 - c$ (restriction of $\overline{T}$ to the x-axis). The flip curves f_{2^0} and f_{2^1} intersect the axis $\gamma = 0$ at $c = c_{2^1}$ and $c = c_{2^2}$, respectively. The bifurcation properties related to Tc_{2^1} are given by Fig. 5(b) putting $i = 1$. So let us follow the parameter path a, b, c, d, e, f of Fig. 5(a), crossing through the fold arc F_{2^1} and Tc_{2^1}. The stability exchange between the period 2^1 cycles (saddles denoted $Sad2^1$, and stable nodes denoted $SN2^1$ with ordinates $y = 0$, or $y < 0$, or $y > 0$) occurs according to Fig. 5(b) scheme, where b, e are fold points, c, d are transcritical points.

The foliated structure related to the neighborhood of Tc_{2^1} is given by Fig. 7 with $i = 1$, the structure for $c < c(Tc_{2^1})$ being described by the left part of Fig. 8, which will be discussed in Sec. 4.2. Here in Fig. 7 the sheet $y = 0$ is separated into two regions by Tc_{2^1}, one related to the stable node $SN2^1$, the other to the saddle $Sad2^1$, located on $y = 0$. For the map restricted to the x-axis these two cycles are respectively the period 2^1 stable cycle, and the

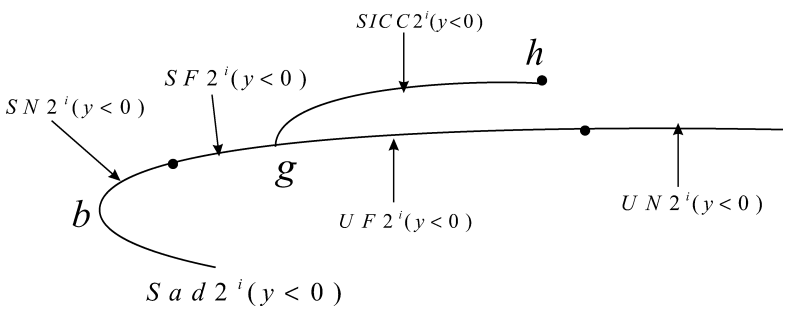

(a)

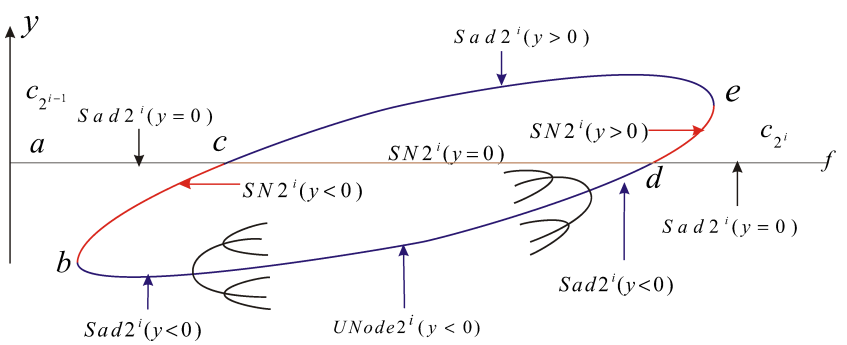

(b)

Fig. 6. Qualitative changes in the phase plane by following the path (bgh) in the parameter plane (Fig. 5). $Sad2^i$, $SN2^i$, denote a period 2^i saddle cycle, and a stable period 2^i node, respectively. $SF2^i$, $SICC2^i$, $UF2^i$, $UN2^i$ are a stable period 2^i focus, a stable period 2^i invariant closed curve, an unstable period 2^i focus, an unstable period 2^i node, respectively.

period 2^1 unstable cycle, resulting from the destabilization of the previous stable one after the flip bifurcation, for $c > c_{b1}$ (i.e. c_{2^1}). Each point of the sheet Sa_{2^1} (resp. Ss_{2^1}) is related to a saddle $Sad2^1(y < 0)$ (resp. a stable node $SN2^1(y < 0)$). Each point of the sheet Sa'_{21} (resp. Ss'_{21}) is related to a saddle $Sad2^1(y > 0)$ (resp. a stable node $SN2^1(y > 0)$).

4. Bifurcations Set of the ω_1 Spectrum

4.1. *Bifurcation curves*

The bifurcation curves organization of Fig. 3, described above considering cycles of periods 2^0 and 2^1, also recurs for the period 2^i cycles, $i = 2, 3, \ldots$ of the ω_1 spectrum (cf. Part I, Sec. 2). Figure 3(c) shows this property for $i = 2$, with $c_{2^2} = 5/4$. This means that each curve f_{2^i} has a flip codimension-two point M^i joining a fold arc $F_{2^{i+1}}$, locus of merging of a period 2^{i+1} saddle and a period 2^{i+1} node, as for the case $i = 1$ considered in Secs. 3.2 and 3.3. The point M^i separates two arcs of f_{2^i}. The arc $c < c(M^i)$ (Fig. 5) is such that, crossing it with γ decreasing, the period 2^i saddle turns into an unstable period 2^i node ($S_1 > 1$, $S_2 < -1$), and gives rise to period 2^{i+1} saddle ($S_1 > 1$, $-1 < S_2 < 1$). The f_{2^i} arc for $c > c(M^i)$ is such that, crossing it with γ increasing, the unstable period 2^i node turns into a period 2^i saddle, but also gives rise to a period 2^{i+1} repelling node ($S_1 > 1$, $S_2 > 1$). Each fold arc F_{2^i} is tangent to an arc N_{2^i} of Neimark bifurcation ($S_{1,2} = e^{\pm j\varphi}$, $j^2 = -1$) at a point N^i ($\varphi = 0$, i.e. $S_1 = S_2 = 1$). With γ decreasing, crossing through the curve N_{2^i} the map gives rise to a stable period 2^i invariant closed curve by destabilization of a period 2^i focus.

Each fold arc F_{2^i} is tangent to a transcritical bifurcation curve Tc_{2^i} at a point E^i. The curve Tc_{2^i} intersects $\gamma = 0$ at the points $c = c_{2^i}$ and $c = c_{2^{i+1}}$, flip points of the Myrberg's map $x' = x^2 - c$. Each flip curve f_{2^i} intersects the axis $\gamma = 0$ at $c = c_{2^{i+1}}$, and the limit f_s intersects this axis at $c = c_s = \lim_{i\to\infty} c_{2^i} \simeq 1.401155189$.

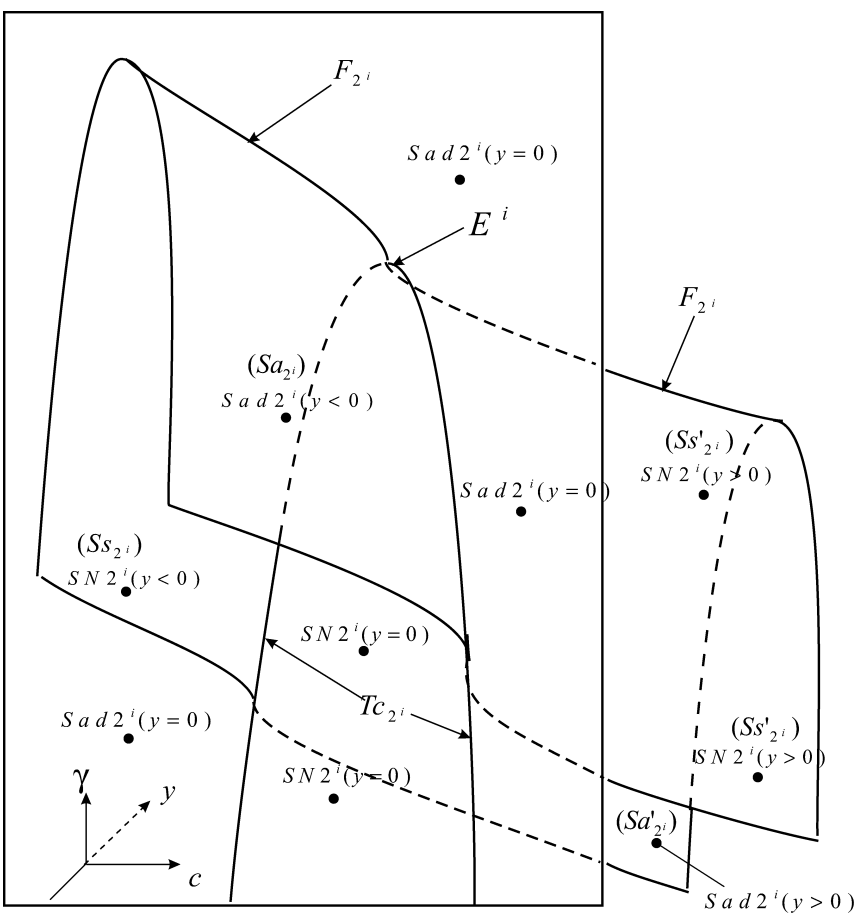

Fig. 7. Foliation of the parameter plane by crossing the transcritical curve Tc_{2^i}. Each sheet is related to a well defined cycle of Fig. 5(b).

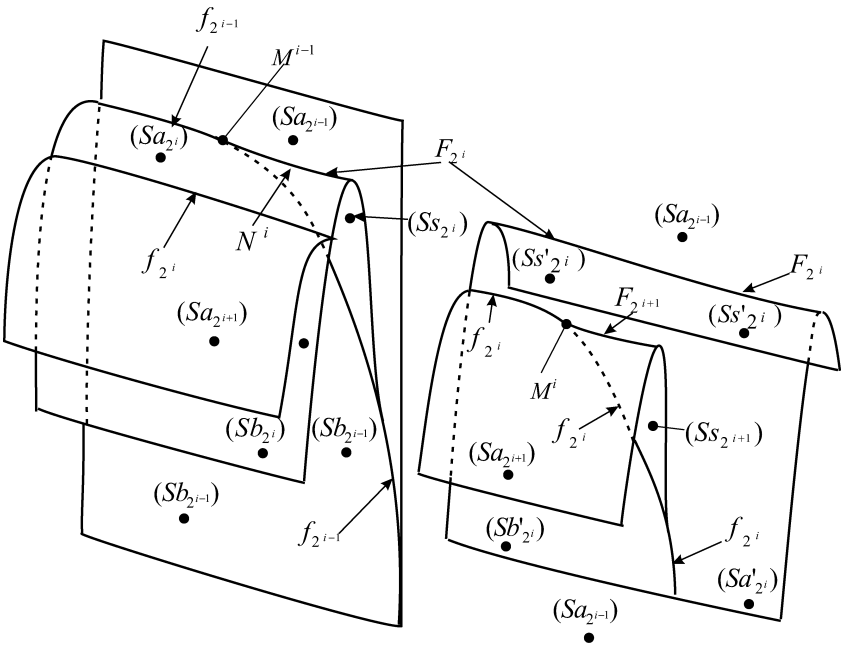

Fig. 8. In relation with Fig. 5(a), additional information on the parameter plane foliation before crossing the transcritical curve Tc_{2^i} (left part of the figure), and after crossing (right part of the figure).

Let us follow the parameter path a, b, c, d, e, f of Fig. 5(a), crossing through the fold arc F_{2^i} and Tc_{2^i}. The stability exchange between the period 2^i cycles (saddles denoted $Sad2^i$, and stable nodes denoted $SN2^i$ with ordinates $y = 0$, $y < 0$, $y > 0$) occurs according to Fig. 5(b) scheme.

4.2. *Foliated bifurcations structure*

The foliated structure is given by Figs. 7 and 8. Each sheet of this structure is related to a well defined cycle. Considering Fig. 8, the sheet Sa_{2^i} is related to the period 2^i saddle cycle (denoted 2^i saddle), born from crossing through the flip curve $f_{2^{i-1}}$. The sheet $Sb_{2^{i-1}}$ related to the period 2^{i-1} unstable node cycle ($S_1 > 1$, $S_2 < -1$). The curve $f_{2^{i-1}}$ is the junction of three sheets. For $c < c(M^{i-1})$ they are the sheets Sa_{2^i}, $Sa_{2^{i-1}}$, and $Sb_{2^{i-1}}$. For $c > c(M^{i-1})$ they are the sheets $Sb_{2^{i-1}}$, $Sa_{2^{i-1}}$, and Ss_{2^i} related to the period 2^i node ($y < 0$) born from the fold curve F_{2^i}. This cycle is always unstable near $f_{2^{i-1}}$ and near the arc $\widehat{M^{i-1}N^i}$ of F_{2^i}. It is stable near the arc $\widehat{N^iE^i}$ of F_{2^i}, then with decreasing γ-values, this period 2^i node turns into a focus, becoming unstable when $c < c(N_{2^i})$. In brief, for decreasing γ values the arc $c < c(M^{i-1})$ of the flip bifurcation $f_{2^{i-1}}$ is characterized by:

$$2^{i-1} \text{ saddle} \rightarrow 2^{i-1} \text{ unstable node} + 2^i \text{ saddle} \quad (6)$$

and the arc $c(M^{i-1}) < c < c_{_{2^i}}$ is characterized by

$$2^{i-1} \text{ saddle} + 2^i \text{ unstable node} \rightarrow 2^{i-1} \text{ unstable node} \quad (7)$$

These cycles have their ordinates $y < 0$, and the bifurcations in (6), (7) concern different sheets.

Whatever be the index i, the foliated structure related to the curve Tc_{2^i}, given in Fig. 7, occupies the empty place of Fig. 8, between the left and the right parts. Here the sheet $y = 0$ is separated into two regions by Tc_{2^i}, one related to the saddle $Sad2^i$, the other to the stable node $SN2^i$, located on $y = 0$. For the map restricted to the x-axis these two cycles are respectively the period 2^i stable cycle, and the period 2^i unstable cycle, resulting from the destabilization of the previous stable one after the flip bifurcation, i.e. $c > c_{bi}$. Each point of the sheet Sa_{2^i} (resp. Ss_{2^i}) is related to a saddle $Sad2^i(y < 0)$ (resp. a stable node $SN2^i(y < 0)$). Each point of the sheet Sa'_{2^i} (resp. Ss'_{2^i}) is related to a saddle $Sad2^i(y > 0)$ (resp. a stable node $SN2^i(y > 0)$).

The arc $\widehat{M^{i-1}N^i}$ of F_{2^i} satisfies ($S_1 > 1$, $S_2 = 1$). The F_{2^i} arc on the right of N^i satisfies ($0 < S_1 < 1$, $S_2 = 1$). Figure 8 gives the three-dimensional foliated representation of the bifurcation curves shown in Fig. 5(a), from which the part related to Fig. 7 is removed for clarity sake. Here the sheet Ss_{2^i} is bounded by the arc $\widehat{M^{i-1}E^i}$ of F_{2^i},

and a $f_{2^{i-1}}$ arc, and the arc $\widehat{E^i c_{2^i}}$ of Tc_{2^i}. It is associated with the unstable, or stable, period 2^i cycle node, or focus, with $y < 0$, born from the fold F_{2^i}.

Let us remark that in the parameter plane the curves f_{2^j}, $j = i, i+1, \ldots$, intersect the curve $f_{2^{i-1}}$ (Figs. 3 and 9), but it is not the case in the three-dimensional foliated representation (Fig. 8). Indeed the flip curves $f_{2^{i-1}}$ and f_{2^i} are located on two different sheets for $x > x(M^{i-1})$.

Remark. The parameter plane properties, given below, were numerically established for only relatively small values of the integer i. Nevertheless it is possible to conjecture the same behavior on the basis of the bifurcation structure generated by the map restricted to the x-axis (the box-within-a-box one). The following reasonable conjecture is also made: the organization of the Figs. 3(a) and 3(b) bifurcation curves recur for each interval $c_{(k)0} \leq c \leq c_{k2^1}$, related to a period k basic cycle. Figure 9 shows this situation for $k = 3$.

4.3. *Regions of the parameter plane with the same qualitative characteristics*

In the interval $-1/4 = c_{(1)0} = c_{2^0} < c \leq c_1^* = 2$, the different arcs of curves described above [Fig. 5(a)] limit regions of the parameter plane with specific properties. For $c > c(E^{i-1})$ below the region R^{i-1} (with lower boundary $F_{2^{i-1}}$) there are the fold curves set F_{2^n}, $n > i-1$, delimiting n slices. Each of these slices corresponds to a period 2^n attractor, $n \leq i-1$, located in the half plane $(y > 0)$, stable node or focus if $(c;\gamma)$ is sufficiently near F_{2^n}. Then, when γ decreases, it turns into an unstable focus surrounded by an invariant closed curve which becomes a chaotic attractor. Considering the colored regions in Fig. 4, if $(c;\gamma) \in R^{i-1}$ the half plane $y < 0$ is without any singularity. The upper region R^0 $(i = 1)$ has for its lower boundary F_{2^0}, which is the fold line $\gamma = 1$. If $(c;\gamma) \in R^0$ the whole phase plane is empty of any singular point, except for the x-axis. In the lower region, when $(c;\gamma) \in R_1^i$, a period 2^{i-1} attractor (cycle, or invariant close curve, or chaotic area), belonging to the half plane $(y > 0)$, exists, and the half plane $(y < 0)$ is without any singularity. When $(c;\gamma) \in R_2^i$, the half plane $(y < 0)$ contains a part D_- of the basin of a stable period 2^{i-1} cycle located on $y = 0$ (the fixed point P^* is related to $i = 1$). The boundary ∂D_- contains the period 2^{i-1} saddle cycle resulting from the crossing through $Tc_{2^{i-1}}$ for $c > c(E^{i-1})$. This cycle turns into an unstable node when $(c;\gamma) \in R_3^i$, and with decreasing γ values, after crossing through the flip curves f_{2^n} unstable period 2^{n-1} nodes, and period 2^n saddles, appear on ∂D_-, with the Myrberg' spectrum ω_1 order (cf. Part I, Sec. 2).

When $(c;\gamma) \in R_4^i$ (cf. Fig. 4), the half plane $(y < 0)$ contains a part D_- of the basin of a stable period 2^{i-1} cycle located on $y = 0$ (the fixed point P^* is related to $i = 1$). For $c \in I_2^i$ from

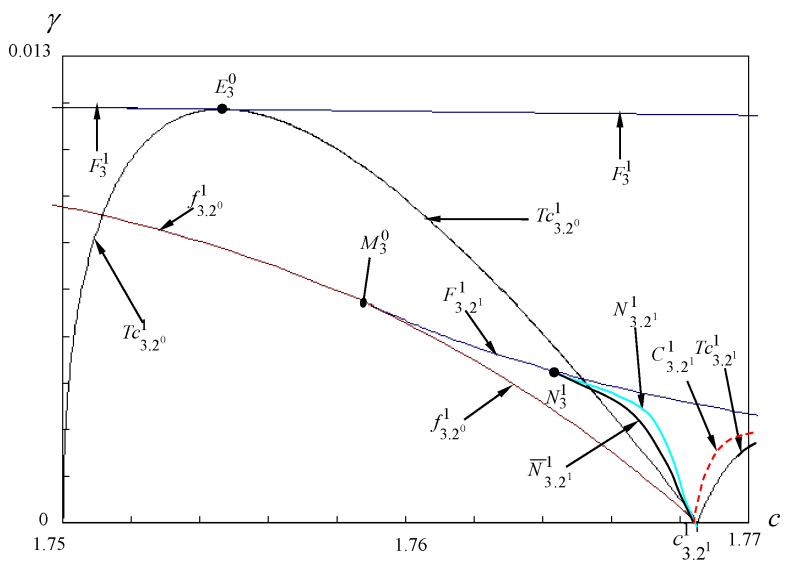

Fig. 9. Basic bifurcation curves of the interval $1.75 = c_{(3)0} \leq c \leq c_{3s}$. Related to a period 3.2^i cycle, $F_{3.2^i}$, $f_{3.2^i}$, $Tc_{3.2^i}$, $N_{3.2^i}$, $i = 0, 1, 2, \ldots$, respectively correspond to fold, flip, transcritical, and Neïmark bifurcations. These curves are similar to the Fig. 3 ones.

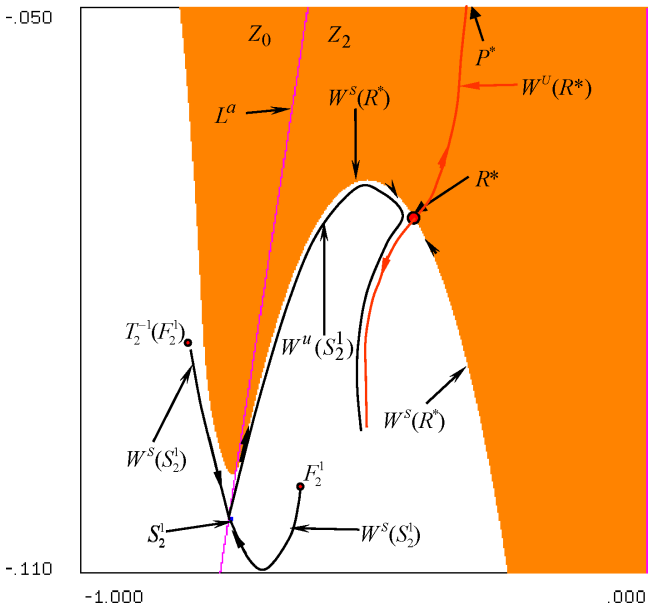

Fig. 10. $c = 0,47$; $\gamma = 0,3881$: phase plane situation before the Fig. 11 bifurcation. R^*, S_2^r, F_2^r, $r = 1, 2$, are respectively a saddle fixed point, a period two saddle, and a period two unstable focus. W^S and W^u denote the stable and unstable manifolds of the saddles. P^* is a stable node located on $y = 0$. L_a is an arc of critical curve separating the phase plane into two regions Z_0 (a point has no preimage) and Z_2 (a point has two rank-one preimages).

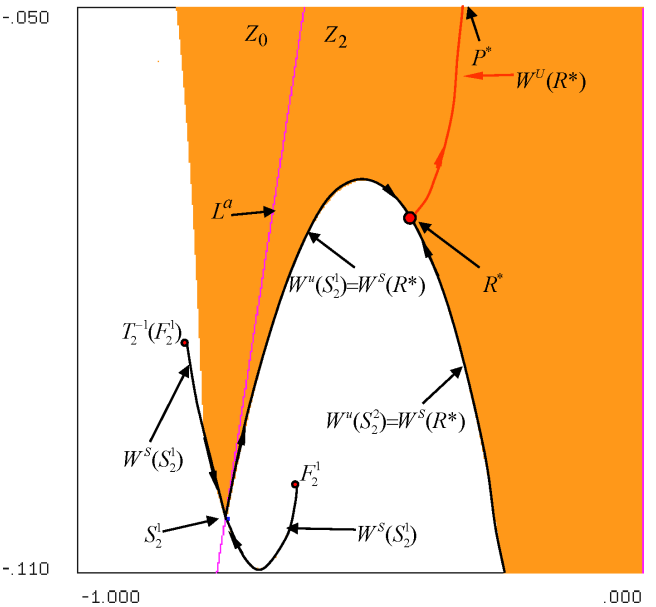

Fig. 11. $c = 0.47$; $\gamma \simeq 0.388062942$: saddle-saddle bifurcation.

the fold bifurcation F_{2^i} a period 2^i saddle $S_{2^i}^r$, $r = 1, 2, \ldots, 2^i$, and a period 2^i unstable node, turning after into an unstable period 2^i focus $F_{2^i}^r$, appear out of ∂D_-. The cycles $S_{2^i}^r$ and $F_{2^i}^r$ belong to the nonconnected boundary of the domain of divergent orbit. With decreasing values of γ and $c \in I_2^i$, a *global bifurcation of "saddle-saddle" type* defined by $W^u(S_{2^i}^r) \equiv W^s(S_{2^{i-1}}^{r'})$, $r' = 1, 2, \ldots, 2^{i-1}$, occurs. For $i = 1$ this bifurcation is described before the bifurcation in Fig. 10 ($c = 0,47$; $\gamma = 0,3881$), at the bifurcation in Fig. 11 ($c = 0.47$; $\gamma \simeq 0.388062942$), and after that in Fig. 12 ($c = 0.47$; $\gamma = 0,388$) for which ∂D_- now contains $F_{2^i}^r$ and the stable manifold of the saddle $S_{2^i}^r$ (for more details cf. below Sec. 5.4).

When $c \in I_3^i \cup I_4^i$ (cf. Fig. 4), $(c;\gamma)$ being sufficiently close to the fold curve F_{2^i} a period 2^i stable node, or focus, or invariant close curve exists in the half plane $y < 0$. The related basins of the 2^i fixed points of $\overline{T}^{2^i}$ and D_- are without any connection, and without common boundary. With new γ decreasing values, this period 2^i attractor becomes unstable, leading the pair period 2^i saddle and unstable focus to the same situation occurring for $c \in I_2^i$. The boundary ∂D_- contains the period 2^{i-1} saddle cycle (the fixed point R^* if $i = 1$) resulting from the crossing through $Tc_{2^{i-1}}$ for $c > c(E^{i-1})$. Now a saddle-saddle bifurcation D_- is nonconnected since it is in Fig. 2(c) situation. The islands (nonconnected parts) have the stable manifold $W^s(S_{2^i}^r)$ of the saddle $S_{2^i}^r$ as limit set, and for $i = 1$, Fig. 13 ($c = 0.6$; $\gamma = 0.25972$) shows the situation. For $i = 1$ the above saddle-saddle bifurcation is described in Figs. 14 ($c = 0.6$; $\gamma \simeq 0.259716125$)

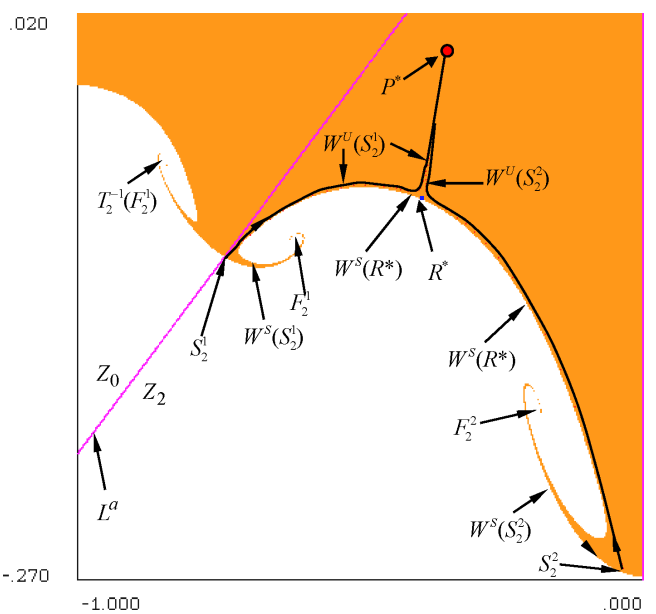

Fig. 12. $c = 0.47$;$\gamma = 0,388$: situation after the saddle-saddle bifurcation. Now the basin boundary ∂D_- contains $F_{2^i}^r$ and the stable manifold of the saddle $S_{2^i}^r$.

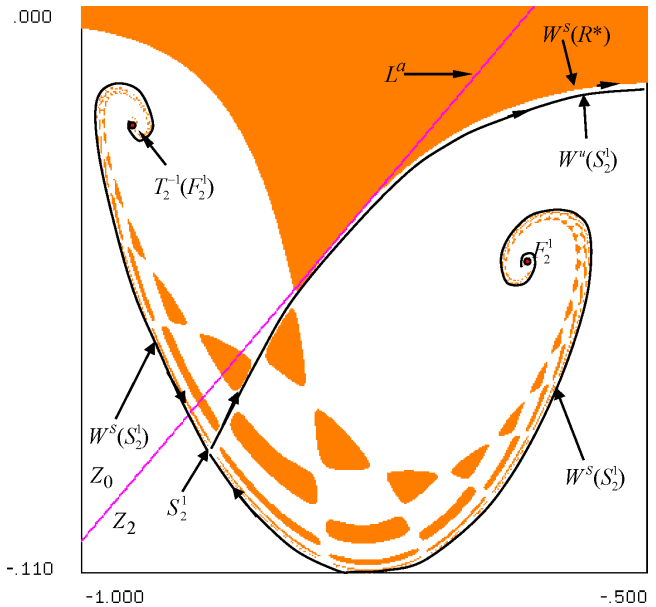

Fig. 13. $c = 0.6$; $\gamma = 0.25972$: due to the creation of a headland (L_a intersects the immediate basin boundary at three points, as in Fig. 2(c)) the basin is nonconnected. The islands (nonconnected parts) have the stable manifold $W^s(S_{21}^r)$ of the saddle S_2^r as limit set.

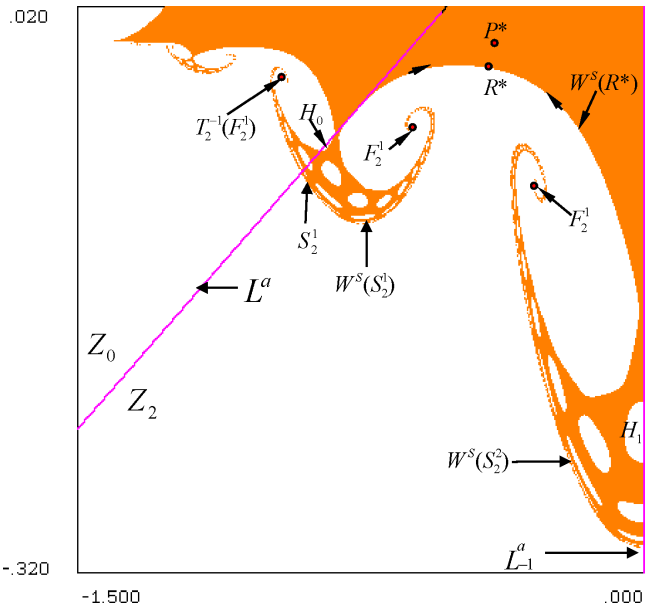

Fig. 15. $c = 0.6$; $\gamma = 0.2597$: multiply connected basin D_- obtained from the Fig. 14 situation, which has induced a *direct transition nonconnected multiply-connected basin.*

and 15 ($c = 0.6$; $\gamma = 0.2597$). It gives rise to a multiply connected basin D_-, being in the Fig. 1(c) situation (more details are given in Sec. 5.4). The basin D_- becomes simply connected (Fig. 16, $c = 0.6$; $\gamma = 0.259653$) via the bifurcation in Fig. 1, beginning with Fig. 1(c) and arriving at the Fig. 1(a) situation. It is worth to underline that, for $c \in I_3^i$, the saddle-saddle bifurcation $W^u(S_{2^i}^r) \equiv W^s(S_{2^{i-1}}^{r'})$ induces a *direct transition nonconnected multiply-connected basin* as in Sec. 4.2 of the paper [Bischi *et al.*, 2006].

If $(c;\gamma) \in R_5^i$, a stable period 2^{i-1} attractor (R^* if $i = 1$) exists in the half plane ($y > 0$) and the segment $(-x(Q^*) \le x \le x(Q^*);\ y = 0)$ belongs

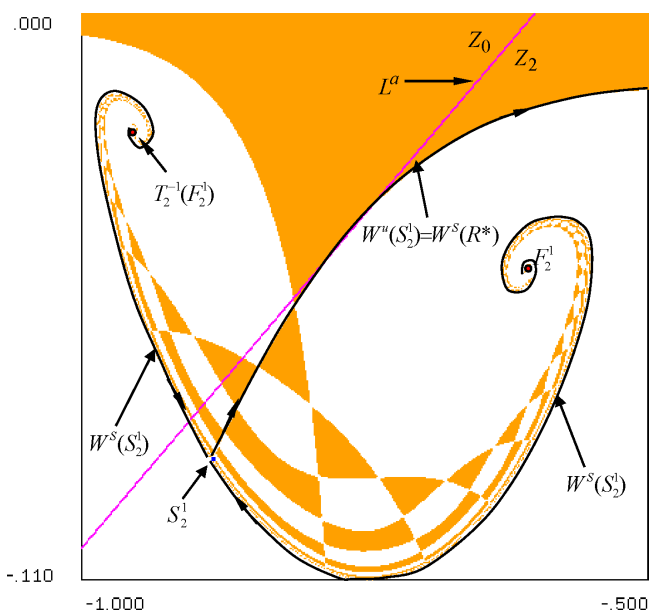

Fig. 14. $c = 0.6$; $\gamma \simeq 0.259716125$: saddle-saddle bifurcation which gives rise to a multiply connected basin D_- (Fig. 1(c) situation) when γ decreases from this value.

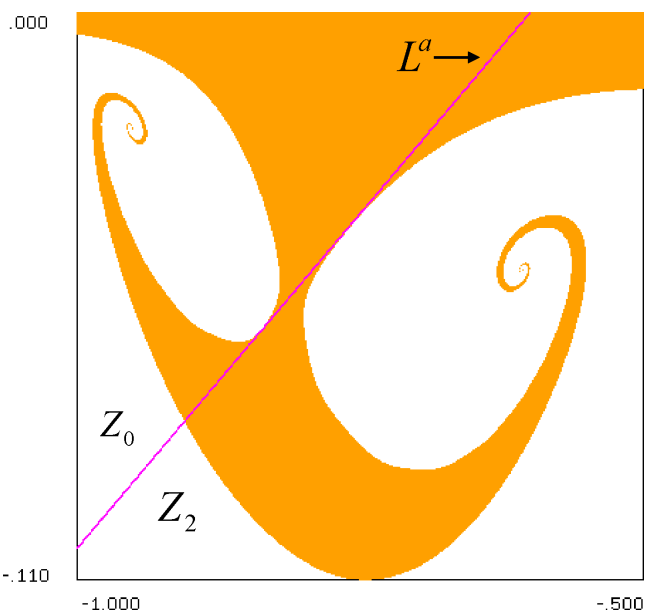

Fig. 16. $c = 0.6$; $\gamma = 0.259653$: the basin D_- becomes simply connected via the bifurcation of Fig. 1, beginning with Fig. 1(c) and arriving at the Fig. 1(a) situation.

to the boundary ∂D of its basin $D \subset (y > 0)$. If $(c;\gamma) \in R_5^i$ is above the curve $\overline{N}_{2^i}$ (cf. Figs. 3(b) and 4) then the half plane $y < 0$ contains the period 2^i singularities mentioned above for $c \in I_4^i$.

The region (R_6^i) is bounded by the arcs $\widehat{E^i c_{2^i}}$ of Tc_{2^i}, $\widehat{E^i c_{2^i}}$ of the arc C_{2^i}. This new arc C_{2^i} (cf. Figs. 3(b) for $i = 1$, and 3(c) for $i = 2$) corresponds to another type of saddle-saddle bifurcation. Now the unstable manifold $W^u(S^r)$, $r = 1, 2, \ldots, 2^i$, of the period 2^i saddle $(y = 0)$ merges with the stable manifold $W^s(S_{2^i}^r)$ of the period 2^i saddle $(y < 0)$. The qualitative view of this new "saddle-saddle" bifurcation is given by Fig. 17(b) for $i = 1$, where the fixed point P^* $(y = 0)$ is an unstable

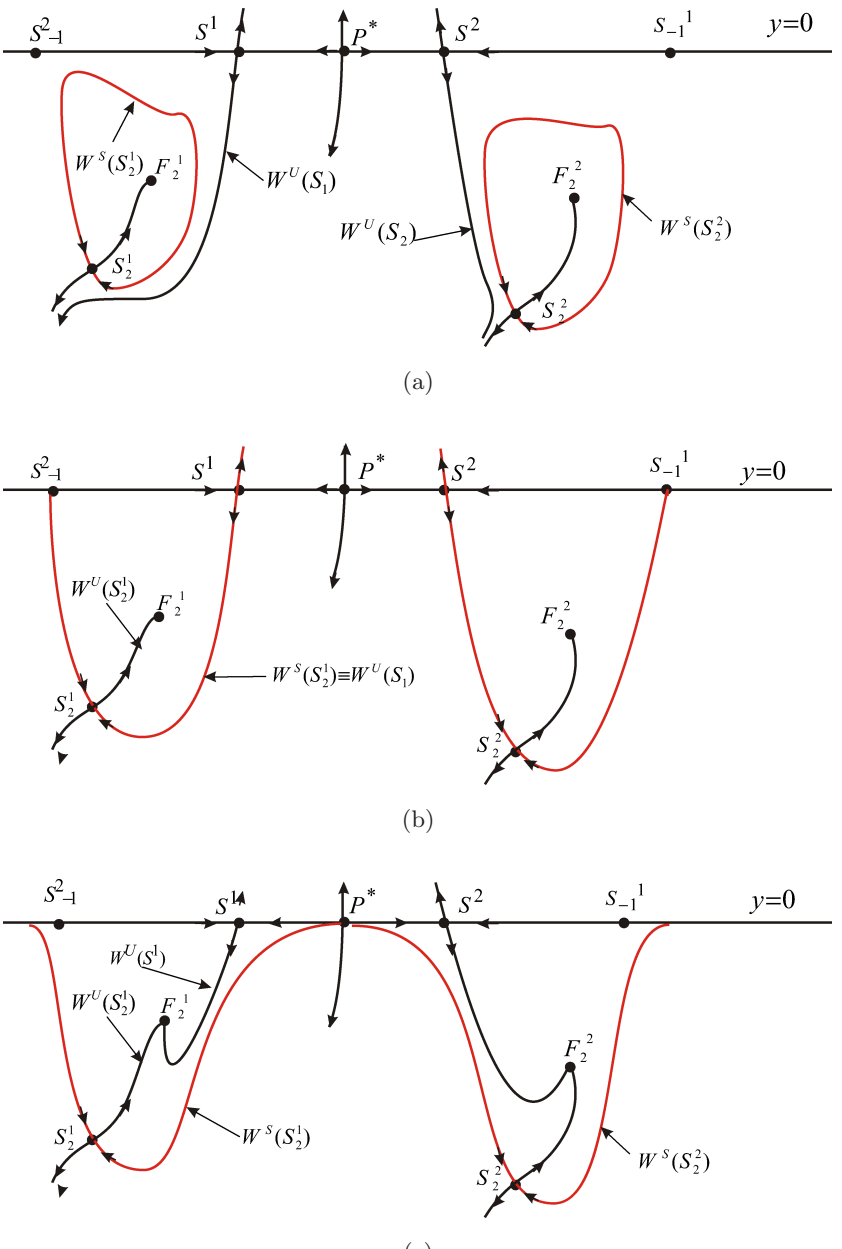

Fig. 17. Other type of saddle-saddle bifurcation. P^* $(y = 0)$ is an unstable node. The period two cycle $(y = 0)$ S^j, $j = 1, 2$, born from P^* by period doubling is a saddle, whose stable manifold (belonging to the x-axis) is $W^s(S^j)$, the unstable one being $W^u(S^j)$. The point S_{-1}^1 is the rank-one preimage of S^1 different from S^2, S_{-1}^2 the rank-one preimage of S^2 different from S^1. The points S_2^j, F_2^j, $j = 1, 2$, are respectively those of the period two saddle cycle and stable node (becoming a focus). (a) Situation before the bifurcation: the immediate basin of the period two attracting set, in the region $y < 0$ of the phase plane, is nonconnected. (b) Situation at the bifurcation: the unstable manifold $W^u(S^r)$, $r = 1, 2$, of the period 2^1 saddle $(y = 0)$ merges with the stable manifold $W^s(S_{2^1}^r)$ of the period 2^1 saddle $(y < 0)$. (c) Situation after the bifurcation.

node. Figure 17(a) represents the situation before the bifurcation, and Fig. 17(c) the situation after the bifurcation. The period two cycle ($y = 0$) S^j, $j = 1, 2$, born from P^* by period doubling is a saddle, whose stable manifold (belonging to the x-axis) is $W^s(S^j)$, the unstable one being $W^u(S^j)$. The point S^1_{-1} is the rank-one preimage of S^1 different from S^2, S^2_{-1} the rank-one preimage of S^2 different from S^1. The points S^j_2, F^j_2, $j = 1, 2$, are respectively those of the period two saddle cycle and stable node (becoming a focus) generated by the fold bifurcation on the arc $\widehat{N^iE^i}$ of F_{2^i}. The stable manifold of S^j_2, and the unstable one, are denoted $W^s(S^j_2)$ (basin boundary of F^j_2) and $W^u(S^j_2)$, respectively. In Fig. 17(b) $W^s(S^j_2)$ has merged into $W^u(S^j)$. The left part of Fig. 5(b) with $i = 1$ [or Fig. 3(b)] corresponds to Fig. 17(c), i.e. a point of the parameter plane is located between C_{2^1} and the arc $\widehat{E^1c_{2^0}}$ of Tc_{2^1} in Fig. 5(a). In the Fig. 17(a) situation the immediate basin of the period two attracting set, in the region $y < 0$ of the phase plane, is nonconnected. It has no contact with $W^s(S^j)$, $j = 1, 2$, which is a part of the basin boundary of the attracting set in the region $y > 0$. In the Fig. 17(c) situation the stable manifold $W^s(S^j)$, $j = 1, 2$, now separates the basin of the period two attracting set in the region $y < 0$ from the basin of the attracting set in the region $y > 0$.

The region (R^i_7) is bounded by the transcritical curve Tc_{2^i}. Its properties are given by Figs. 5 and 7. The region R^{i+1} contains the regions R^{i+1}_m, $m = 1, 2, \ldots, 7$, having the above properties but for period 2^{i+1} cycles. In the neighborhood of the Tc_{2^i} arc $\widehat{E^ic_{2^{i+1}}}$, these cycles have ordinates $y < 0$ (Fig. 5).

4.4. *Global view: bifurcation aspects in the half plane $y \leq 0$*

If $\gamma > 0$ the half planes $(y > 0)$ and $(y \leq 0)$ are both trapping, with $\overline{T}(y > 0) \subseteq (y > 0)$ and $\overline{T}(y < 0) \subseteq (y < 0)$. For $\gamma = 0$ the negative half plane is invariant ($\overline{T}(y < 0) = (y < 0)$) and the positive one is still trapping.

As already mentioned, for $\gamma = 0$ the map $\overline{T}$ is topologically semiconjugate to the complex quadratic map T_Z in (1) in the half plane $y < 0$, with $\overline{T} \circ h = h \circ T_Z$, where $h(x, y) = (x, -y^2)$. This property leads to the following remarks:

(a) inside the half plane $y \leq 0$ with $\gamma > 0$ decreasing and keeping fixed the value of c, $-1/4 < c \leq 2$, the map $\overline{T}$ generates more and more sets of infinitely many real cycles. For $\gamma = 0$ all the possible cycles have been created, "conjugated" to those of the (complex) quadratic map T_Z in (1). All these cycles are unstable with multipliers $|S_1| = |S_2| > 1$. The limit set of these cycles constitute a Julia set $J = (E')$. The case $\gamma = 0$ includes two exceptional situations. The first one is related to fold and flip bifurcations c-values giving rise to a domain of convergence (but not a basin), bounded by J, toward a cycle of $y = 0$ belonging to J (cf. Part I, Sec. 3.4, Sec. 3.6, and below Sec. 6.4.1). The second situation is the *dendrite* ones (cf. Part I, Sec. 5.5, and below Sec. 9). One of them gives rise to a domain of convergence toward a chaotic set A^{Ch} in the half plane $y \geq 0$, a subset set of A^{Ch} touching $J \cap (y = 0)$ at a periodic chaotic segment CH for the map reduced to the x-axis (cf. Part I, Sec. 2.1). With respect to the two-dimensional map $\overline{T}$, CH is a weak Milnor attractor (on $y = 0$) for the points in the CH neighborhood with $y > 0$.

(b) For $c = c^*_1 = 2$ all the cycles of the quadratic map T_Z in (1) and their limit points are on the x-axis. Thus also for $\overline{T}$ with $\gamma = 0$, these cycles are located on the segment $-2 \leq x \leq 2$, $y = 0$. These cycles are the ones generated by the Myrberg's map $x' = x^2 - c$, $c = 2$, denoted $(k; j)$, k being the period, j the cyclic permutation of one of their points by k successive iterations by $\overline{T}$ (cf. Part I, Sec. 2).

(c) Consider the transcritical curve Tc_{2^0}, which is made up of the two branches $H_-(c, \gamma) = 0$ $(c = (1 - \gamma)/4 - (\sqrt{1 - \gamma}/2))$ and $H_+(c, \gamma) = 0$ $(c = (1 - \gamma)/4 + (\sqrt{1 - \gamma}/2))$ joining at the point $(c = 0, \gamma = 1)$. Remind that the first branch (resp. second branch) is related to a stability exchange between P^* and S^*(resp. R^*). The first branch intersects $\gamma = 0$ at the point $c = c_{2^0} = c_{(1)0} = -1/4$ first basic fold bifurcation of the Myrberg's map, the $S^* = P^*$ multipliers being $S_1 = S_2 = 1$. For $\gamma = 0$ and $c = c_{2^1} = 3/4$ (i.e. c_{b1}) the R^* multipliers are $S_1 = -S_2 = \sqrt{4 - 4c}$, that is $S_1 = -S_2 = 1$. Then the second Tc_{2^0} branch (related to R^* with $S_1 = +1$) intersects the flip curve f_{2^0} (related to R^* with $S_2 = -1$) at the point $c = c_{2^1} = 3/4$ (i.e. c_{b1}) and $\gamma = 0$.

We note that for $\gamma = 0$, the Julia set $J \subset (y \leq 0)$, $J \equiv \partial D_-$, made up of all the unstable cycles and

their limit points, is nowhere smooth, except for two cases. The first is $c = 0$, when the fixed point on the x-axis is superstable, with multiplier $S = 0$, and J reduces to a circle. The second case corresponds to c-values of fold and flip bifurcations (cf. Sec. 6.4) for which boundary ∂D_- has a numerable set of points where the tangent can be defined, elsewhere ∂D_- having no tangent.

For $\gamma = 0$, on the c-axis of the parameter plane, a situation equivalent to that of Tc_{2^0} takes place for each transcritical curve Tc_{2^i}, related to the period 2^i cycle with multipliers $S_1 = -S_2 = 1$, and with its points ordinate $y = 0$. That is, it results that each point $c_{2^{i-1}}$ on $\gamma = 0$ is also a meeting of the bifurcation curves: transcritical $Tc_{2^{i-1}}$, flip $f_{2^{i-1}}$, Neimark N_{2^i}, and C_{2^i}. The points c_{2^j}, $j = 0, 1, 2, \ldots$, form the Myrberg *spectrum* ω_1 (Sec. 2) with $c_{2^\infty} = c_{1s} \simeq 1.401155189$.

Then the curves $Tc_{2^{i-1}}$, $f_{2^{i-1}}$, N_{2^i}, C_{2^i} and also the fold one F_{2^i}, tangent to $f_{2^{i-1}}$ and Tc_{2^i}, are reproduced by the ω_1 period doubling in the parameter plane (c, γ). We have the same property for all the spectra ω_k^n, $k = 3, 4, \ldots$, $n = 1, 2, 3, \ldots$, which are organized according the fractal box-within-a-box bifurcation structure. Equivalently it is possible to define a transcritical curve $Tc_{k2^i}^n$, flip $f_{k2^i}^n$, Neimark $N_{k2^i}^n$, and $C_{k2^i}^n$, intersecting at flip points $c_{k2^i}^n$ of the spectrum ω_k^n, and a fold one $F_{k2^i}^n$. This means that these curves form spectra organized according to the box-within-a-box structure in the parameter plane $(c; \gamma)$. From these considerations the following proposition can be formulated:

Proposition. *Consider the flip points* $c_{k2^{i-1}}^n$, $k = 1, 3, 4, \ldots$ (*for* $k = 1$ $c_{k2^{i-1}}^n = c_{2^{i-1}}$), $n = 1, 2, 3, \ldots, N_\lambda(k)$, $i = 2, 3, \ldots$, *related to the cycles* (k, n) *of the Myrberg's map* $x' = x^2 - c$ (*restriction of the map* $\overline{T}$ *to the* x*-axis*), $c_{k2^{i-1}}^n$ *belonging to the spectrum* ω_k^n (*cascade of period doubling bifurcations*). *On the* $\gamma = 0$ *axis of the parameter plane* (c, γ) *each point* $c = c_{k2^{i-1}}^n$ *is a meeting of five bifurcation curves*: *the two transcritical* $Tc_{k2^{i-1}}^n$ *and* $Tc_{k2^i}^n$, *the flip* $f_{k2^{i-1}}^n$, *the Neimark* $N_{k2^i}^n$, *and* $C_{k2^i}^n$ *related to a saddle-saddle bifurcation. For* $i = 0, 1, 2, \ldots$, *all these curves, and the fold ones* $F_{k2^i}^n$, *constitute a spectrum* Ξ_k^n *in the* (c, γ) *plane. The set of all the spectra* Ξ_k^n, $k = 1, 3, 4, \ldots$, *are organized according to the fractal box-within-a-box structure defined in Sec. 2 of Part I.*

This proposition is illustrated in Fig. 9, with $k = 3$, $n = 1$, $c_{3.2^0}^1 = 7/4$, $c_{3.2^1}^1 \simeq 1.786853$ which is the flip bifurcation $\lambda = \lambda_{3b1}^1$ of the Myrberg's map. It can be compared with Figs. 3–5 and 9 noticing the reproduction of the same bifurcation curves organization. The Fig. 5 configuration recurs with the basic cycle $(3; 1)$ for the whole spectrum Ξ_3^1, as for all the Ξ_k^j spectra with $(k; j)$ as basic cycle.

(d) Consider a fixed c value of the interval $-1/4 = c_{(1)0} = c_{2^0} < c < c_1^* = 2$, $(c; \gamma \geq 0) \in \Xi_k^j$. The number of cycles of $\overline{T}$ inside the half plane $y < 0$ increases (thus are created) as γ decreases, because we know (as remarked above in (a)) that for $\gamma = 0$ all the possible cycles in the region $(y \leq 0)$ have been created, and they are conjugated to those of the (complex) quadratic map T_Z in (1). Such cycles can be also identified by the symbolism $(k; j)$, defined in Part I, Sec. 2.1, the index j being defined from the permutation of the abscissae of the cycle points (the validity of this symbolism is discussed below in Sec. 6.1). This also means that starting from $\gamma = 0$, with increasing γ values and a given value of c, it is possible to follow the cycles $(k; j)$ evolution until they disappear by a fold or flip bifurcation. For $c \to c_1^* = 2$ the spectra are such that $\Xi_k^j \to (\gamma = 0)$. When $c = c_1^*$ no cycle with $y < 0$ is created for $\gamma > 0$ in the region $(y \leq 0)$, the only cycles are those of the set $J = (E') = [-2; 2]$.

The numerical study of the bifurcations, leading to the results presented below, shows two different bifurcation sequences, obtained with a fixed value of the parameter c and with γ decreasing values, $1 > \gamma \geq 0$.

(i) For the first sequence, inside an interval $-1/4 < c < c_l$, the arcs of fold and flip bifurcation curves of the $(c; \gamma)$ parameter plane are met in the same order as the $(k; j)$ cycles of the Myrberg's map with increasing λ values. These arcs do not intersect and are organized according to the box-within-a-box bifurcations structure represented by Fig. 1 of Part I.

(ii) For the second sequence, $c > c_l$, arcs of fold F_k^j or flip bifurcation curves, associated with various $k \neq 2^i$ and j, intersect (see Figs. 18 and 19). This situation generates a disruption of the Myrberg cycles order: it is as if the bifurcation parameter γ axis has underwent a fold (see below Figs. 20–22). The Myrberg order is respected but following a folded axis.

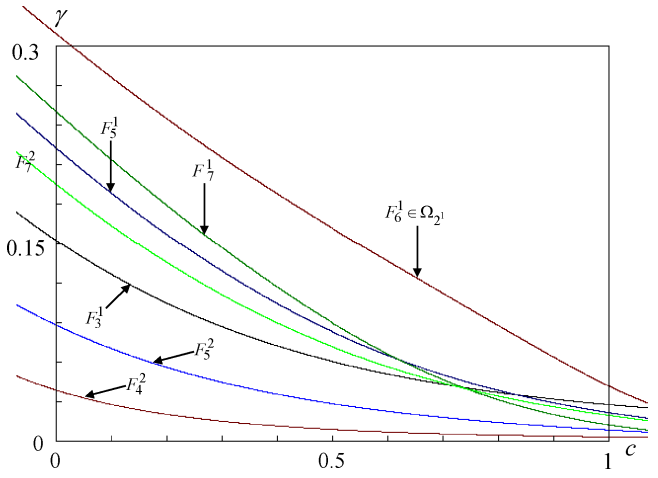

Fig. 18. Arcs of fold F_k^j, associated with various $k \neq 2^i$ and j, $k = 3, \ldots, 7$. After intersection of these bifurcation curves a disruption of the Myrberg cycles order occurs.

4.5. *General view: half plane $y < 0$ properties for $c_{2^0} < c \leq c_{1s}$*

Let D be the basin of the attractor A (fixed point, or cycle) located either in the half plane $y < 0$ or on $y = 0$, ∂D its boundary, $D_- = D \cap (y < 0)$ the part inside the half plane $(y < 0)$, ∂D_- its boundary, and $-1/4 = c_{(1)0} = c_{2^0} < c \leq c_{1s} = 1.401, \ldots$. We note that other attractors may exist in the half plane $(y > 0)$. The basin D_- may be connected (simply connected or multiply connected) or disconnected, in which case it is made up by an immediate basin D_0 and all its preimages of any rank. Outside D_- other singularities may exist (unstable cycles and their stable and unstable sets). The following

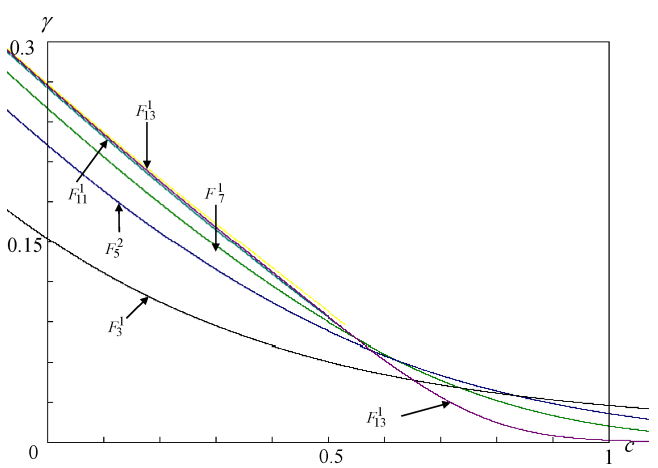

Fig. 19. Arcs of fold F_k^j, associated with various $k \neq 2^i$ and j, $k = 3, \ldots, 7$. The arcs $k = 11$ and 13 are added. After intersection of these bifurcation curves, a disruption of the Myrberg cycles order occurs.

situations can be identified.

(a1) A and thus D_- does not exist: no cycle belongs to the half plane $y < 0$.

(a2) A and thus D_- does not exist: but the half plane $y < 0$ contains period 2^i unstable cycles.

(b1) $A \in (y = 0)$ is the stable node fixed point P^*, D_- and ∂D_- are simply connected, (regions R_2^1, and $R_3^1 \cap I_1^1$, of Fig. 4 for which the fixed point P^* is the unique attractor of $\overline{T}$).

(b2) $A \in (y = 0)$ is the fixed point P^*, D_- is connected but not simply, ∂D_- is nonconnected, due to the existence of internal holes (cf. Fig. 15), or D_- is nonconnected (cf. Fig. 13).

(b3) $A \in (y = 0)$ is the fixed point P^*, D_- is simply connected, and the boundary ∂D_∞ of the domain of divergence (basin of an attractor on the Poincaré 's equator) contains a period two cycles pair: an unstable node (or focus) and a saddle with its stable manifold (cf. Sec. 5.3, Fig. 10).

(b4) $A \in (y = 0)$ is a stable period 2^i node, $i = 1, 2, \ldots$, D_- is nonconnected, ∂D_- is connected, due to a tangential contact with $y = 0$ at points of period 2^{i-1} unstable nodes, $i = 1, 2, \ldots$, and their increasing rank preimages (see below Fig. 36, $c = 1.08$; $\gamma = 0.17$).

(b5) $A \in (y = 0)$ is a stable period 2^i cycle, $i = 1, 2, \ldots$, D_- is nonconnected, due to a tangential contact of ∂D_{0-} (boundary of its immediate basin) with $y = 0$ at points of a period 2^{i-1} unstable node $(y = 0)$, $i = 1, 2, \ldots$, and its increasing rank preimages, and also to the creation of a strange repeller SR inside the half plane $y < 0$ out of the closure $\overline{D}_{0-}$ of D_{0-}. A strange repeller is created before the islands birth (see Figs. 20–22).

(b5) $A \in (y = 0)$ is a stable period 2^i node, $i = 1, 2, \ldots$, D_- and ∂D_- are nonconnected, due to a tangential contact of ∂D_- with $y = 0$ at points of period 2^{i-1} unstable nodes, $i = 1, 2, \ldots$, and their increasing rank preimages, and due to the creation of islands having as limit set a strange repeller SR (cf. below Fig. 51, where q_{21} and q_{22} are the two points of the period 2^1 cycle).

(c1) $A \in (y < 0)$, a period 2^i cycle, or a period 2^i attracting set (invariant closed curve, or chaotic attractor), $i = 1, 2, \ldots$, is the unique attractor of the half plane $y < 0$ (no attractor on $y = 0$, in particular $y(R^*) > 0$, i.e. $H_+ > 0$) $D(A) \subset (y < 0)$, $(y = 0) \cap \partial D(A) = \varnothing$. Each

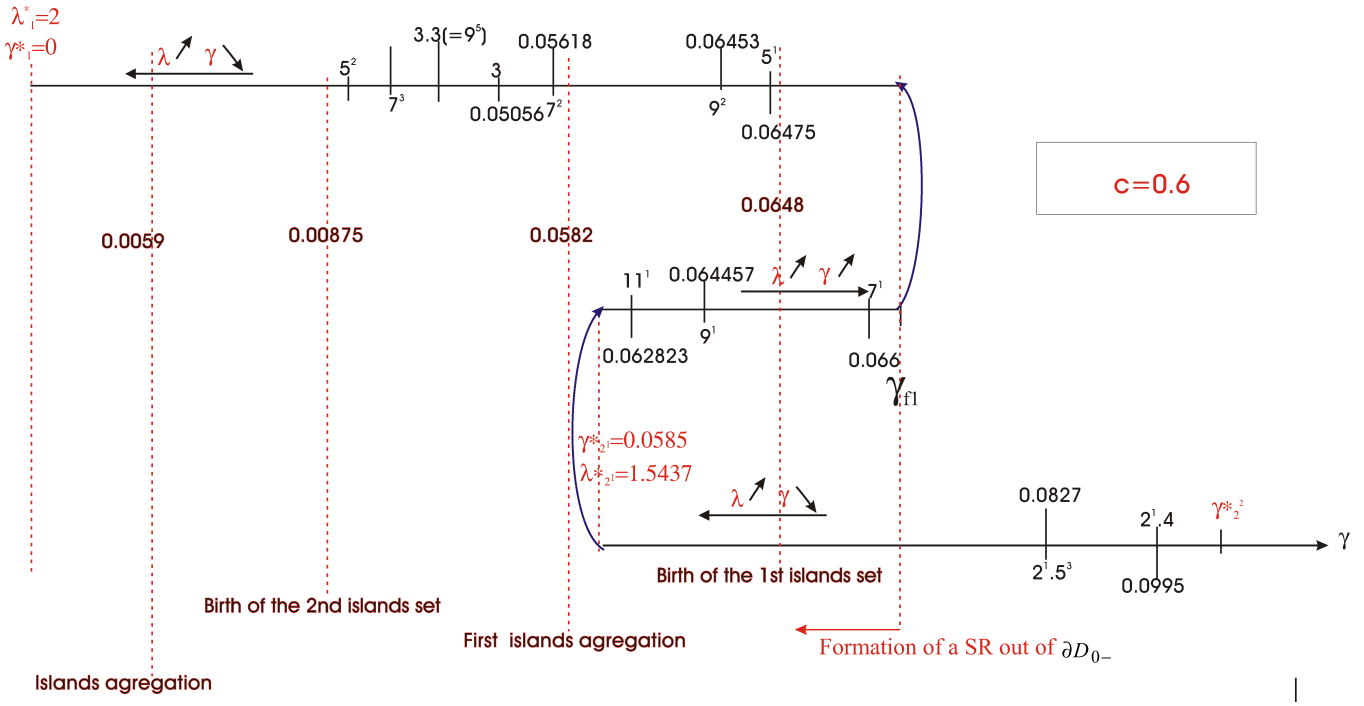

Fig. 20. $c = 0.6$. Disruption of the Myrberg cycles order: it is as if the bifurcation parameter γ axis has underwent a fold. In this figure λ is the parameter of the Myrberg's map $x' = x^2 - \lambda$, directly related to γ. A cycle $(k; j)$ (resp. $(2^i \cdot k; 1, j)$) is here denoted k^j (resp. $2^i k^j$). It is associated (below, or above the symbol) with a γ-value for which it is stable. Parameter γ^* and λ^* are defined in Sec. 2 of Part I. They correspond to the merging of a rank-r, $r > 2$, critical point with a point of an unstable period k, $k = 1, 3, \ldots$, or unstable period $2^i \cdot k$ cycle.

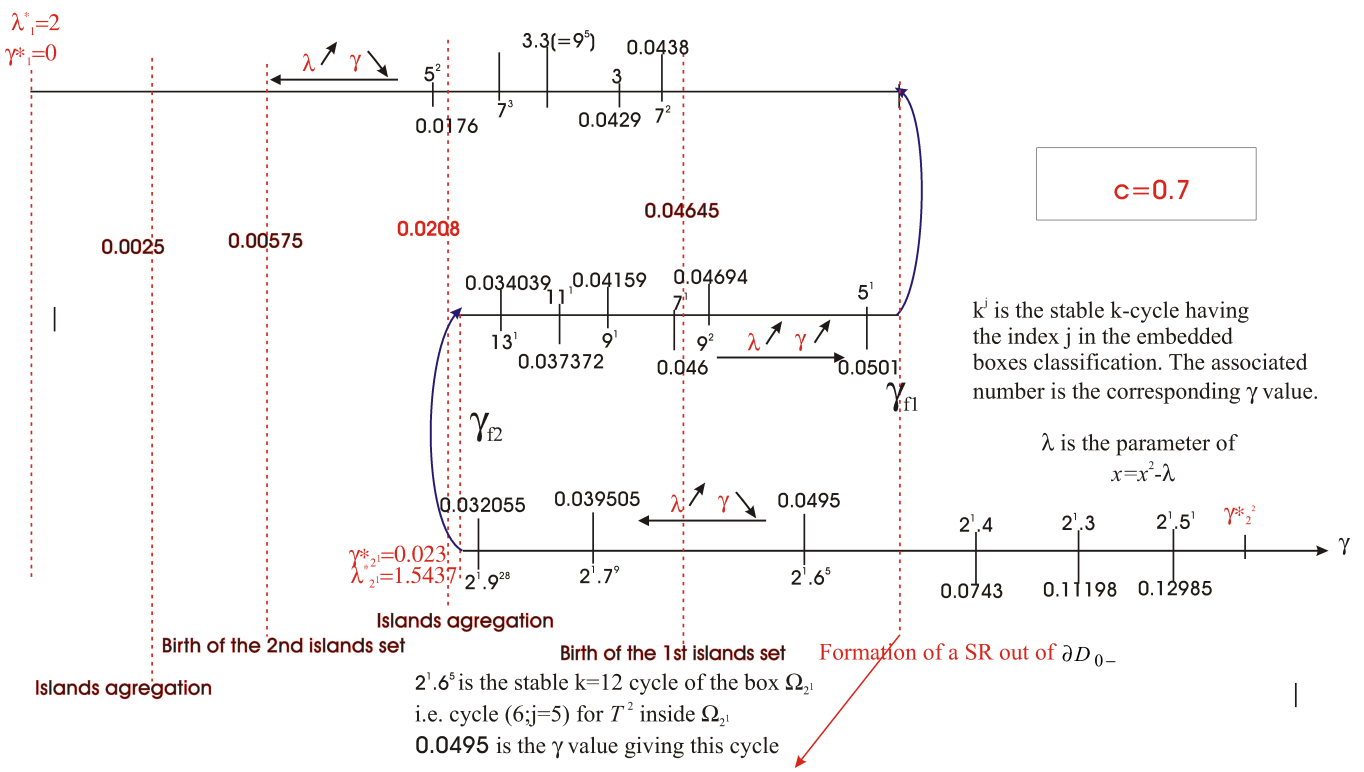

Fig. 21. $c = 0.7$. Disruption of the Myrberg cycles order. The symbols are defined as in Fig. 20.

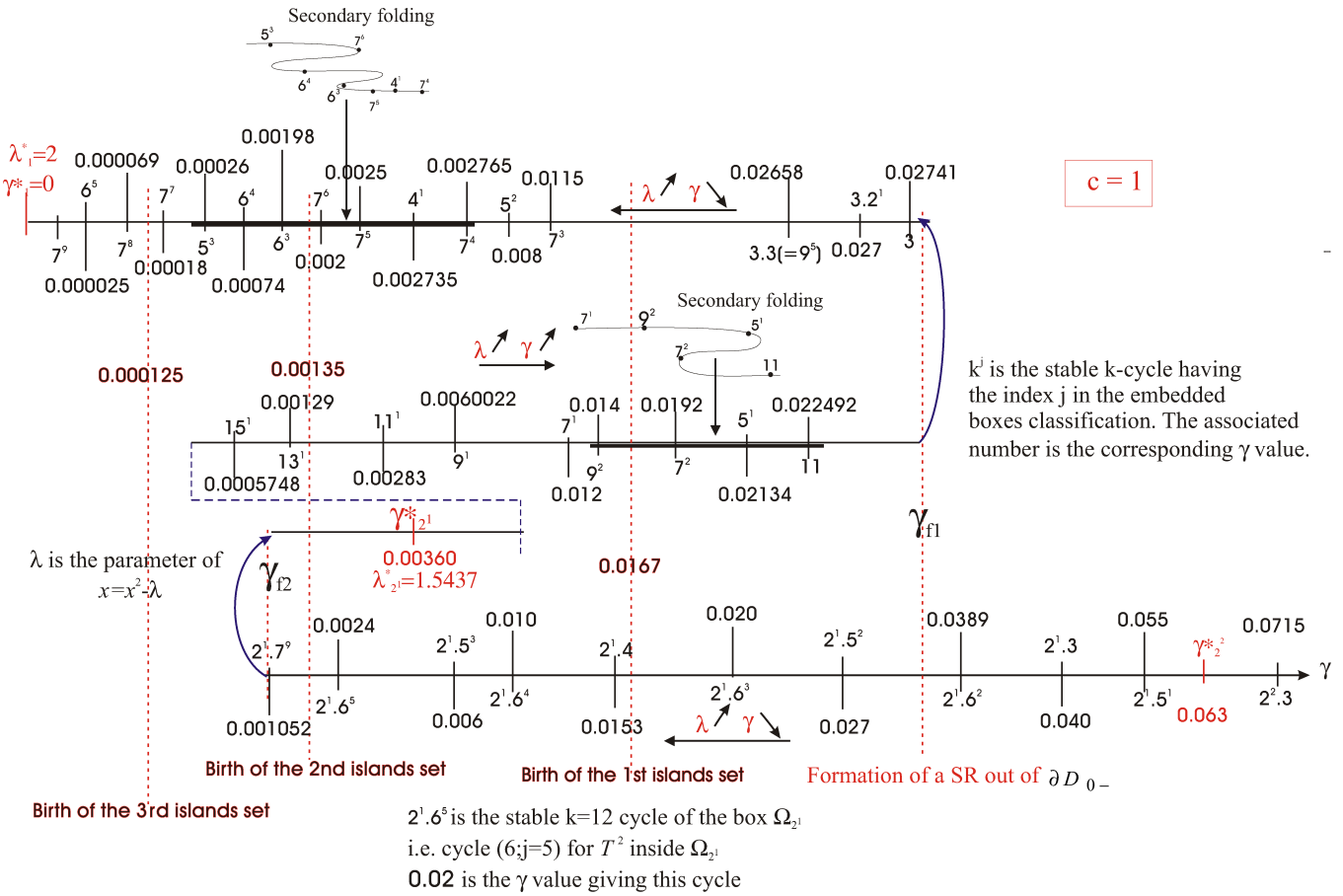

Fig. 22. $c = 1$. The number of disruptions of the Myrberg cycles order has increased. The symbols are defined as in Fig. 20.

of the 2^i cycle points (fixed points of the map $\overline{T}^{2^i}$), or each of the period 2^i attracting set, have a basin boundary without any common arc with the basin boundary of the other cycle points [cf. case of Fig. 17(a)]. A coexists with a period 2^i saddle located on $\partial D(A)$.

(c2) $A \in (y < 0)$, a period 2^i cycle, or a period 2^i attracting set (invariant closed curve, or chaotic attractor), $i = 1, 2, \ldots$, is the unique attractor of the half plane $y < 0$, $D(A) \subset (y < 0)$, $(y = 0) \cap \partial D(A) = \varnothing$, but a stable period 2^{i-1} cycle A_{cy} exists on $y = 0$, with a basin $D(A_{cy})$ intersecting the half plane $(y < 0)$, $D(A_{cy}) \cap (y < 0) = D(A_{cy})_-$. Figure 23 ($c = 0.557$, $\gamma = 0.359$) illustrates this situation: $D_-(P^*)$ exists, and $y(R^*) \in \partial D_-(P^*)$ is such that $y(R^*) < 0$, i.e. $H_+ < 0$.

(c3) $A \in (y < 0)$ is a period 2^i cycle, $i = 1, 2, \ldots$, D_- is nonconnected, but ∂D_- is connected from unstable period 2^{i-1} node cycles located on $y = 0$, $(y = 0) \cap \partial D \neq \varnothing$ [Fig. 17(c)].

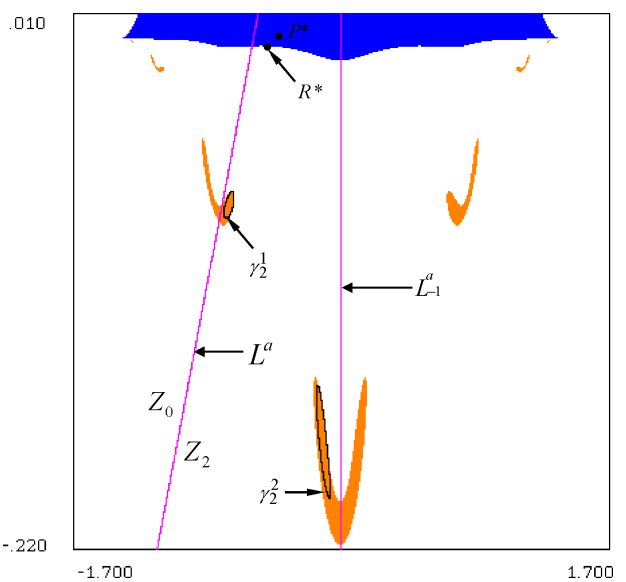

Fig. 23. $c = 0.557$, $\gamma = 0.359$. A stable period 2^1 invariant closed curve γ_2^r, $r = 1, 2$, is the unique attractor of the half plane $y < 0$. It coexists with the stable fixed point P^* (period 2^0), its basin $D(P^*)$ intersecting the half plane $(y < 0)$, with $y(R^*) \in \partial D_-(P^*)$, $y(R^*) < 0$.

5. Bifurcations Analysis for $c =$ Constant. Case of Period 2^n Cycles

This section is devoted to analyze the bifurcation situations occurring in the interval J^1 defined in Fig. 5 with $i = 1$, for a constant value of c and decreasing values of γ, $\gamma(f_{1s}) < \gamma < 1$, $f_{1s} = \lim f_{2^n}$ when $n \to \infty$. These bifurcations are essentially those of the unstable period 2^n cycles, $n = 0, 1, 2, \ldots$, either located on the basin boundary arc ∂D_- (i.e. belonging to $(y < 0)$), or those of $(y < 0)$ belonging to the disconnected part of the boundary $\partial D_{-\infty}$ of the divergence domain (basin of an attractor on the Poincaré equator), which progressively are integrated to ∂D_- when γ decreases. The limitation to period 2^n cycles means that γ is here limited to values not too small, for the restriction T_r of the map (2) to ∂D_-. The interval J^1 (in Fig. 4 with $i = 1$) is the union of intervals I_p^1, $p = 1, \ldots, 5$, each of them being related to a well defined bifurcations sequence.

5.1. *Interval* I_1^1

This interval is defined by $c(E^0) < c < c(M^0)$, E^0 $(c = 0, \gamma = 1)$, M^0 $(c \simeq 0.2049, \gamma \simeq 0.5482)$ (Fig. 4 with $i = 1$). Above Tc_{2^0} $(H_+ > 0$, i.e. $y(R^*) > 0)$ and with γ close to 1, R^* is stable with a basin without any part inside the region $(y \leq 0)$. The half plane $(y < 0)$ contains no singularities (situation (a1) of Sec. 4.5). With decreasing γ values, limited to the ω_1 spectrum, from a point below Tc_{2^0} $(H_+ < 0$, i.e. $y(R^*) < 0)$, P^* $(y = 0)$ is the unique attractor, and we have the situation (b1) of Sec. 4.5. Then the restriction T_r of the map (2) to $\partial D_-(P^*)$ (the basin boundary of P^*) generates from the saddle $R^* \in \partial D_-(P^*)$ the classical bifurcations of the Myrbeg's ω_1 spectrum [Agliari *et al.*, 2004].

A similar behavior occurs in the interval I_0^1 defined by $-1/4 < c < 0 = c(E^0)$ [see Fig. 3(a)]. When γ is close to 1, S^* belongs to $(y < 0)$ and is stable with a basin inside $(y < 0)$ and R^* is a saddle on this basin boundary. With decreasing values of γ, on the bifurcation curve Tc_{2^0} the fixed points S^* and P^* merge (on $y = 0$), and after P^* becomes stable while the saddle S^* enters the region $y > 0$ [see Fig. 3(a)]. From now on, as γ decreases, the properties are the same as those occurring in the interval I_1^1. This will appear below in Figs. 43(a)–43(d).

5.2. *Interval* I_2^1

The interval I_2^1 is defined by $c(M^0) \simeq 0.2049 < c < c(N^1)$, $N^1 = (c \simeq 0.4799, \gamma \simeq 0.39557)$ (Figs. 4 and 5 for $i = 1$). We remind that N^1 is the tangential contact point of the fold arc F_{2^i} with the arc N_{2^1} of Neimark bifurcation ($S_{1,2} = e^{\pm j\varphi}$, $j^2 = -1$, at N^1 $\varphi = 0$, i.e. $S_1 = S_2 = 1$). Above Tc_{2^0} and below F_{2^0} $(\gamma = 1)$ one has the case (a1) of Sec. 4.5. Below Tc_{2^0} and above the fold curve F_{2^1} the behavior is the same as in I_1^1 (case b1): the saddle R^* is the unique singularity belonging to the half plane $(y < 0)$. After crossing through F_{2^1} the map generates two new singularities: a period two saddle (sheet Sa_{2^i} in Fig. 8) and a period two unstable node inside $(y < 0)$.

For example let $c = 0.47$ be the fixed value for the parameter c, and consider decreasing values of γ. The corresponding γ value on the fold curve F_{2^1} is $\gamma_{b1} \simeq 0.3996821$. From this bifurcation, the period two saddle S_2^i, $i = 1, 2$, and the period two unstable node (turning after into an unstable period two focus F_2^i) appear out of D_- and out of ∂D_-. They belong to the disconnected part of the boundary $\partial D_{-\infty}$ of the divergence domain (basin of an attractor on the Poincaré equator), which gives the case (b3) in Sec. 4.5. Figure 10 $(\gamma \simeq 0,3881)$ has shown this situation with the unstable (resp. stable) manifolds $W^u(S_2^i)$ (resp. $W^s(S_2^i)$) of the saddle S_2^i, and the unstable (resp. stable) manifolds $W^u(R^*)$ (resp. $W^s(R^*)$) of the saddle fixed point R^*, $W^s(S_2^i) \subset \partial D_{-\infty}$. Here $T_2^{-1}(F_2^1) \in Z_0$ is the determination of the F_2^1 inverse different from F_2^1, $T_1^{-1}(F_2^1) \equiv F_2^1 \in Z_2$.

Section 4.3 *global bifurcation of "saddle-saddle" type*, $W^u(S_2^i) \equiv W^s(R^*)$, occurs for $\gamma_{b2} \simeq 0,388062942$ (Fig. 11), from which $W^s(S_2^i)$, $W^s(R^*)$, and F_2^i belongs to ∂D_- with a "mushroom" shape when $\gamma_{b3} < \gamma < \gamma_{b2}$ (cf. Fig. 12, $\gamma = 0.388$), γ_{b3} being defined below. So when $\gamma < \gamma_{b2}$ we are still in the situation (b1) in Sec. 4.5. For decreasing values of γ, the "mushroom" swells (Fig. 24, $\gamma = 0.35$) and disappears. The unstable period two focus F_2^i, $i = 1, 2$, turns into an unstable node N_2^i which merges with the saddle fixed point R^* (becoming an unstable node) when the parameter point $(c = 0.47; \gamma = \gamma_{b3})$ belongs to the flip curve f_{2^0}. For $\gamma \leq \gamma_{b3}$ the boundary ∂D_- contains the unstable node R^* and the period two saddle S_2^i, $i = 1, 2$. When γ decreases, this period two point undergoes the classical cascade of bifurcations by period

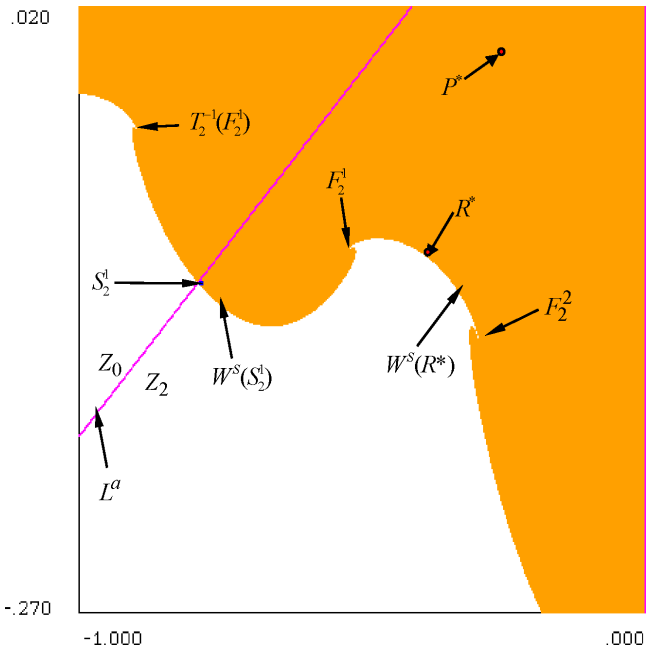

Fig. 24. $c = 0.47$, $\gamma = 0.35$. From the Fig. 12 situation ($\gamma = 0.388$), with decreasing values of γ the "mushroom" shape swells and disappears after.

doubling, belonging to the spectrum ω_1 in the Myrberg's map.

The restriction of the map $\overline{T}$ to ∂D_- generates the singular points (cycles and cyclical chaotic arcs) of the box-within-a-box bifurcation structure (Part I, Sec. 2.2), $\gamma = 0$ corresponding to λ_1^*.

5.3. *Interval* I_3^1

The interval I_3^1 is defined by $c(N^1) \simeq 0.4799 < c < c(A^1)$, $A^1 = (c \simeq 0.5662,\ \gamma \simeq 0.35988)$ (Figs. 4 and 5 for $i = 1$). Now the crossing through the fold curve F_{2^1} with decreasing values of γ gives rise to the generation of a period two saddle (sheet Sa_{2^i} in Fig. 8) and a *period two stable node*. This occurs with $y(R^*) < 0$, i.e. $H_+ < 0$, and P^* as a stable node on $y = 0$, with a basin $D(P^*)$ intersecting the half plane $(y \leq 0)$, $D(P^*) \cap (y \leq 0) = D(P^*)_-$. Due to the very narrow closeness of the curves N_{2^1}, $\overline{N}_{2^i}$ and F_{2^1} the node quickly turns into a period two stable focus F_2^i, $j = 1, 2$, which becomes unstable generating a period two stable invariant close curve (γ_2^i). The basins $D(F_2^1)$ of F_2^1 (resp. $D(\gamma_2^1)$ of (γ_2^i)), $D(F_2^2)$ of F_2^2 (resp. $D(\gamma_2^2)$ of γ_2^2), and D_- are without any connection, and without common boundary (situation c2 in Sec. 4.5, and Fig. 23). After a contact of (γ_2^i) with $\partial D_0(\gamma_2^j)$ $(\gamma = \gamma(\overline{N}_{2^i}))$ the boundary of the immediate basin $D_0(\gamma_2^j)$, γ_2^j is destroyed, letting the pair period two saddle-unstable focus in the situation of Sec. 5.2, i.e. for decreasing values of γ the sequence of bifurcations is the same.

5.4. *Interval* I_4^1

In this interval, defined by $c(A^1) < c < c_{2^1} = 3/4$ (i.e. c_{b1}), the fold curve F_{2^1} is now above the transcritical curve Tc_{2^0}, $\gamma(F_{2^1}) > \gamma(Tc_{2^0})$. This means that $y(R^*) > 0$, if γ is not too small [Fig. 3(b)]. For $\gamma > \gamma(F_{2^1})$ the fixed point R^* is stable, and the half plane $(y < 0)$ is void of singularities. Crossing through the fold curve F_{2^1} (Figs. 4 and 5 for $i = 1$) with decreasing values of γ, the map gives rise to the generation of a period two saddle (sheet Sa_{2^i} in Fig. 8) and a *period two stable node*, as for the interval I_3^1. The node turns into a period two stable focus F_2^l, $l = 1, 2$, which generates a period two attracting closed invariant curve (γ_2^i), when it becomes unstable. The situation when F_2^l is stable corresponds to the case in Fig. 17(a). It is shown in Fig. 25 ($c = 0.6$, $\gamma = 0.3473$), where the red region corresponds to the basin of the point R^*, the blue one to the F_2^l basin. For $c(A^1) < c < c_a < c_{2^1}$, $c_a \simeq 0.65$, $\gamma(\overline{N}_{2^i}) \simeq 0.284527$ [cf. Fig. 3(b)] the map behaves as in the interval I_3^1, i.e. the bifurcation arc $\overline{N}_{2^i}$ corresponds to the contact of (γ_2^i) with the boundary of its immediate basin $\partial D_0(\gamma_2^i)$, which leads to the destruction of (γ_2^i) for $\gamma < \gamma(\overline{N}_{2^i})$. For $c_a < c$ the behavior is different, due to the fact that

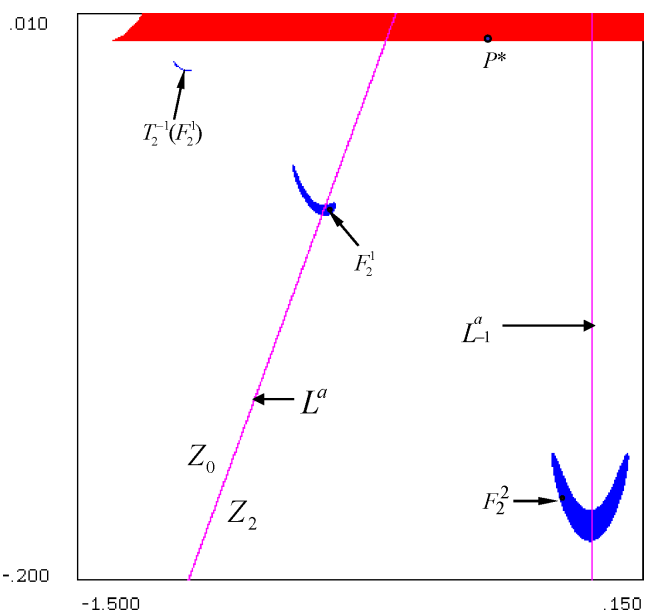

Fig. 25. $c = 0.6$, $\gamma = 0.3473$. The period two focus F_2^r, $r = 1, 2$, is stable and corresponds to the Fig. 17(a) situation. The red region corresponds to the basin of the stable fixed point R^*, $y(R^*) > 0$, the blue one to the F_2^r basin.

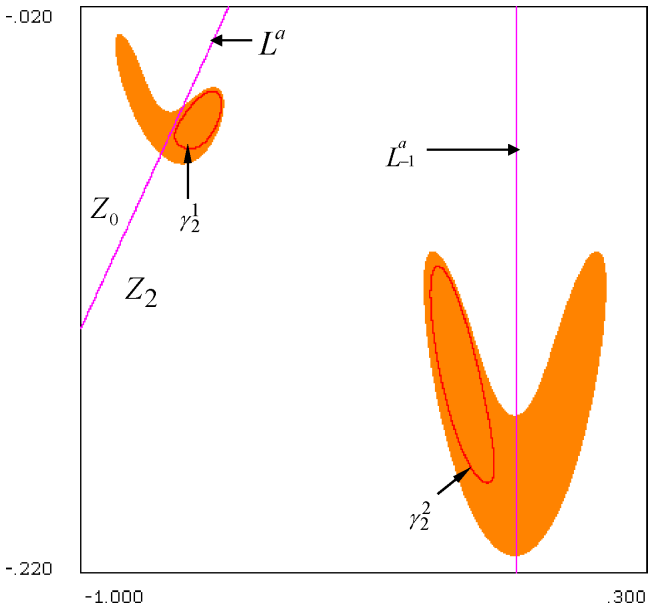

Fig. 26. $c = 0.6$, $\gamma = 0.335$. The period two focus F_2^l is now unstable, and has generated the period two stable invariant closed curve γ_2^l.

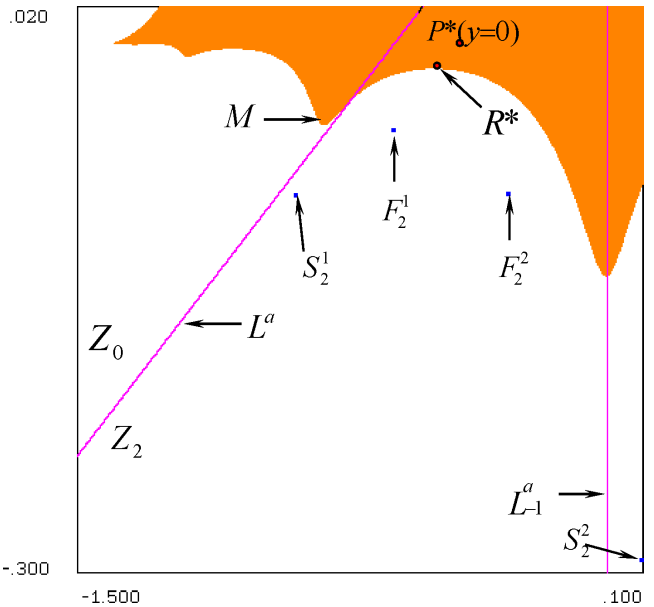

Fig. 27. $c = 0.6$, $\gamma = 0.26$. After crossing through the transcritical curve Tc_{2^0}, the fixed point R^* has turned into a saddle with $y(R^*) < 0$. P^* is now a stable node, and its basin $D(P^*)$ has a part $D_-(P^*)$ inside the half plane $(y < 0)$, coexisting with the pair period two saddle-unstable focus, located out of the closure $\overline{D_-(P^*)}$ of $D_-(P^*)$.

(γ_2^i) turns into a period two chaotic attractor after a bifurcations sequence (Chap. 6 in [Mira *et al.*, 1996a]), as this will be shown below.

The first subinterval $c(A^1) < c < c_a$, with γ decreasing values, is illustrated for $c = 0.6 < c_a$. When the period two focus F_2^l becomes unstable it generates the period two stable invariant closed curve γ_2^l (Fig. 26, $c = 0.6$, $\gamma = 0.335$). The immediate basins $D_0(F_2^1)$ of F_2^1 (resp. $D_0(\gamma_2^1)$ of γ_2^1), $D_0(F_2^2)$ of F_2^2 (resp. $D_0(\gamma_2^2)$ of γ_2^2), and D_- are without any connection, and without common boundary (Figs. 25 and 26). The bifurcation curve $\overline{N}_{2^1}$ corresponds to a contact of γ_2^l with $\partial D_0(\gamma_2^l)$, the boundary of $D_0(\gamma_2^l)$. Below $\overline{N}_{2^1}$ γ_2^l is destroyed, letting the pair period two saddle and unstable focus as only singularities belonging to $(y < 0)$.

Crossing through the transcritical curve Tc_{2^0}, due to $y(R^*) < 0$, P^* becomes a stable node, and its basin $D(P^*)$ has a part $D_-(P^*)$ inside the half plane $(y < 0)$, coexisting with the pair period two saddle and unstable focus, located out of the closure $\overline{D_-(P^*)}$ of $D_-(P^*)$ (Fig. 27, $c = 0.6$, $\gamma = 0.26$). The value $\gamma \simeq 0.259749$ is a bifurcation with transition from $D_-(P^*)$ connected to $D_-(P^*)$ nonconnected by creation of an headland: $D_-(P^*)$ intersecting the critical arc L^a at three points near the point M in Fig. 27. This bifurcation gives rise to infinitely many islands, the limit set of which is the stable manifold $W^s(S_2^l)$ of the period two saddle S_2^l, $l = 1, 2$ (Fig. 13, $c = 0.6$, $\gamma = 0.25972$), with the unstable manifold $W^u(S_2^l)$ being out of $D_-(P^*)$, the boundary of which is defined by the manifold $W^s(R^*)$, of the saddle R^*.

The bifurcation of "*saddle-saddle*" *type* described in Sec. 4.3 occurs when $\gamma \simeq 0.259716125$, with $W^u(S_2^l) \equiv W^s(R^*)$, and $\partial D_-(P^*)$ having a nontransverse contact with L^a and L^a_{-1}. Crossing through this γ value with decreasing values leads to the *direct transition nonconnected basin to multiply connected basin* for $D_-(P^*)$ (Fig. 14). Figure 15 ($c = 0.6$, $\gamma = 0.2597$) has shown the situation immediately after the bifurcation with creation of a *bay* H_0, the rank-one lake being $H_1 = \overline{T}^{-1}(H_0)$, the infinitely many others being $\bigcup_{n>0} \overline{T}^{-n}(H_1)$ with $W^s(S_2^l)$ as limit set. When H_0 disappears $D_-(P^*)$ becomes simply connected (Fig. 28(a), $c = 0.6$, $\gamma = 0.25$). A new γ decrease leads to the Fig. 28(b) ($c = 0.6$, $\gamma = 0.2$) situation. The unstable period two focus F_2^l, $l = 1, 2$, turns into an unstable node N_2^l. This period two node merges with the saddle fixed point R^* which becomes an unstable node, when the parameter point $(c = 0.6; \gamma = \gamma_{b3})$ belongs to the flip curve f_{2^0} from the bifurcation (7). For $\gamma_{b4} < \gamma \leq \gamma_{b3}$ the boundary ∂D_- contains the unstable node R^* and the period two saddle S_2^l, $l = 1, 2$. When γ decreases, $\gamma(f_{1s}) < \gamma < \gamma_{b4}$, $f_{1s} = \lim f_{2^n}$ when $n \to \infty$, from S_2^l the flip

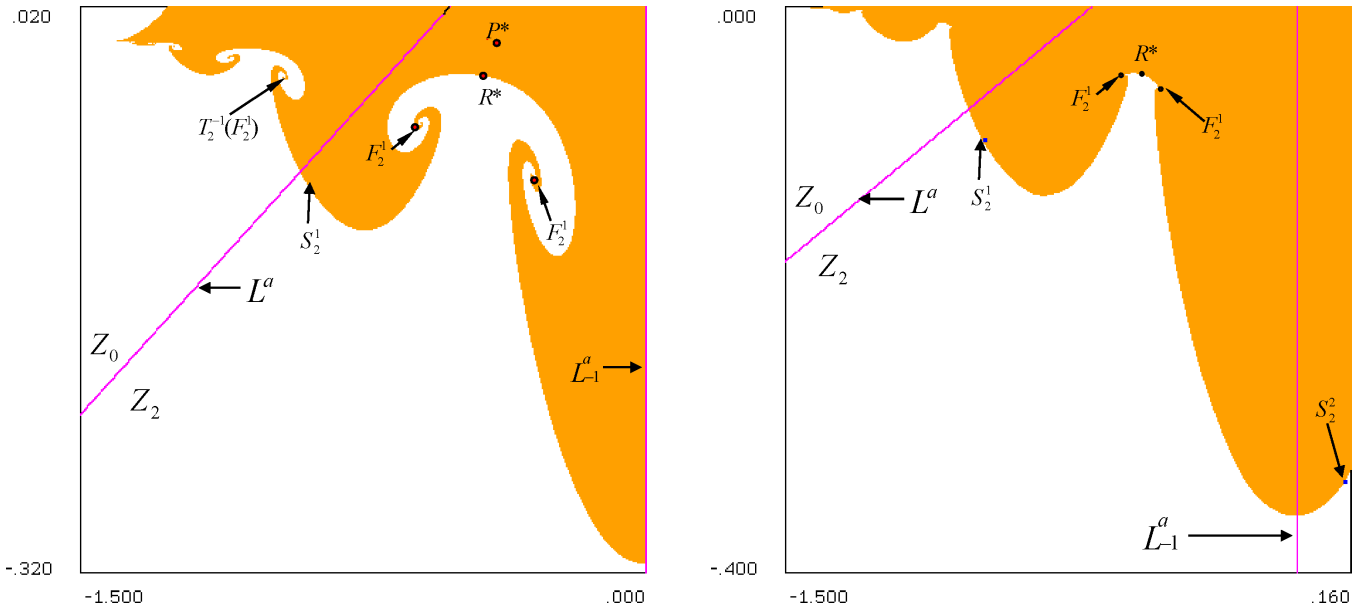

Fig. 28. (a) $c = 0.6$, $\gamma = 0.25$. The basin part $D_-(P^*)$ becomes simply connected. (b) $c = 0.6$, $\gamma = 0.2$. The unstable period two focus F_2^l, $l = 1, 2$, turns into an unstable node.

bifurcations of the Myrberg' spectrum ω_1 occur, by crossing through the curves f_{2^i} with bifurcations of the type given in (6). For $0 < \gamma < \gamma(f_{1s})$ Secs. 5.7 and 6 will show that the restriction of the map $\overline{T}$ to ∂D_- generates the singular points (cycles and cyclical chaotic arcs) of the box-within-a-box bifurcation structure (Part I, Sec. 2), but with a folding of the γ-axis (Figs. 20–22), $\gamma = 0$ corresponding to λ_1^*.

The interval I_4^1 differs from I_3^1 by the fact that for $c > c_a$ the bifurcation arc $\overline{N}_{2^i}$ is no longer a contact of a period two attracting closed curve (γ_2^l) with $\partial D_0(\gamma_2^l)$. Indeed for $c > c_a$ and decreasing values of γ, now the period two closed invariant curve γ_2^l undergoes a series of bifurcations, described in Chapter 6 of [Mira *et al.*, 1996a], which leads to a period two chaotic area (d_l), $l = 1, 2$, (Fig. 29, $c = 0.7$, $\gamma = 0.1937$). For a parameter point $(c; \gamma)$ belonging to $\overline{N}_{2^i}$ the (d_l) boundary $\partial(d_l)$, made up of arcs of critical curves (cf. [Mira *et al.*, 1996a, pp. 273–276, 392–399]), has a contact with the immediate basin boundary $\partial D_0(d_l)$. When $\gamma < \gamma(\overline{N}_{2^i})$ (d_l) is destroyed. Moreover, with γ decreasing, from the period two saddle S_2^i, $i = 1, 2$, a sequence of bifurcations by period doubling occurs (the ones of the ω_1 spectrum). After the rth bifurcation a period 2^{r+1} saddle $S_{2^{r+1}}^i$ coexists with a set of period 2^h unstable nodes, $h = 2, 3, \ldots, r$, located on the stable manifold $W^s(S_{2^{r+1}}^i)$, an extremity of which is the unstable period two focus F_2^i. This manifold and SR_2^i belongs to the boundary of the divergence domain inside Π_- $(y < 0)$. So for $c = 0.7$, $\gamma = 0.1937$, $r = 1$, the saddle has period four. New γ decreasing values give rise to the bifurcations related to the interval $]\lambda_{1S}; \lambda_{2^1}]$ (see Fig. 1 of Part I), and to a period $2^m k$ saddle $S_{2^m k}^i$ with its

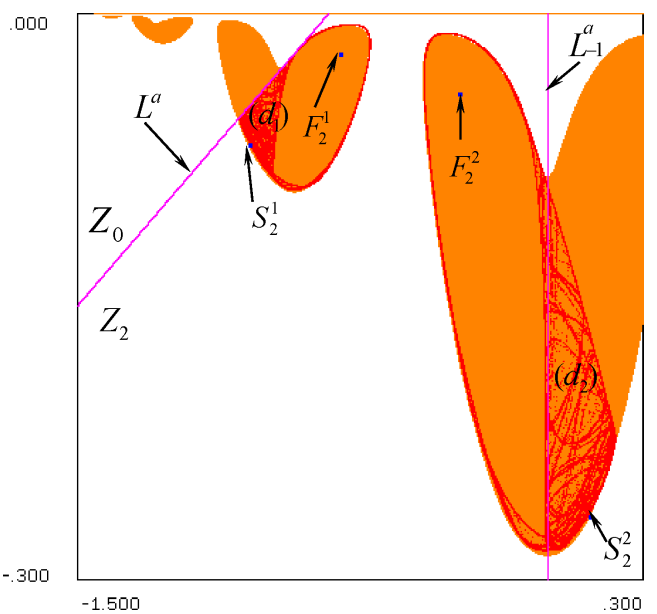

Fig. 29. $c = 0.7$, $\gamma = 0.1937$. The period two closed invariant curve γ_2^l (Sec. 3.3) undergoes a series of bifurcations, which leads to a period two chaotic area (d_l), $l = 1, 2$.

stable manifold an extremity of which is the unstable period two focus F_2^i. After crossing through Tc_{2^0} ($y(R^*) < 0$) a subset D_- of the basin of the stable fixed point P^* exists inside the half plane ($y \leq 0$). Then the *global bifurcation of* "saddle-saddle" *type* (Sec. 4.3) occurs, $W^u(S^i_{2^m k}) \equiv W^s(R^*)$, from which $W^s(S^i_{2^m k})$, $W^s(R^*)$, and F_2^i belongs to ∂D_- which has either a simply connected "mushroom" shape, or associated with islands, or lakes, as for I_3^1. Figure 30 ($c = 0.7$, $\gamma = 0.0978$) shows the "mushroom" case with lakes, with a period $2^m k$ saddle (born in the $[\lambda_{2^1}; \lambda_{1_S}[$ interval) difficult to be exactly defined, but the existence of which is confirmed by the presence of a period $6, 8, 10, 12$ unstable nodes on the numerically obtained stable manifold $W^s(S^i_{2^m k})$ of Fig. 30. For decreasing values of γ the "mushroom" swells and disappears. The unstable period two focus F_2^i, $i = 1, 2$, turns into an unstable node N_2^i which merges with the saddle fixed point R^* (becoming an unstable node) when the parameter point belongs to the flip curve f_{2^0}.

Generally, a chaotic area contains infinitely many unstable cycles with increasing period (cycle before contained in (d_l)), and their limit sets when the period tends toward infinity. So when $\gamma < \gamma(\overline{N}_{2^1})$ (d_l) being destroyed, it might give rise for $\gamma < \gamma(\overline{N}_{2^i})$ to a period two strange repeller SR_2^l (Chapter 5 of [Mira *et al.*, 1996a]) made up of these unstable cycles, and their limit sets. Nevertheless not any of these cycles, which might be generated in the interval $\omega_1 \cup]\lambda_{1_S}; \lambda_{2^1}]$ (Fig. 1 of Part I), was numerically found. The fact that the cycles of $\omega_1 \cup]\lambda_{1_S}; \lambda_{2^1}]$ are found on the manifold $W^s(S^i_{2^m k})$ leads to conjecture that the cycles of SR_2^l disappear by inverse bifurcations before creation of the cycles on $W^s(S^i_{2^m k})$ having the same period.

As indicated in Fig. 21, when γ decreases a strange repeller SR is created out of ∂D_-, for $\gamma < \gamma_{f_1}$, followed by D_- becoming nonconnected by generation of islands.

5.5. *Interval* I_5^1

With decreasing values of γ, and $\gamma(C_{2^1}) < \gamma < \gamma(F_{2^1})$, the behavior is the same as in the interval I_4^1, cf. Figs. 31 ($c = 0.78$; $\gamma = 0.285$) and 32 ($c = 0.8$; $\gamma = 0.285$), that is, we are in the situation of Fig. 17(a). For $\gamma(Tc_{2^1}) < \gamma < \gamma(C_{2^1})$ we have the situation of Fig. 17(c) (Fig. 33, $c = 0.8$; $\gamma = 0.239$). For $\gamma < \gamma(Tc_{2^1})$, sufficiently close to Tc_{2^1}, the period two cycle ($y = 0$) N^i, $i = 1, 2$, is stable. The basin situation is shown in Fig. 34 ($c = 0.8$; $\gamma = 0.1$) where $\overline{S}_2^n$ ($y > 0$), $n = 1, 2$, is the saddle of the branch $Sad2^i(y > 0)$ of Fig. 5(b).

5.6. *Interval* J^2

This interval corresponds to J^{i+1} in Fig. 4 with $i = 1$. It repeats the organization of the intervals I_n^1, $n = 1, \ldots, 5$, but with a period doubling of the cycles, as shown in the examples given below.

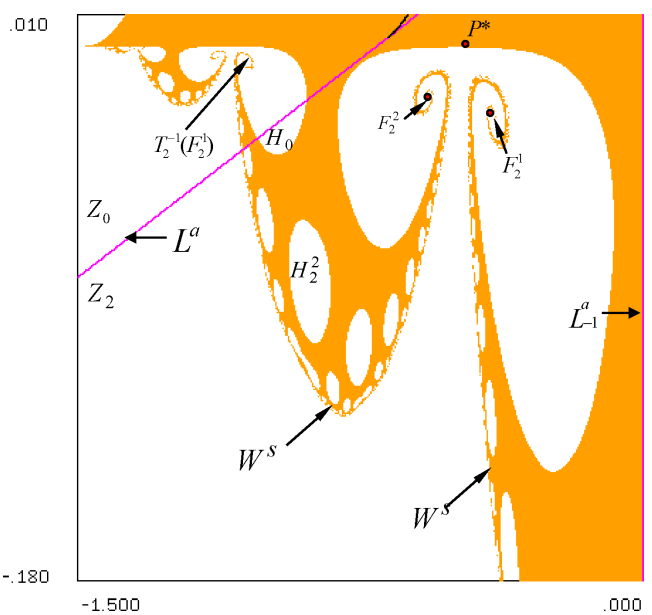

Fig. 30. $c = 0.7$, $\gamma = 0.0978$. "Mushroom" case with lakes, and a period $2^m k$ saddle on the stable manifold $W^s(S^i_{2^m k})$.

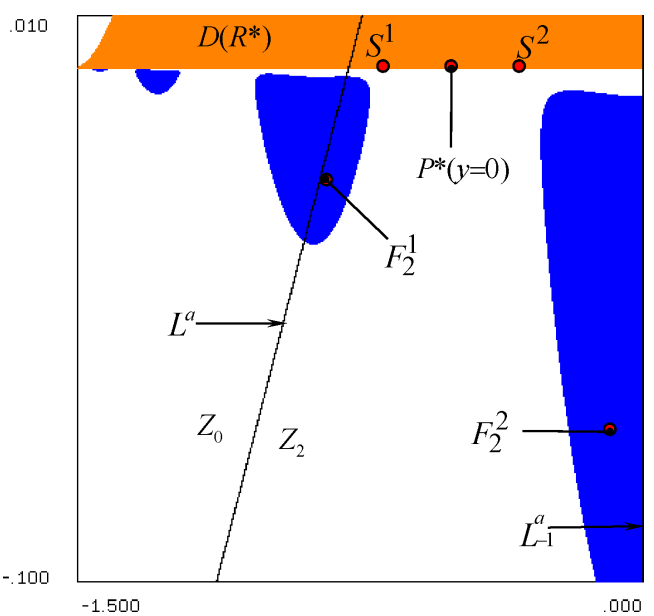

Fig. 31. $c = 0.78$; $\gamma = 0.285$. The behavior is the same as in the interval I_4^1.

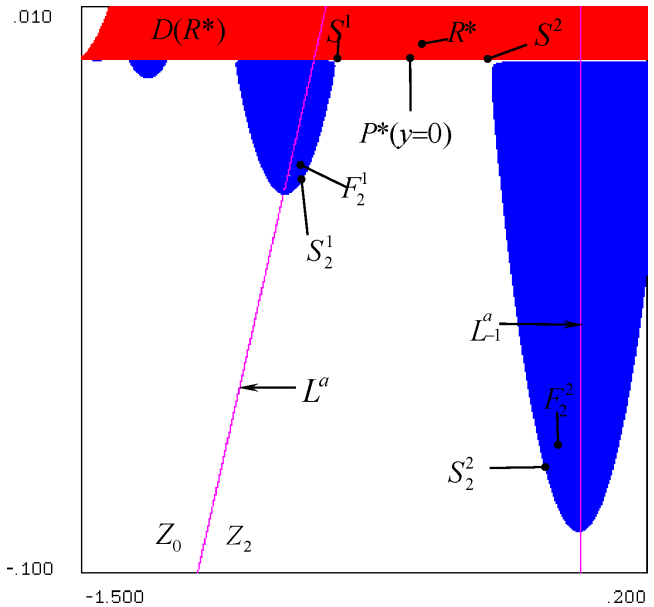

Fig. 32. $c = 0.8$; $\gamma = 0.285$. Figure 17(a) situation.

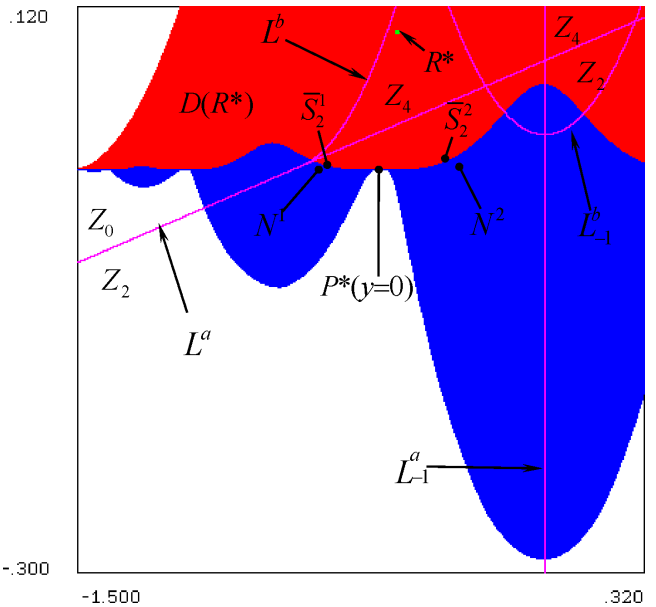

Fig. 34. $c = 0.8$; $\gamma = 0.1$ Basins situation. $\overline{S}_2^n$ $(y > 0)$, $n = 1, 2$, is the saddle of the branch $Sad2^i(y > 0)$ of Fig. 5(b).

Figure 35 ($c = 1.08$; $\gamma = 0.21$), $(c, \gamma) \in I_1^2 \cap R^1$ $(i = 2)$, gives the situation (a1) in Sec. 4.5. R^* is a stable fixed point in $(y > 0)$ with the blue colored basin. N^1 and N^2 is the period two stable node $(y > 0)$ in Figs. 5(a), 5(b) $\widehat{de}$ arc $(i = 1)$ its basin being red colored. $\overline{S}_2^1$ and $\overline{S}_2^2$ are the period two saddles $(y > 0)$ on Fig. 6(b) $\widehat{ce}$ arc.

Figure 36 ($c = 1.08$; $\gamma = 0.17 < \gamma(Tc_{2^1}) \simeq 0.186$), $(c, \gamma) \in I_1^2 \cap R_2^2$ $(i = 2)$, gives the Sec. 4.5 situation (b1). R^* $(y > 0)$ is a stable fixed point with the red colored basin. Having crossed through Tc_{2^1} now the period two stable node $N^1 \cup N^2$ belongs to the x-axis. This bifurcation and those of the period two saddle $(y > 0)$ $\overline{S}_2^1 \cup \overline{S}_2^2$, and the period two saddle $(y < 0)$ $\widetilde{S}_2^1 \cup \widetilde{S}_2^2$, are represented on the Fig. 5(b) $(i = 1)$ red segment cd $(y = 0)$, the blue arc ce $(y > 0)$, and the blue arc bd $(y < 0)$, respectively.

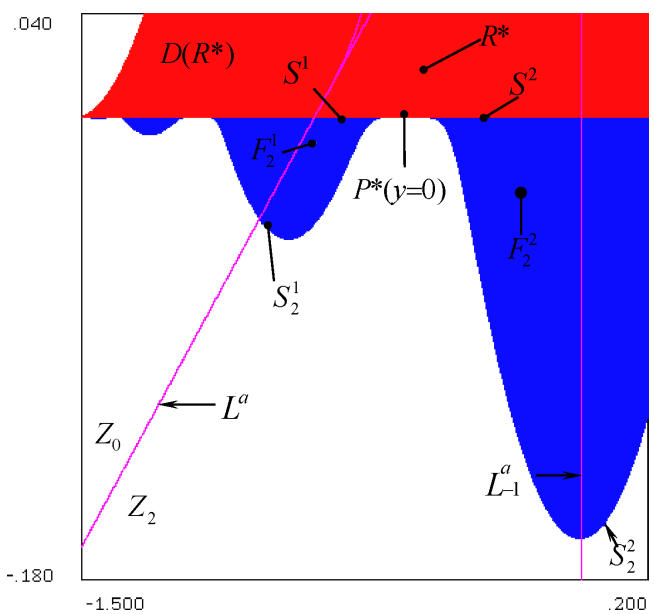

Fig. 33. $c = 0.8$; $\gamma = 0.239$. Figure 17(c) situation.

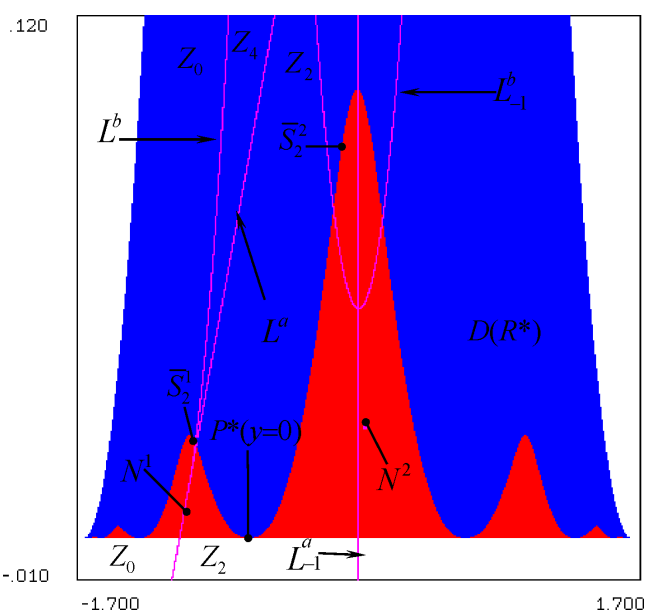

Fig. 35. $c = 1.08$; $\gamma = 0.21$. Situation (a1) of Sec. 4.5.

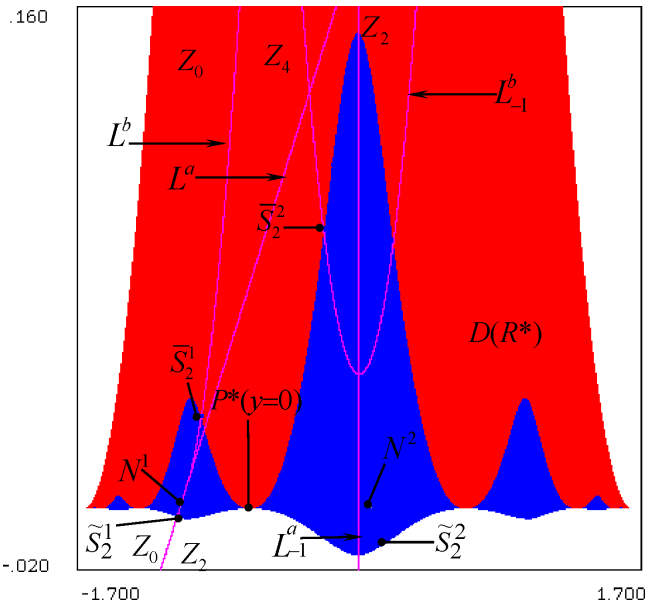

Fig. 36. $c = 1.08$; $\gamma = 0.17$. Situation (b4) of Sec. 4.5.

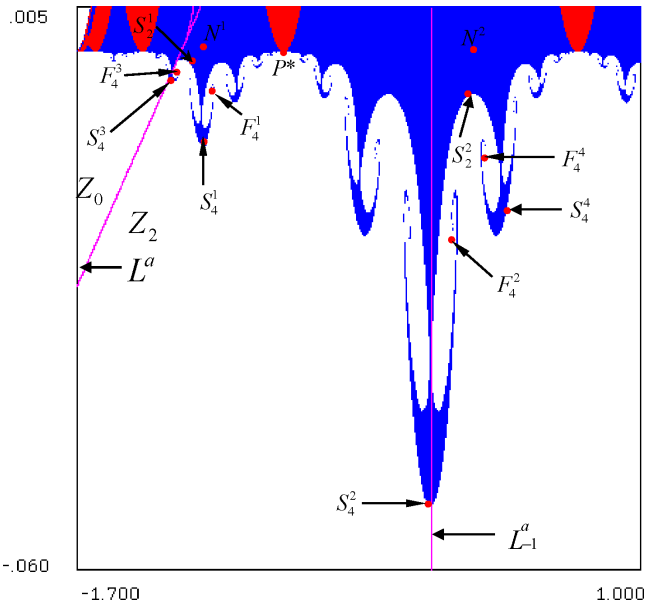

Fig. 37. $c = 1.2$; $\gamma = 0.0544$. "Mushrooms" shaped situation (b1) obtained with γ decreasing after the Figs. 13–16 case (creation of islands, lakes) but from period 2^2 saddle and unstable focus.

The value $c = 1.2$ belongs to the interval I^2_4, $\gamma(F_{2^1}) \simeq 0.20589$, $\gamma(F_{2^2}) \simeq 0.06473$, $\gamma(Tc_{2^1}) \simeq 0.0637$. So for $\gamma(F_{2^2}) < \gamma < 1$, the Sec. 4.5(a1) situation is obtained with a period two stable node ($y > 0$). For $\gamma(Tc_{2^1}) < \gamma < \gamma(F_{2^2})$ (region R^2_5), one has the Sec. 4.5(c1) situation, the attractor $A \in (y < 0)$ being a period 2^2 cycle, with a nonconnected immediate basin $D_{0-}(A)$. The region $I^2_4 \cap R^2_4$ ($\gamma < \gamma(Tc_{2^1})$) reproduces the R^1_4 behaviors with a cycles period doubling. Figure 37 ($c = 1.2$; $\gamma = 0.05442$) is the "mushrooms" shaped situation (b1) obtained with γ decreasing after the Figs. 13–16 case (creation of islands, lakes) but from period 2^2 saddle and unstable focus. Here the points S^1_2, S^2_2, $F^r_{2^2} \equiv F^r_4$, $S^r_{2^2} \equiv S^r_4$, $r = 1, \ldots, 4$, are respectively a period two saddle, an unstable period four focus, and a period four saddle with $y < 0$. The red region with $y > 0$ is the basin of the stable fixed point R^* ($y > 0$), the blue one is the basin of the period two stable node N^1 and N^2 ($y = 0$). With γ decreasing, Fig. 38 ($c = 1.2$; $\gamma = 0.024$) corresponds to the Fig. 37 evolution after $F^r_{2^2}$ changing into an unstable $N^r_{2^i} \equiv N^r_4$ node, followed by the flip bifurcation described in Eq. (7) with the merging of the node $N^r_{2^2}$ and saddle S^j_2 ($j = 1, 2$), giving rise to the unstable period two node N^j_2. The red region with $y > 0$ is the basin of the stable fixed point R^*, the blue one is the basin of the period two stable node N^1 and N^2 ($y = 0$). For this value $\gamma = 0.024$ the unstable period 2^i nodes $N^r_{2^i}$, $r = 1, 2, \ldots, 2^i$, of the ω_1 spectrum have been created, for $i = 1, 2$, and are located on the basin boundary $\partial D_-(N^1, N^2)$.

Figure 39 ($c = 1.25$, $\gamma = 0.048$) corresponds to the Sec. 4.5 situation (c1), $(c, \gamma) \in (I^2_4 \cap R^2_5)$. Here the points S^1_2, S^2_2, $F^r_{2^i} \equiv F^r_4$, respectively belong to period two saddle [$y = 0$, cf. Fig. 17(a)], and a stable period four focus ($y < 0$) with a nonconnected immediate basin $D_0(F^r_4)$. The blue region

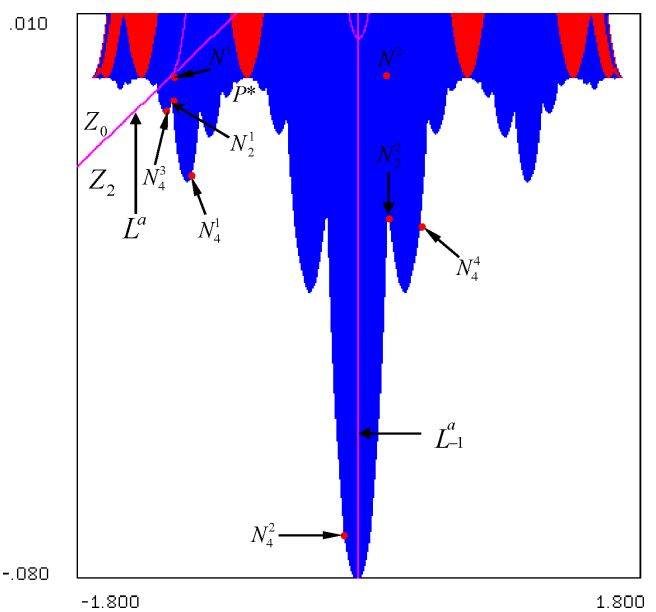

Fig. 38. $c = 1.2$; $\gamma = 0.024$. With γ decreasing Fig. 37 evolution after $F^r_{2^2}$ changing into an unstable $N^r_{2^i} \equiv N^r_4$ node, followed by the flip bifurcation described in Eq. (7).

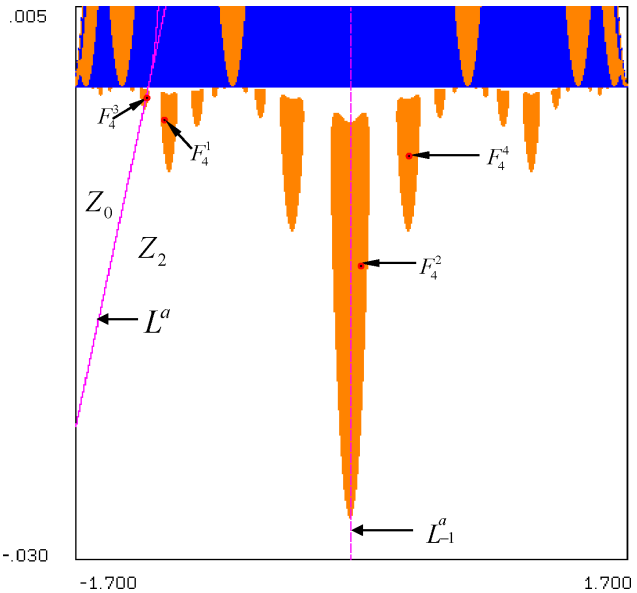

Fig. 39. $c = 1.25$, $\gamma = 0.048$. Situation (c1) of Sec. 4.5, with a stable period four focus ($y < 0$) having a nonconnected immediate basin $D_0(F_4^r)$. The blue region with $y > 0$ is the basin of the stable fixed point R^*, the brown one with $y > 0$ is the basin of the stable period two fixed point N^1 and N^2 ($y > 0$).

with $y > 0$ is the basin of the stable fixed point R^*, the brown one with $y > 0$ is the basin of the stable period two fixed points N^1 and N^2 ($y > 0$).

In the Fig. 40 ($c = 1.3$, $\gamma = 0.012 < \gamma(Tc_{2^2})$) case, $(c, \gamma) \in I_5^2 \cap R_7^2$, the blue basin is related to the

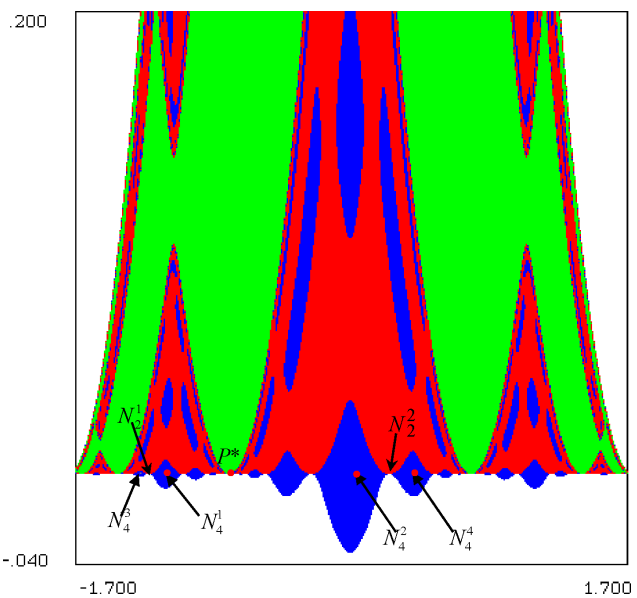

Fig. 40. $c = 1.3$, $\gamma = 0.012$. The blue basin is related to the stable period 2^2 cycle N_4^r, $r = 1, \ldots, 4$, located on $y = 0$ (red segment cd of Fig. 5(b) with $i = 3$). The red area is the basin of a stable period two cycle, the green one the basin of a period four cycle, located in $y > 0$.

stable period 2^2 cycle N_4^r, $r = 1, \ldots, 4$, located on $y = 0$ (red segment cd of Fig. 5(b) with $i = 3$). Its basin boundary contains a period 2^2 saddle ($y > 0$, blue arc ce of Fig. 5(b) with $i = 3$) and a period 2^2 saddle ($y < 0$, blue arc bd of Fig. 5(b) with $i = 3$). The red area is the basin of a stable period two cycle, the green the basin of a period four cycle, located in $y > 0$.

5.7. *Disruption of the ω_1 Myrberg's ordering*

Consider the parameter c with a fixed value, and with decreasing values, and the Myrberg's order of the spectrum ω_1, related to the period 2^n cycles belonging to the half plane ($y < 0$). The disruption of this order occurs as soon as $\gamma(f_{2^0}) < \gamma(f_{2^1})$, i.e. for $c \gtrsim 0.52259$, which takes place in the interval I_3^1 (Fig. 4). For example consider $c = 0.6$. As shown in Secs. 4.3 and 5.4, with decreasing values of γ, the pair of period two saddle and unstable focus cycles S_2^i, F_2^i, $i = 1, 2$, generated from the fold bifurcation curve F_{2^1}, belongs to the boundary of the immediate basin of P^* from $\gamma \simeq 0.259716125$, i.e. the *global bifurcation of "saddle-saddle" type*, $W^u(S_2^i) \equiv W^s(R^*)$, $i = 1, 2$, (Fig. 14). The saddle S_2^i undergoes the flip bifurcation represented by (6) with $i = 2$ (curve f_{2^1}) for $\gamma \simeq 0.25209$. It turns into an unstable period two node UN_2^i and gives rise to a period four saddle S_4^r, $r = 1, \ldots, 4$. Moreover with γ decreasing values the focus F_2^i becomes an unstable node $UN_2'^i$ which merges with the saddle fixed point R^* for $\gamma(f_{2^0}) \simeq 0.1856$. For $\gamma < \gamma(f_{2^0})$ the basin boundary of P^* contains all these points and those resulting from the crossing through flip curves f_{2^i} via the bifurcations (6). Then for $c = 0.6$ with γ decreasing values, the ω_1 spectrum order is disrupted only for the first flip bifurcation in (6) ($i = 1$), and starting from the period 2^1 saddle S_2^i the Myrberg's order is respected. For intervals J^m, $m > 1$, (Fig. 4), we have an equivalent property but starting from the period 2^m saddle S_m^i, $m = 1, \ldots, 2^m$.

6. Other Properties for Decreasing Values of γ

6.1. *General presentation*

First let us remark that in the half plane $y < 0$ the attractor (when it exists) is unique, but in $y \leq 0$ two attractors may exist, one on the x-axis, the other with a nonconnected basin belonging to $y < 0$ as

shown in Fig. 23. The bifurcations study in Secs. 4 and 5 have shown that this last situation disappears when γ becomes sufficiently small. So this section considers the case of a unique attractor in $y \leq 0$, then located either on $y = 0$, or in $y < 0$. It is particularly devoted to the bifurcations of unstable period k cycles, $k \neq 2^n$, $n = 1, 2, \ldots$, belonging to the half plane ($y < 0$), and so not to the x-axis (the case of period 2^n cycles has been seen in the previous sections). Such cycles are not generated from the ω_1 spectrum. When $\gamma = 0$, this attractor is located on $y = 0$, and considering the semi-conjugacy property related to (2), it is the one having a Julia set as basin boundary (cf. Sec. 3 of Part I).

Remind that the symbolism $k = 2^n$ concerns cycles generated from the ω_1 spectrum. So it is about to consider the cycles generated from the box Δ_1 and to see how the Myrberg's order (cf. Sec. 2.2 and Fig. 1 of Part I) can be perturbed, $\gamma = 0$ corresponding to λ_1^*. A cycle $k \neq 2^n$ is characterized by the Sec. 2 symbolism $(k; j)$, the index j being defined from the permutation of the abscissae of the cycle points. As long as the basin boundary part $\partial D_- \subset (y < 0)$ is simply connected, and each abscissa x is associated with only one point of ∂D_-(*single-valued situation*) it appears that the cycles bifurcations are those of the map restricted to ∂D_- having the box-within-a-box structure for an interval equivalent to $\lambda_{(1)_0} < \lambda < \lambda_c \in \Delta_1$ (Fig. 1 of Part I). If there are x-intervals, each one associated with more than one arc of ∂D_- (multivalued situation), at first view it would seem that the choice of j based on the permutation of the abscissae of the cycle points cannot work. Nevertheless it was observed that all the period k cycles abscissae (some of them until the period 18), having helped to identify the ∂D_- properties, satisfy the necessary and sufficient condition for a permutation of k integers be the one of a cycle generated by an unimodal map (cf. [Mira, 1987], pp. 136–138). So in spite of the multivalued situation, it is as if the permutation of the k points on ∂D_- remains the one of a cycle of a unimodal map, then represented by the symbolism $(k; j)$ defined in Part I. We conjecture this property for all the ∂D_- cyles, j being based on the permutation of the abscissae of the cycle points, which implies a particular location of the cycles points with respect to the "multivalued" arcs of ∂D_-.

Consider the total basin $D_-(A)$, A being the attractor belonging to the half plane $y \leq 0$, ∂D_- its boundary. As we have seen, it is possible that repelling cycles exist out of ∂D_-, these cycles belong to the boundary $\partial D_{-\infty}$ of the diverging orbits domain.

Let $\overline{T}_r$ be the map restricted to ∂D_-. When γ decreases, c having a constant value, $-1/4 < c < c_{1s}$ (c belonging to the ω_1 spectrum), the repelling $(k; j)$ cycles, $k \neq 2^n$, appear outside ∂D_- with the Myrberg's order if $-1/4 < c < c_p$, and with a disruption of this order if $c > c_p$, when repelling cycles exist outside ∂D_-. Estimating the c_p value is not an easy task. It is only possible to say that this order is disrupted as soon as the fold curves F_k^j related to $(k; j)$ cycles intersect, but the first intersections occurs for cycles with a period $k \to \infty$. Our conjecture is that a *very rough* estimation of the beginning of folds intersection is $0.4 < c_p < 0.5$.

When $c_p < c < c_{1s}$ ($c_{1s} = \lim c_{2^n}$ when $n \to \infty$) the Myrberg's order is disrupted in the sense that unstable (repelling) $(k; j)$ cycles appear before their natural place, and so coexist with "regular" cycles with respect to this order. It is as if one has a folding of the γ axis, with overlapping of several γ intervals. This situation is represented by Figs. 20 ($c = 0.6$), 21 ($c = 0.7$), 22 ($c = 1$), where the γ fold bifurcation $F_k^{j'}$ of a $(k; j')$ cycle is denoted $k^{j'}$ in the nonembedded representation, and $(2^m k; j')$ in the embedded representation of boxes Ω_{2^m}. These bifurcations are associated with their numerical approximations, and also with bifurcations $\gamma_{2^i}^*$ related to the $c_{2^i}^*$ ones (cf. Sec. 2 of Part I). The first irregularity in the order occurs for $\gamma = \gamma_{f1}$, giving rise to unstable "irregular" cycles. Via the several numerical experiences made for this study, the following important property appears.

Property. *When the "irregular" repelling cycles appear, they are located out of ∂D_-, and they belong to the boundary $\partial D_{-\infty}$ of the domain of diverging orbits. With γ decreasing, infinitely many such sets of unstable cycles are created from $\gamma = \gamma_{f1} - \varepsilon$, $\varepsilon > 0$, $\varepsilon \to 0$, which gives rise to a strange repeller $SR \subset (y < 0)$ out of $D_- \cup \partial D_-$. As soon as an islands set is created, such a SR becomes its limit set, and so SR belongs now to $\partial D_-(SR \subset \partial D_-)$.*

The first set of irregular repelling cycles occurs when D_- is simply connected, before the creation of an islands set. Figure 41 ($c = 0.53$; $\gamma = 0.010974$) shows that the unstable $(k; j)$ cycle $k = 12$, $j = 40$, out of ∂D_{0-} as belonging to a strange repeller SR limit of islands (belonging to D_-) which are generated for $\gamma < \gamma_{f1}$. The same situation is obtained for

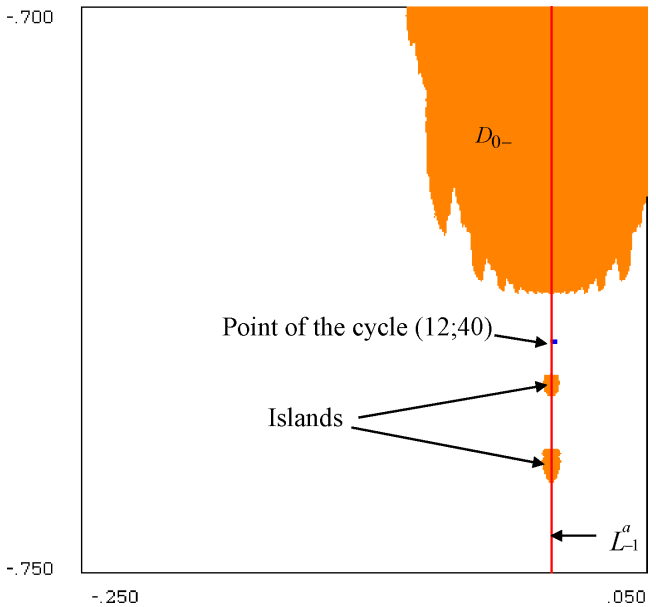

Fig. 41. $c = 0.53$; $\gamma = 0.010974$. The unstable $(k; j)$ cycle $k = 12$, $j = 40$, out of ∂D_{0-} as belonging to a strange repeller SR limit of a islands set.

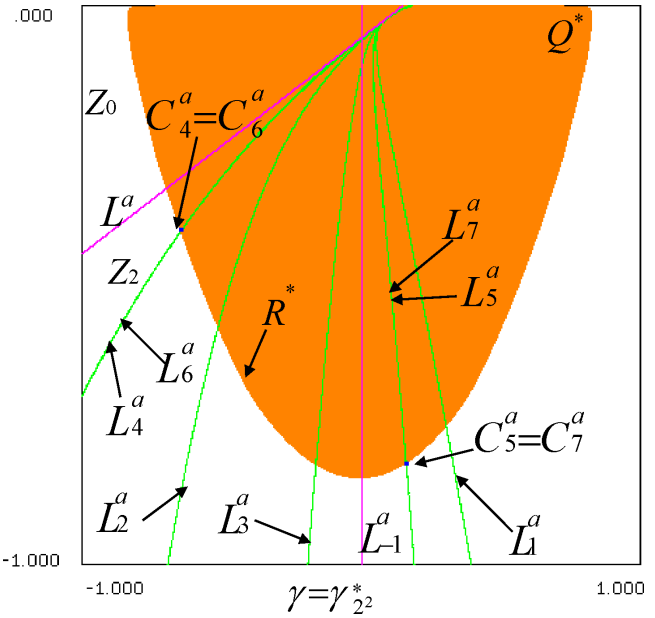

Fig. 42. $c = -0.15$; $\gamma = \gamma^*_{2^2} = 0.3865$. The rank n critical point C^a_{n-1} of $\overline{T}_r$, $n = 1, 2, 3, \ldots$, $C^a_0 \equiv C^a$, is given by $C^a_{n-1} = \partial D_- \cap L^a_{n-1}$, $L^a_{n-1} = \overline{T}L^a$ being the rank $n-1$ image of the critical arc L^a.

$c = 0.53$, $\gamma = 0.011064229$ with an unstable $(k; j)$ cycle $k = 11$, $j = 25$.

6.2. *Conservation of the Myrberg's order on ∂D_-*

For $-1/4 < c < c_p$, with γ decreasing values, and for period $k \neq 2^i$ cycles, the basin D_- and its boundary ∂D_- located in $(y < 0)$ are simply connected, with preservation of the Myrberg's order on its boundary ∂D_-. The map $\overline{T}_r$ restricted to ∂D_- can be considered as conjugate to the Myrberg's map. This situation is described in [Agliari *et al.*, 2004] for $c = -0.15$. Different situations are represented by Figs. 42 ($c = -0.15$; $\gamma = \gamma^*_{2^2} = 0.3865$), 43(a) ($c = -0.15$; $\gamma = 0.33$, $\gamma^*_{2^1} < \gamma < \gamma^*_{2^2}$), 43(b) ($c = -0.15$; $\gamma = 0.3242$, $\gamma = \gamma^*_{2^1}$), 43(c) ($c = -0.15$; $\gamma = 0.315$, $\gamma^*_1 = 0 < \gamma < \gamma^*_{2^1}$). In these figures the rank n critical point C^a_{n-1} of $\overline{T}_r$, $n = 1, 2, 3, \ldots$, $C^a_0 \equiv C^a$, is given by $C^a_{n-1} = \partial D_- \cap L^a_{n-1}$, $L^a_{n-1} = \overline{T}L^a$ being the rank $n-1$ image of the critical arc L^a. The saddle cycles $(k; j) \in \partial D_-$ of the two-dimensional map $\overline{T}$ in (2) are the stable cycles of the one-dimensional unimodal map $\overline{T}_r$.

6.3. *Disruption of the Myrberg's order in the Δ_1 interval*

We use the "compact" notation k^j to represent the fold bifurcation $\gamma^j_{(k)_0}$ (c being fixed) of the $(k; j)$ cycle as in Figs. 20–22. We note that their Myrberg's order (the one for $-1/4 < c < c_p$) is given by the inequalities:

$$\begin{aligned}
&\gamma_{1s} > \cdots > \gamma^*_{2^2} \cdots > 2^1 \cdot 5^1 > 2^1 \cdot 3 > 2^1 \cdot 5^2 \\
&> 2^1 \cdot 4 > 2^1 \cdot 5^3 > 2^1 \cdot 6^5 > 2^1 \cdot 7^9 > 2^1 \cdot 8^{16} \\
&> 2^1 \cdot 9^{28} \cdots > \gamma^*_{2^1} > \cdots > \cdots 17^1 > \cdots > 13^1 \\
&> \cdots > 11^1 > \cdots > 9^1 > \cdots > 7^1 > 9^2 > 5^1 \\
&> \cdots > .9^3 > 7^2 > 9^4 > \cdot 8^3 > \cdots > 3 \\
&> 3 \cdot 2^1 (= 6^2) > \cdots > 3 \cdot 3 (= 9^5) > \cdots 8^4 \cdots \\
&> 7^3 > 8^5 > \cdots > 5^2 > \cdots > 7^4 > \cdots > 6^3 \\
&> \cdots > 7^5 > \cdots > 4^2 > \cdots > 7^6 > \cdots 6^4 \\
&> \cdots > 7^7 > \cdots > 5^3 > \cdots > 7^8 \cdots > 6^5 \\
&> \cdots > 7^9 \cdot > \cdots > \cdots \gamma^*_1 \\
&= 0.
\end{aligned}$$

Figures 20 ($c = 0.6$), 21 ($c = 0.7$) and 22 ($c = 1$) use this notation, and show that the more c increases, the more the above Myrberg's order is disrupted, giving rise to overlapping of γ intervals defined by horizontal lines. The order is preserved (but with inversion of the sense of γ increase) on the horizontal lines with a jump for $\gamma = \gamma_{fn}$, $n = 1, 2, \ldots$. Consider the interval $c_p < c < c_{1s} \simeq 1.401$, and γ decreasing values from a value giving period $k \neq 2^i$ "regular" cycles belonging to ∂D_-, i.e. ∂D_- contains a *strange repeller*, say Ω, made up of all the repelling cycles on ∂D_{0-} their limit

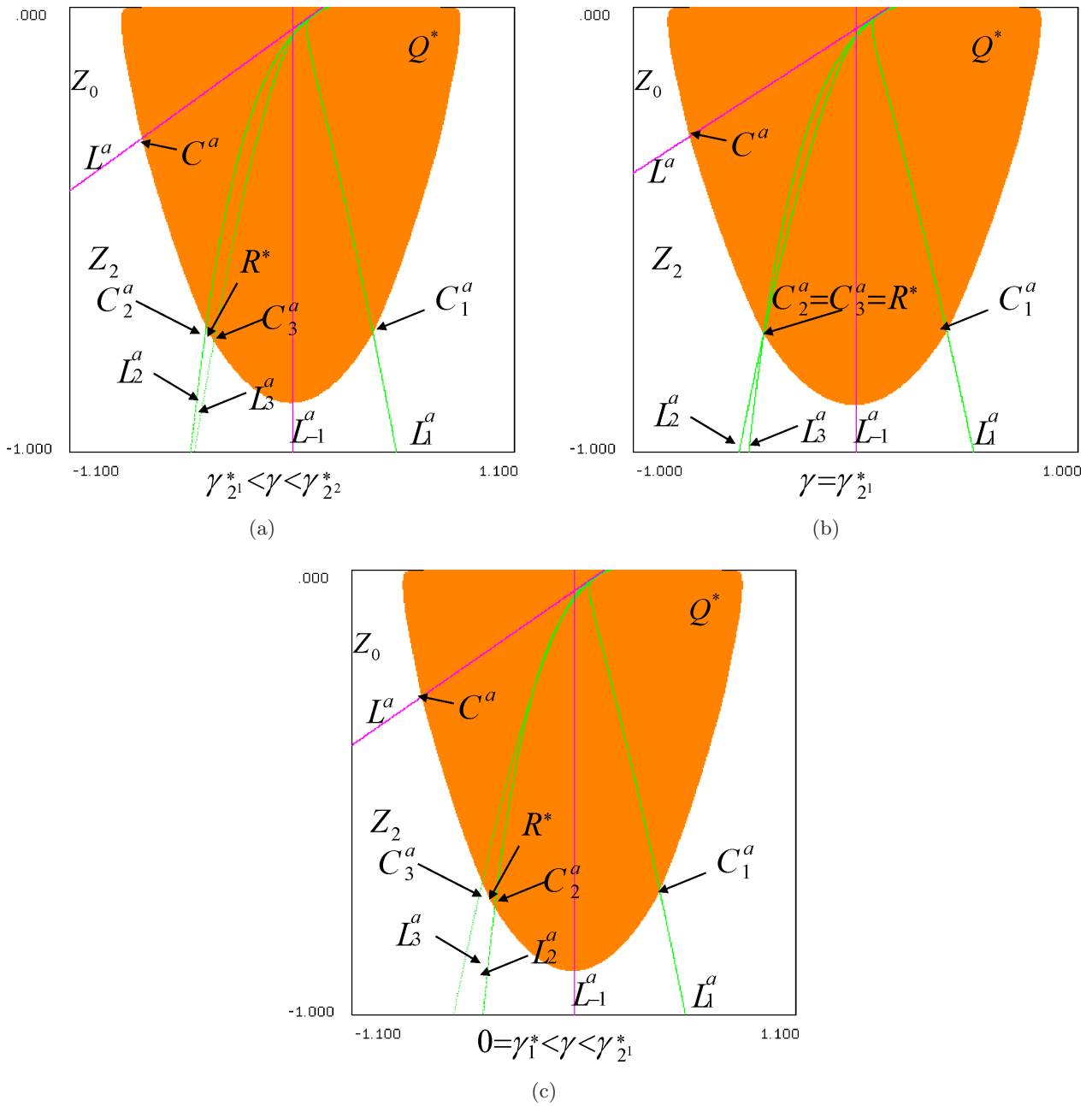

Fig. 43. (a) $c = -0.15$; $\gamma = 0.33$, $\gamma_{2^1}^* < \gamma < \gamma_{2^2}^*$. (b) $c = -0.15$; $\gamma = 0.3242$, $\gamma = \gamma_{2^1}^*$. (c) $c = -0.15$; $\gamma = 0.315$, $\gamma_1^* = 0 < \gamma < \gamma_{2^1}^*$. Here the rank n critical point C_{n-1}^a of $\overline{T}_r$, $n = 1, 2, 3, \ldots$, $C_0^a \equiv C^a$, is given by $C_{n-1}^a = \partial D_- \cap L_{n-1}^a$, $L_{n-1}^a = \overline{T} L^a$ being the rank $n-1$ image of the critical arc L^a.

set, all the increasing rank preimages of all these points. Then the map restricted to this boundary is chaotic. The basin D_- may be either simply connected, or nonconnected. From $\gamma = \gamma_{f1}$ "irregular" (unstable) cycles appear before their natural place in the Myrberg's order, i.e. such cycles, resulting from the first overlapping intervals of the γ axis, are external to D_- and ∂D_-, and give rise to a *strange repeller* SR_1 belonging to the boundary $\partial D_{\infty -}$ of the domain of diverging orbits. In other words from the first point of overlapping $\gamma = \gamma_{f1}$, with decreasing values of γ, the unstable cycles related to the lines above the lower horizontal line of Figs. 20–22 are located out of $D_- \cup \partial D_-$, this before the birth of a set of infinitely many islands. The presence of an unstable period $k \neq 2^i$ "irregular" cycle implies infinitely many such cycles belonging to the strange repeller SR_1.

Considering Figs. 20–22 for a given c-value, as γ decreases in the range $\gamma_{2^1}^* < \gamma < \gamma_{1s}$ the critical line

L^a approaches the x-axis and the preimages of the period 2^{i-1} cycle cross through L^a entering from Z_0 in Z_2 ($\gamma^*_{2^i}$ is a *homoclinic* bifurcation value). Although the frontier ∂D_- includes (for $\gamma < \gamma_{1s}$) a strange repeller, it has a smooth shape when $c \le c_p$. For $\gamma < \gamma^*_{2^1}$, cycles of odd period begin to appear, with other cycles of even period, however not necessarily confined to ∂D_-. This means that some bifurcation sequences create cycles and strange repellers SR also outside the frontier of the immediate basin, which maintain a smooth shape.

When c decreases from $c = 1$ to $c = c_p$, the Figs. 20–22 structures unfold, i.e. with less and less overlapping, until obtaining the Myrberg's order $-1/4 = c_{2^0} < c < c_p$ for the cycles birth on ∂D_- [Agliari *et al.*, 2004].

6.4. *Strange repellers and birth of islands sets*

From a γ value $\gamma = \widetilde{\gamma}_1 < \gamma_{f1}$, $c > c_p$, after the birth of a strange repeller SR_1, a set of infinitely many islands is created according to the bifurcation described in Figs. 2(a)–2(c), SR_1 being the limit set of these islands. So independently of the cycles external to $\partial D_- \cup D_-$ and numerically found, the existence of SR_1 (which contains such cycles) becomes obvious after the islands birth. Such non-connected parts of D_- are due to the contact bifurcation of ∂D_- with the critical line L^a, followed by its crossing which creates a headland Δ^0 (Fig. 2). In this case the strange repeller SR_1, created for $\gamma \le \gamma_{f1}$, belongs to the limit set of the islands $\cup_{n\ge1} T^{-n}(\Delta_0)$. Now $\Lambda^* = SR_1 \cup \Omega$ is the total limit set of these islands, and SR_1 belongs to ∂D_-. The main island D_1 is the one crossing through L^a_{-1}, $D_1 = T^{-1}(\Delta_0)$. After the contact bifurcation the basin D_- consists of the immediate basin D_{0-} (which includes the headland Δ^0) and all its preimages of any rank:

$$D_- = D_{0-} \bigcup_{n\ge1} T^{-n}(\Delta^0).$$

In Figs. 20–22, the formation of strange repellers, and the birth of islands sets, are red colored. For $c_p < c < c_{2^1} = 3/4$ (i.e. c_{b1}), with $\gamma > 0$ decreasing values, an islands *aggregation* occurs before attaining $\gamma = 0$, which corresponds to the inverse bifurcation in Figs. 2(a)–2(c), i.e. in the sense (c, b, a). Such an aggregation changes the shape of D_-, which now presents infinitely many parts with a peduncle shape, that we call *appendices*. Without islands aggregation, it also happens that appendices occur when, without attaining the Fig. 2(b) case, the Fig. 2(a) situation presents a very strong variation of the distance between the ∂D_- points and the critical line L.

In a fractal way each island $T^{-n}(\Delta^0)$, $n = 1, 2, 3, \ldots$, reproduces on its boundary the immediate basin boundary behavior, i.e. an island boundary contains around it a limit set of a subset of islands. As γ decreases, more and more islands sets are created. They are due to the formation of headlands Δ^j, $j = 1, \ldots, p$, each one giving rise to a new islands set $\bigcup_{n\ge1} T^{-n}(\Delta^j)$, and also to the intersection of one of the islands with L^a (see Sec. 3.1). When no islands aggregation occurs ($c \ge c_{2^1}$ i.e. $c \ge c_{b1}$), all these islands have a common limit set SR out of $\partial D_- \cup D_-$, made up of the SR_1 points increased by new "irregular cycles", related to unstable cycles sets SR_j, $j = 2, 3, \ldots$, born for $\gamma < \gamma_{fj}$. If an islands aggregation ($c_p < c < c_{2^1} = 3/4$) takes place, or in presence of appendices, the index j is bounded. Nevertheless appendices can give rise to new sets of islands (see Fig. 21 for $c = 0.7$, for $\gamma \simeq 0.00575$), but when $\gamma \to 0$ this process ceases in order to obtain the fifth type of Julia set (cf. Part I). For $c_{2^1} \le c \le 1$ islands aggregation does not occur.

If c belongs to the interval $c_{2^1} \le c < c_{1s}$, as γ approaches 0, the critical line L^a approaches the x-axis, and infinitely many contact bifurcations occur with creation of headlands and related islands, and also when one island crosses through L^a from Z_0 to Z_2, etc. (as described in [Mira *et al.*, 1994], and in [Mira *et al.*, 1996b]). At the same time, the box-within-a-box bifurcation structure increases the unstable cycles sets of the strange repeller Ω on the immediate basin boundary ∂D_{0-}, and of the strange repeller SR out of ∂D_{0-}.

At $\gamma = 0$, a subset of islands belonging to $T^{-n}(\Delta^0)$ have a contact with ∂D_{0-} at the points of Ω. The other islands have contacts at the points of SR_j. The union of the limit sets Ω and SR gives the points of a Julia set.

7. Toward the Julia Set for $c \in \omega_1$

7.1. *General properties*

Remind that for $\gamma = 0$, the map $\overline{T}$ gives rise to a Julia set, we denote J' (differently from J related to the complex map T_Z), the boundary ∂D_- of the basin part, or of the convergence domain (if $|S_i| = 1$, $i = 1, 2$), located in ($y \le 0$). This set J' consists of the closure of all the unstable cycles, their limit

sets, their increasing rank preimages, generated by the bifurcations of the box-within-a-box structure of the map $\overline{T}_r$ restricted to ∂D_-. Due to the fact that $\overline{T}_{\gamma=0}$ is semiconjugate to T_Z in the invariant half plane ($y \leq 0$), the Part I results (dealing with the J structure) define completely the properties of the boundary ∂D_-.

Section 5 of Part I has shown that five very different types of Julia sets J, depending on c intervals and their boundaries, are generated by the complex map T_Z. Then, it is the same for the ∂D_- shapes generated by $\overline{T}$ when $\gamma = 0$. The first, second, fifth types correspond to boundaries of parameter c intervals, the crossing of which gives rise to a nonsmooth change of the shape of the Julia set J'. Inside the c-intervals associated with the third and fourth types smooth changes of ∂D_- (semi-conjugate of J) occur. The purpose of this section is a study of the bifurcations route toward each of these ∂D_- type, when $\gamma > 0$ decreases up to $\gamma = 0$, limiting to a constant value of the parameter $c \in \omega_1$. It is worth noting that a γ decrease is associated with a decrease of the slope of the critical arc L^a, corresponding to a rotation of L^a with the center point ($x = -c$, $y = 0$). The slope tends toward zero as $\gamma \to 0$. This property permits to explain some behaviors of ∂D_- during the route toward the Julia set J'.

In the ω_1 interval $c_{(1)_0} \leq c < c_{1s}$, an attracting (resp. neutral, i.e. $|S_i| = 1$) period 2^n cycle exists on the x-axis. It is generated by a sequence of period doubling from the fixed point P^*. If γ is sufficiently close to zero, this cycle has an immediate basin (resp. immediate domain of convergence, for simplifying also called basin) denoted $D_0(2^n)$, made up of 2^n open regions invariant by $\overline{T}^{2^n}$. For $\gamma = 0$ the total basin $D(2^n)$ has a portion in ($y > 0$), the boundary part $\partial D_-(2^n)$ located in the half plane ($y \leq 0$) becomes the Julia set J'. In this half plane $\partial D_-(2^n)$ separates the domain of diverging trajectories from the domain of the period 2^n cycle belonging to $y = 0$. Denoting $\partial D_0(2^n)$ the boundary of $D_0(2^n)$, we have:

$$\partial D_0(2^n) \cap (y \leq 0) \subset J',$$

$$\partial D(2^n) \cap (y \leq 0) = \partial D_-(2^n) \equiv J', \quad \text{when } \gamma = 0$$

The segment $[Q^*_{-1}, Q^*]$ (denoted $[q_1^{-1}, q_1]$ in Part I) of the x-axis contains all the unstable period 2^l cycles, $l = 0, 1, 2, \ldots, n-1$, generated for $c < c_{2^n}$ (or $c < c_{bn}$ as in Part I), their increasing rank preimages restricted to $y = 0$, and the limit set of all these points. When γ is sufficiently close to zero, the basin $D(2^n)$ has the following properties:

- *The unstable period 2^{n-1} cycle ($y = 0$) belongs to the boundary $\partial D_0(2^n)$.*
- *All the other unstable period 2^h cycles ($y = 0$), $h = 0, 1, 2, \ldots, n-2$, belong to $\partial D(2^n)$. They are limit points of a subset of increasing rank preimages of the unstable period 2^{n-1} cycle, and of increasing rank preimages of the unstable period 2^r cycles, $r = h+1, \ldots, n-2$. They are also limit points of a subset of increasing rank preimages of $D_0(2^n) \cap (y \leq 0)$.*

When $\gamma > 0$ decreases toward $\gamma = 0$ with $c \in \omega_1$, depending on the parameter point position with respect to the curves Tc_{2^n}, $F_{2^{n+1}}$, $N_{2^{n+1}}$, $\overline{N}_{2^{n+1}}$, a stable period 2^n cycle exists on the x-axis, or in the half plane $y < 0$. If this cycle belongs to the x-axis, $D_0(2^n)$ and a subset of its increasing rank preimages intersects $y = 0$. When $D_0(2^n)$ belongs to the half plane $y < 0$, with $c \in R_5^n$ (cf. Fig. 4), the closure of its immediate basin $D_0(2^n)$ is nonconnected (Figs. 25, 31 and 39). Then a subset of the increasing rank preimages of $D_0(2^n)$ has also for limit set of all the unstable period 2^l cycles, $l = 0, 1, 2, \ldots, n-1$ of the x-axis, generated for $c < c_{2^n}$, their increasing rank preimages restricted to $y = 0$, and the limit set of all these points. When $D_0(2^n)$ belongs to the half plane $y < 0$ with $c \in R_4^n$ (cf. Fig. 23), as for the case $c \in R_5^n$, a γ decrease toward zero leads to the situation of $D(2^n)$ becoming the basin of a stable period 2^n cycle on the x-axis with $D(2^n) \cap (y > 0) \neq \emptyset$.

7.2. *Toward the Julia sets of the interval $c_{(1)0} \leq c \leq c_{2^1}$ (i.e. c_{b1})*

7.2.1. *Behavior for the bifurcation values $c_{(1)0}$ and c_{2^1}*

For $c \in \omega_1$, $\gamma = 0$, the first type of Julia set (classification of Part I) corresponds to the fold bifurcation $c = c_{2^0} = c_{(1)0} = -1/4$. For these parameter values the fixed points P^*, Q^*, and S^* merge at ($x = 1/2$, $y = 0$), and belong to ∂D_-. In such a situation the region D_- is not a basin, because its boundary ∂D_- (Julia set) limits a domain of convergence toward the neutral fixed point $P^* \equiv Q^*$ (which is the point $q_2 \equiv q_1$ in Part I).

The fixed point R^* ($x = -1/2$, $y = -1$) belongs to the Julia set $J' \equiv \partial D_-$, which has an horizontal tangent at $P^* \equiv Q^* \equiv S^*$. The boundary ∂D_- contains a numerable set made up of the increasing

rank preimages of this point, where the tangent can be defined with a cusp point. Elsewhere ∂D_- has no tangent (Part I, Sec. 5.1). The rank-one preimage of $P^* \equiv Q^* \equiv S^*$ in the half plane $y > 0$ is the point S^*_{-1} ($x = 0$; $y = 1/4$) apex of ∂D_+ (Fig. 44(a), $c = -1/4$; $\gamma = 0$). In this case, the map $\overline{T}$ has no attractor in the whole plane except for the neutral fixed point $P^* \equiv Q^* \equiv S^*$. The total domain of convergence $D = D_- \cup D_+$ toward P^* is bounded by ∂D_- and the boundary ∂D_+. As this will be shown below it is not the case of D_+ at a fold $c^j_{(k)_0}$ or $c^{j_1 \ldots, j_a}_{(k_1 \ldots k_a)_0}$ bifurcation values (belonging to Δ_1) with $\gamma = 0$, which give rise to an attracting set with a basin D_+.

With $c = -1/4$, and $\gamma > 0$ decreasing values from $\gamma = 1$, the fixed point S^* ($y < 0$) is stable, and D_+ does not exist [cf. Fig. 3(a)], i.e. the half plane $y > 0$ belongs to the domain of diverging orbits (Fig. 44(b), $c = -1/4$; $\gamma = 0.1$). On the basin boundary ∂D_- the bifurcations occur with the Myrberg's order inside the interval $1 > \gamma \geq 0$. The boundary ∂D_- remains smooth but with more and more "oscillations" as γ tends toward 0. At $\gamma = 0$ (the Julia set case) it becomes nonsmooth with a numerable set of cusp points [Fig. 44(a)]. The domain of convergence D_+ exists only for $\gamma = 0$. So with γ decreasing values, the domain of convergence toward ($x = 1/2$, $y = 0$) undergoes a sudden increase when $\gamma = 0$, due to the "jump" of the point S^*_{-1}.

The second type of Julia set (classification of Part I) corresponds to the flip bifurcation $c_{2^1} = 3/4$ (i.e. c_{b1} in Part I) of the ω_1 spectrum. When $\gamma = 0$, the fixed point P^*(point q_2 in Part I) has merged with R^*, $x(P^*) = x(R^*) = -1/2$, $y(P^*) = y(R^*) = 0$. It is neutral with multipliers $S_1 = S_2 = -1$. It belongs to $y = 0$ and also to ∂D_- [an arc limiting a domain of convergence toward P^*, Fig. 45(a)].

Consider γ decreasing values for $c = c_{b1} = 3/4$ (i.e. c_{2^1}), boundary between the intervals I^1_4 and I^1_5 (Fig. 4). We are in the Fig. 17(a) situation but with the period two saddle S^j, $j = 1, 2$, merging into P^*. Figure 3(b) shows that the curves N_{2^1} and C_{2^1} are not crossed when γ decreases. When $\gamma < \gamma(F_{2^1})$, D_- is the basin of the period two focus $F^j_{2^j}$, $j = 1, 2$, basin which is always non-connected for $\gamma > 0$, with increasing rank preimages (islands) of its immediate basin. More precisely, as indicated in Sec. 5.4, the immediate basins $D_0(F^1_2)$ of F^1_2 (resp. $D_0(\gamma^1_2)$ of γ^1_2), $D_0(F^2_2)$ of F^2_2 (resp. $D_0(\gamma^2_2)$ of γ^2_2), are without any connection, without common boundary, and without contact

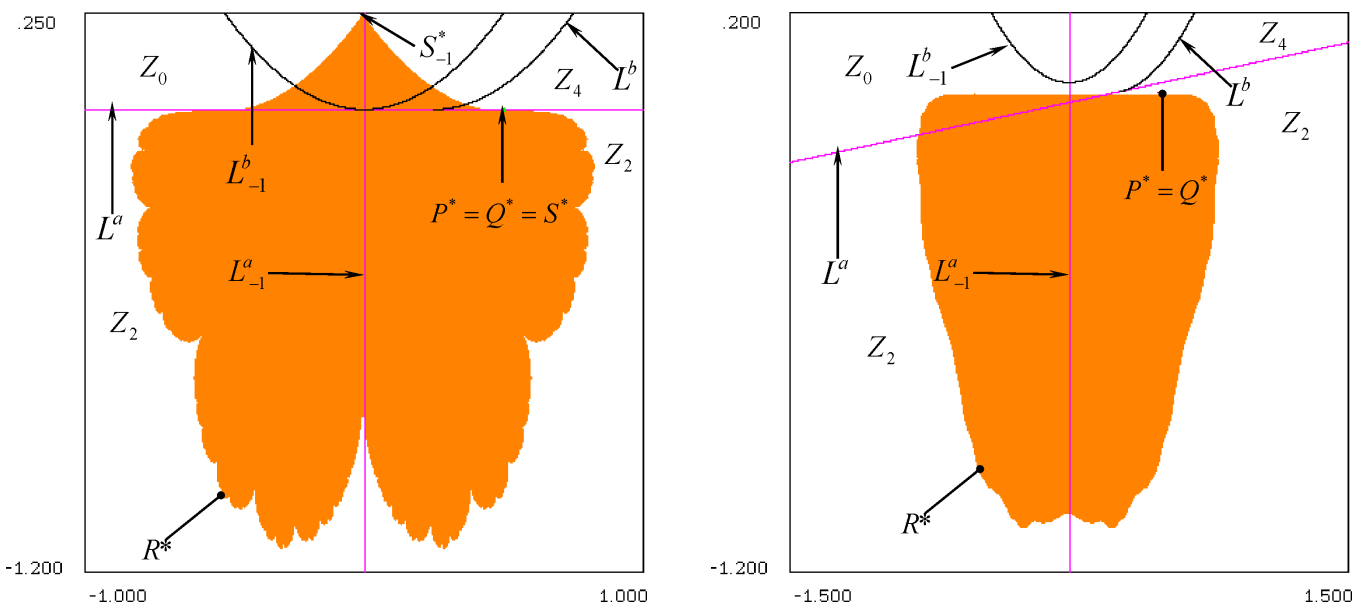

(a) (b)

Fig. 44. (a) $c = -1/4$; $\gamma = 0$. The rank-one preimage of $P^* \equiv Q^* \equiv S^*$ in the half plane $y > 0$ is the point S^*_{-1} ($x = 0$; $y = 1/4$) apex of ∂D_+. The total domain of convergence $D = D_- \cup D_+$ toward P^* is bounded by ∂D_- and the boundary ∂D_+. (b) $c = -1/4$; $\gamma = 0.1$. The fixed point S^* ($y < 0$) is stable, and D_+ does not exist [cf. Fig. 3(a)], i.e. the half plane $y > 0$ belongs to the domain of diverging orbits.

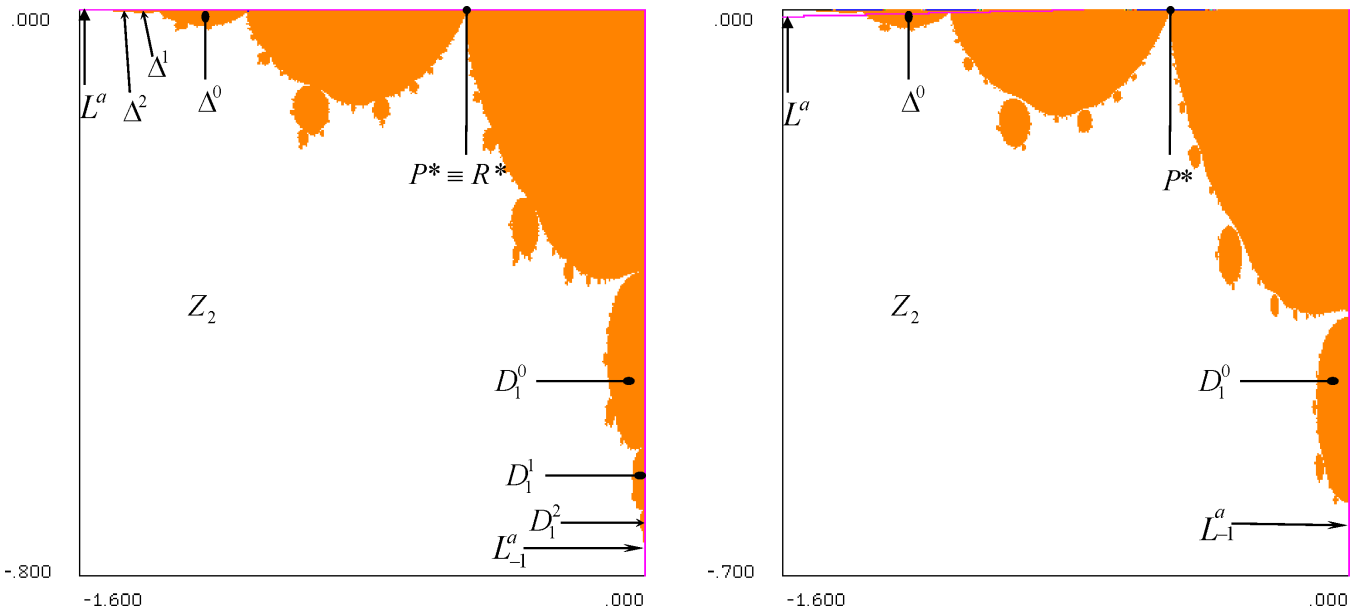

Fig. 45. (a) $c = 3/4$; $\gamma = 0$. Julia set semi-conjugate of the one generated by $z' = z^2 - 3/4$. (b) $c = 3/4$, $\gamma = 0,01$. The islands (nonconnected parts of the basin) have a strange repeller as limit set. The main island D_1^0 intersects symmetrically $L_{-1}^{(a)}$.

with $y = 0$. The total basin D_- is nonconnected with infinitely many islands having the fixed point Q^* and Q^*_{-1} its rank one preimage as limit set. On the boundary ∂D_{0-} of the immediate basin of F_2^j, decreasing γ-values give rise to more and more sequences of infinitely many repelling cycles. With their limit set, and all their increasing rank preimages, a strange repeller $\Omega \subset \partial D_{0-}$ results. From $\gamma < \gamma_{f1}$ now a first strange repeller SR_1 is created but out of ∂D_{0-} (Figs. 21 and 22), followed after by a new islands set resulting from a new intersection of ∂D_- with the critical arc $L^{(a)}$. Each island reproduces on its boundary this behavior, i.e. it contains a limit set of a subset of islands around it (Fig. 45(b), $c = 3/4$, $\gamma = 0.01$). The main island D_1^0 intersects symmetrically $L_{-1}^{(a)}$.

As γ decreases, more and more headlands Δ^j, $j = 0, 1, \ldots, q$, are created, and when $\gamma \to 0$, $q \to \infty$, with main island D_1^j, and the period two focus F_2^j, $j = 1, 2$, tends toward P^*. The way L^a crosses through D_- implies that the inverse bifurcation of Fig. 2 cannot happen. *This results in the impossibility of having islands aggregation* for $\gamma > 0$. At the limit $\gamma = 0$, R^* merges into the fixed point P^* ($y = 0$), ∂D_- and islands sets have contacts.

The first island set $IS^0 = \bigcup_{n\geq 1} T^{-n}(\Delta^0)$ is created from $\gamma \simeq 0.0167$ with the headland Δ^0, belonging to the second bulge on the left of P^*, $D_1^0 = T^{-1}(\Delta^0)$ being the "main" island (the one intersecting L^a_{-1}). The limit set Λ^{*0} of the islands is the strange repeller SR^0, and the set Ψ^{*0} of the unstable cycles (with their limits points, and increasing rank preimages) belonging to ∂D_{0-}, $\Lambda^* = SR^0 \cup \Psi^*$. With γ decreasing values, the L^a slope decreases, more and more islands sets $IS^q = \bigcup_{n\geq 1} T^{-n}(\Delta^q)$, $q = 1, 2, 3, \ldots$, with main island D_1^q, appear from headlands Δ^q, belonging to the $(q+1)$th bulge on the left of P^*, without vanishing of the previous islands sets IS^h, $h < q$. Before the IS^q birth a strange repeller SR^q was created. The limit set of the islands $\bigcup_{j=0}^q IS^j$ so created is Λ^{*q}. When $\gamma = 0$, $q = \infty$, a perfect set results, the Julia set ∂D_-, without any aggregation, with only contact points of the islands between themselves and with the boundary of the basin D_{0-}.

Figure 45(a) ($c_{2^1} = 3/4$, $\gamma = 0$) has shown the Julia set ∂D_-, where Δ^q and D_1^q are respectively headlands and main islands. The contact of the islands limits and ∂D_{0-} limit are located on fractal hollows of D_-. The formation of the first main island D_1^0 from the headland Δ^0, approaching a hollow of D_- is illustrated in Fig. 45(b) ($c_{2^1} = 3/4$, $\gamma = 0.01$).

7.2.2. *Behavior in the interval* $c_{(1)0} < c < 0$

Inside the interval $-1/4 = c_{(1)0} < c < c_{2^1} = 3/4$, $\gamma = 0$ gives rise to Julia sets of fourth type with *Class A* (Sec. 5.4 of Part I), having the same *structure*. We remind that here the qualifier "structure" is only related to the identification of the localization of the $(k; j)$ unstable cycles, the J outline not being considered. (cf. Sec. 1 of Part I).

For the parameter values $c = 0$ and $\gamma = 0$, at which the fixed point P^* of the x-axis has the multipliers $S_1 = S_2 = 0$, P^* is the only attractor of the map. The boundary $\partial D_- = J'$ is made up of an arc [Fig. 46(a)] semi conjugate to the circle $|z| = 1$ generated by the complex map T_Z. When γ decreases from $\gamma = 1$ to $\gamma = 0$, the box-within-a-box bifurcations take place on ∂D_- without any disruption. The basin boundary ∂D_- remains smooth, but now with small "oscillations" [resulting from a sign change of the curvature radius Fig. 46(b)], which disappear at $\gamma = 0$. The parameter value $c = \gamma = 0$ separates two subintervals for which the J *shape* (directly related to its outline) undergoes a qualitative change.

When $\gamma = 0$, a continuous variation of the Julia set $J' = \partial D_-$ occurs, for $-1/4 < c < 0$. The Julia set J' has the same bumpy shaped fractal aspect (*petal-like*), which reduces until attaining $c = 0$. This aspect results from a continuous modification of the case $c = c_{(1)0} = -1/4$, but for $-1/4 < c < 0$ now J' is nowhere differentiable.

For $c_{(1)0} = -1/4 < c < 0$, when γ decreases from $\gamma = 1$, the fixed point P^* is the only attractor of the map $\overline{T}$, the box-within-a-box bifurcations take place without any disruption on the arc ∂D_- of the basin boundary of P^*. The arc ∂D_- remains smooth [Figs. 43(a)–43(c)], but with more and more "oscillations" [Fig. 47(a)] as γ approaches 0, and at $\gamma = 0$ (the Julia set case) it becomes nonsmooth [Fig. 47(b)].

7.2.3. *Interval* $0 < c < c_p$

When $c(E^0) = 0 < c < c_p$ (c_p is defined in Sec. 6.1) the Δ_1 Myrberg's order on ∂D_- is not disrupted for γ decreasing values. The fixed point $R^* \in \partial D_-$ ($y(R^*) < 0$) is located on a local "dip" of D_-, now with a pointed shape of the Julia set ∂D_- (Fig. 48, $c = 0.3$, $\gamma = 0$). When γ decreases from the global bifurcation of "saddle-saddle" type (cf. Secs. 4.3 and 5.2), and after the merging of the period two unstable focus (Fig. 24) F_2^j, $j = 1, 2$, with R^*, D_- presents a sequence of bulges separated by R^* and its increasing rank preimages. This gives rise to a "dampened oscillations" shape of ∂D_- toward $Q^* \cup Q^*_{-1}$, which leads to the Fig. 48 situation when

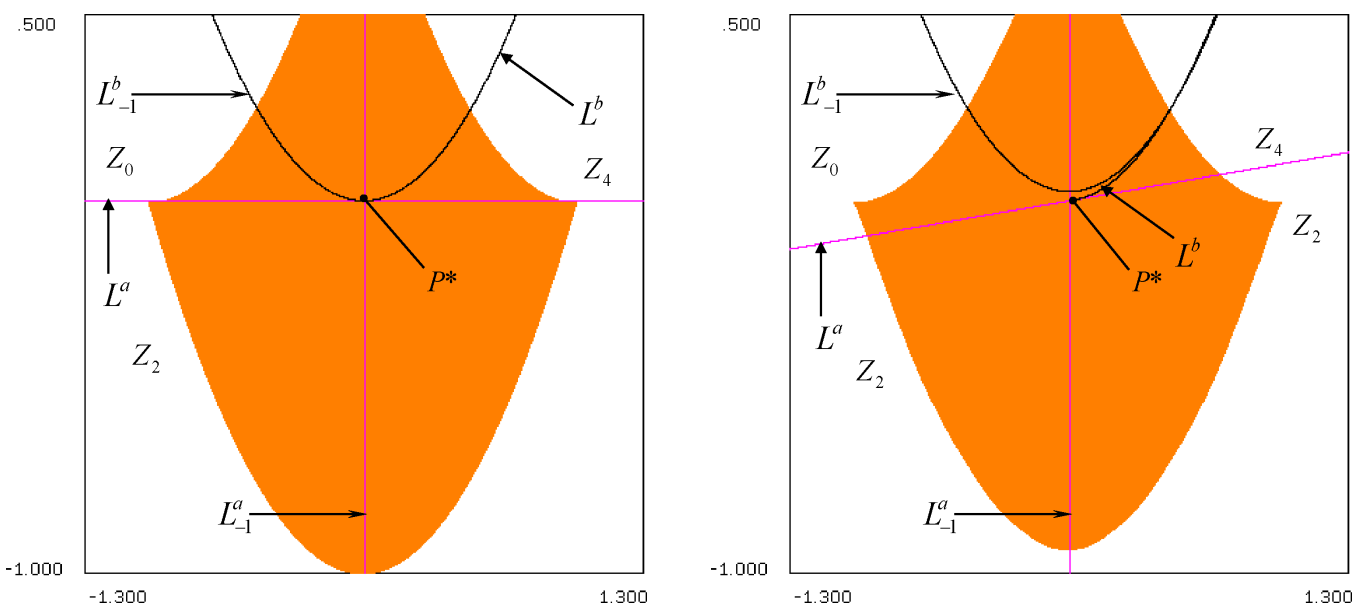

Fig. 46. (a) $c = \gamma = 0$. The fixed point P^* of the x-axis is the only attractor of the map. The boundary $\partial D_- = J'$ is made up of an arc semi conjugate to the circle $|z| = 1$ generated by the complex map $z' = z^2$. (b) $c = 0$; $\gamma = 0.1$.

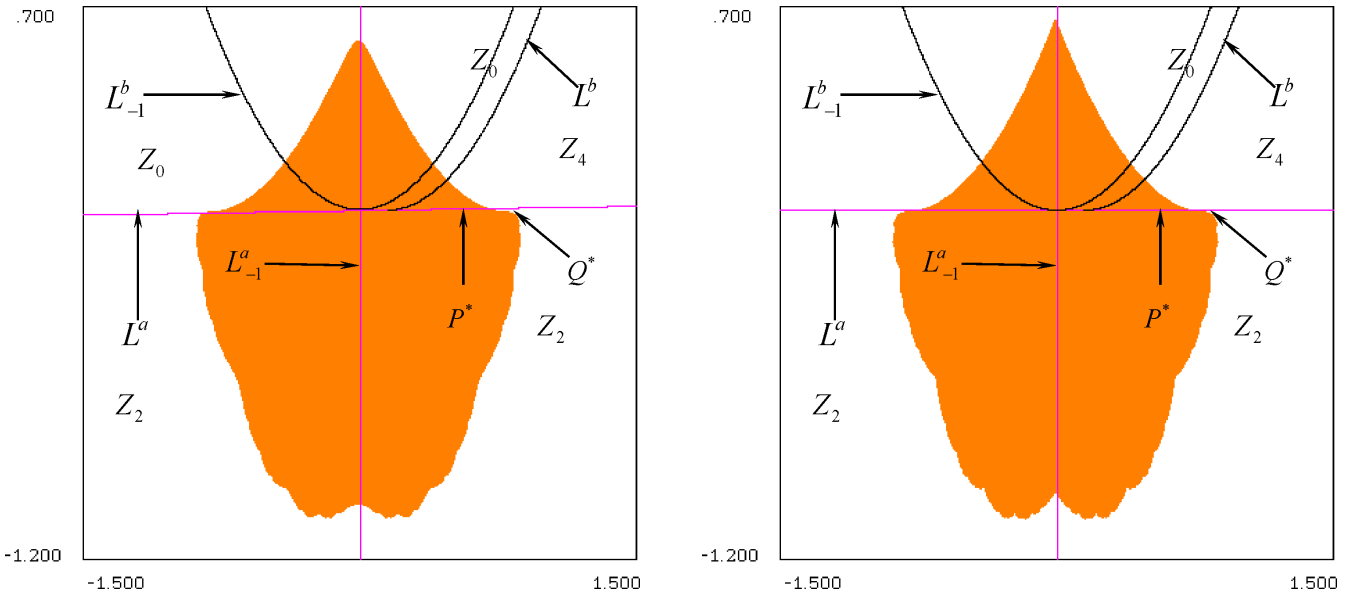

Fig. 47. (a) $c = -0.15$; $\gamma = 0.01$. The basin arc ∂D_- remains smooth but with more and more "oscillations" as γ approaches 0. (b) $c = -0.15$; $\gamma = 0$. Julia set case. The arc ∂D_- is nowhere smooth.

$\gamma = 0$. As for the route toward this Julia set, all unstable cycles of ∂D_-, and their limit sets, result from all the box-within-a box bifurcations (Part I, Fig. 1) without any perturbation, when γ decreases.

7.2.4. *Interval* $c_p < c < c_{b1} = 3/4$

In the interval $c_p < c < c_{2^1} = 3/4$, the Δ_1 Myrberg's order on ∂D_- is disrupted, and $y(R^*) \to 0$ with negative values, when $c \to c_{b1} \equiv c_{2^1}$. This interval is characterized by the birth of island sets followed by aggregation of these islands to the immediate basin D_0 when γ decreases. Births of island sets (or related aggregations) are infinitely many, either by creation (or destruction) of headlands, or when an island intersects the critical line L^a. When $\gamma = 0$, this situation leads to a new aspect of the fractal set $\partial D_- = J$, represented by Fig. 49(a) ($c = 0.6$, $\gamma = 0$).

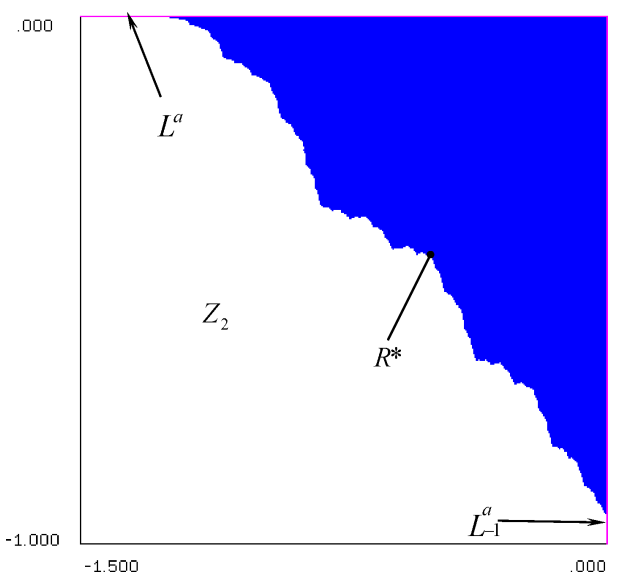

Fig. 48. $c = 0.3$, $\gamma = 0$. Shape of the Julia set ∂D_-.

Consider γ decreasing values, from $\gamma = \gamma_{b3}$ (Sec. 5.4), $(c; \gamma_{b3}) \in f_{2^0}$. In order to see how Fig. 49(a) is obtained we consider the basin situation for $c = 0.6$, $\gamma = 0.0595$ [Fig. 49(b)], with a non-connected basin D_-. We remark that the immediate basin boundary ∂D_{0-} is made up of a sequence of "bulges" of decreasing size, in the form of a dampened half oscillations, tending toward the points Q^* and Q^*_{-1} on $y = 0$. Remind that Q^*_{-1} is a rank-one preimage of the fixed point Q^*, $T^{-1}(Q^*) = Q^* \cup Q^*_{-1}$, $x(Q^*_{-1}) = -x(Q^*)$. The "bulges" are created from the "mushroom" shaped basin (for $\gamma > \gamma_{b3}$, cf. Secs. 5.3, 6.4). This shape disappears when γ decreases. The second bulge on the left of R^* creates the headland Δ^0, the island $D^0_1 = T^{-1}(\Delta^0)$ crossing through L^a_{-1}, and infinitely many islands $\bigcup_{n\geq 1} T^{-n}(\Delta^0)$ constituting the first islands set of Fig. 20. The limit set Λ^* of the islands is the strange repeller SR, and also the set Ω made up of the unstable cycles, their limit points, and increasing rank preimages, belonging to ∂D_{0-}, $\Lambda^* = SR \cup \Omega$.

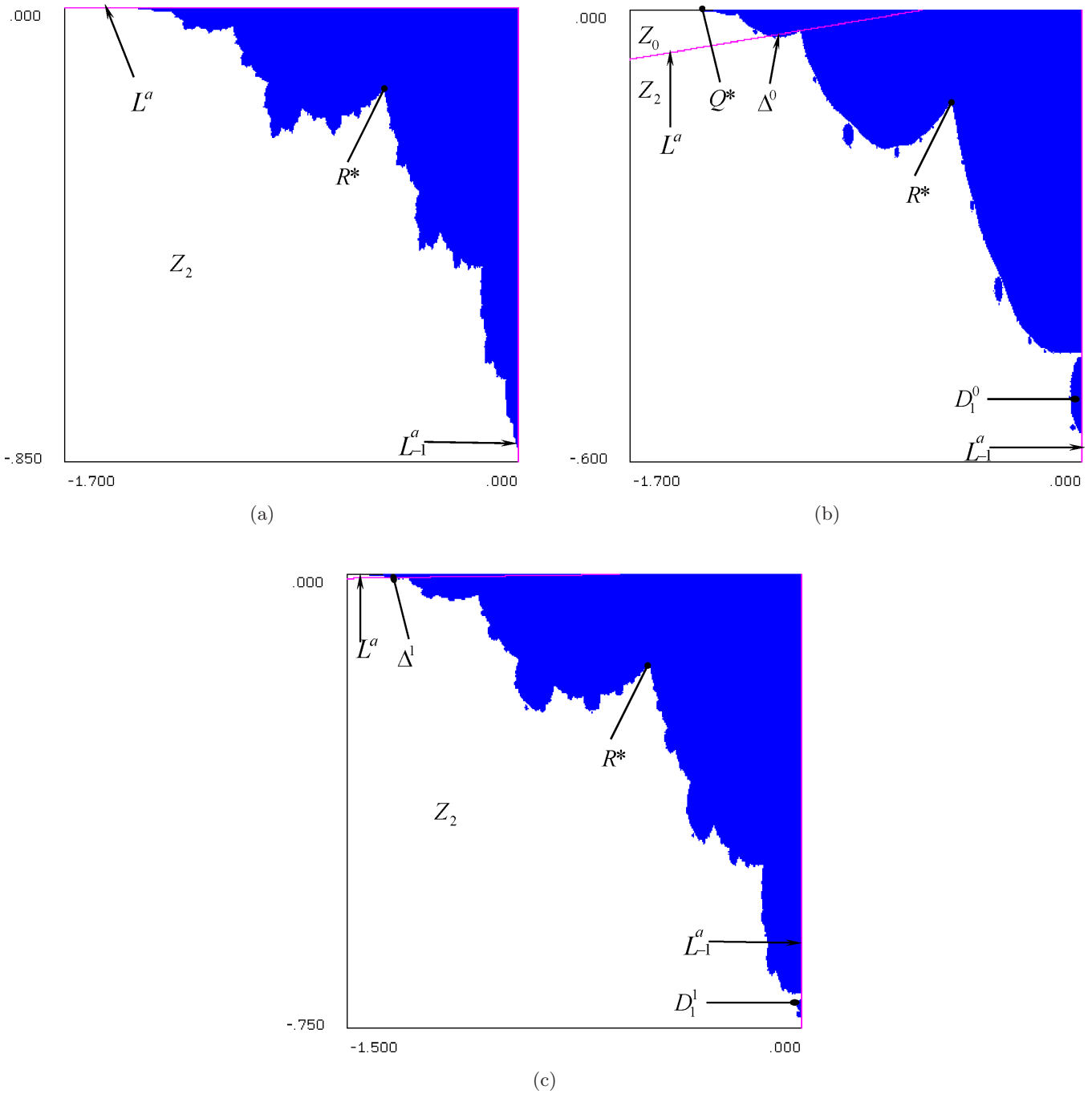

Fig. 49. (a) $c = 0.6$, $\gamma = 0$. Shape of the Julia set ∂D_-. (b) $c = 0.6$, $\gamma = 0.0595$. Nonconnected basin D_-. (c) $c = 0.6$, $\gamma = 0.0075$. Swellings of D_- resulting from the aggregation of the first set of islands.

When γ decreases, the slope of the critical arc L^a decreases by rotation with center point $(x = -c; y = 0)$ and tends toward zero if $\gamma \to 0$. For $c = 0.6$ the inverse bifurcation of Fig. 2 (sense $\overrightarrow{cba}$) leads to the aggregation of the islands set to D_{0-} for $\gamma \lesssim 0.0582$. A second islands set, due to the headland Δ^1 in the third bulge on the left of R^*, appears from $\gamma \simeq 0.00875$, $D^1_1 = T^{-1}(\Delta^1)$, being the island crossing through L^a_{-1}. Figure 49(c) ($c = 0.6$, $\gamma = 0.0075$) shows this case and swellings resulting from the first islands aggregation. Decreasing values of γ cause the aggregation of these islands when $\gamma \lesssim 0.0059$. This situation is followed by a sequence of global bifurcations with formation of island sets, due to the headland Δ^n in the rank $(n + 2)$ bulge on the left of R^*, followed by islands aggregation,

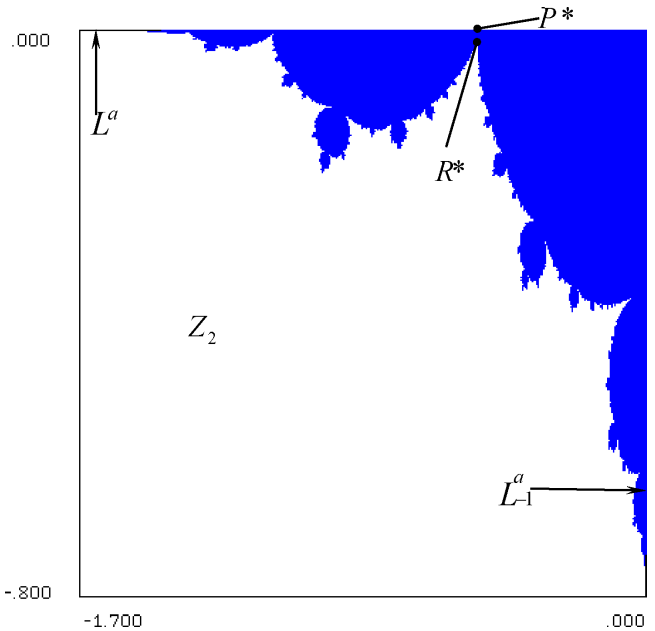

Fig. 50. $c = 0.74$, $\gamma = 0$. Julia set ∂D_-.

$n \to \infty$ when $\gamma \to 0$. The fractal Julia set ∂D_- of Fig. 49(a) ($c = 0.6$, $\gamma = 0$) is the result of such infinitely many global bifurcations.

When c is not far from $c_{2^1} = 3/4$, and with decreasing γ values, $\gamma < \gamma(f_{2^0})$, the alternation of islands birth and aggregations no longer occurs, i.e. several births of islands sets happen before an aggregation. This gives rise to the fractal Julia set ∂D_- of Fig. 50 ($c = 0.74$, $\gamma = 0$) where the swellings basis is smaller.

7.3. *Toward the Julia Set generated between the flip bifurcations c_{2^i} and $c_{2^{i+1}}$*

The parameter interval considered here is $c_{2^i} \leq c \leq c_{2^{i+1}}$, $i = 1, 2, 3, \ldots$, which belongs to the Myrberg's spectrum ω_1. Here c_{2^i} is the flip bifurcation denoted c_{bi} in Part I. When $\gamma = 0$, the neutral period 2^i cycle, with multipliers $S_1 = S_2 = -1$, belongs to $y = 0$ and also to ∂D_- which is an arc limiting a domain of convergence toward this neutral cycle inside the half plane $y \leq 0$. In the simplest case $c = c_{2^1} = 3/4$ (i.e. c_{b1}), $\gamma = 0$, the cycle is the fixed point P^* (point q_2 in Part I), which merges with R^* (see the previous section).

For $c = c_{2^i}$, $i = 2, 3, 4, \ldots$, consider the total domain of convergence $D(2^i) = D_-(2^i) \cup D_+(2^i)$ of the neutral period 2^i cycle located on $y = 0$, $D_+(2^i) = D(2^i) \cap (y > 0)$, $\partial D_-(2^i) = \partial D_- = J'$ is such that $D_+(2^i)$ coexists with an attractor in the half plane $y > 0$, with a basin D_+.

The fourth type of Julia set (with *class A*) is obtained for each c-value of the interval $c_{2^n} < c < c_{2^{n+1}}$ (denoted $c_{bn} < c < c_{b(n+1)}$ in Part I) of the ω_1 spectrum, $n = 1, 2, \ldots$, and $\gamma = 0$. This situation is described in Sec. 5.4 of Part I. For $n = 1$ and $c = c_{2^1}$, R^* merges into the fixed point P^* located on $y = 0$ [Fig. 45(a)]. When $c > c_{2^1}$ one has $y(R^*) > 0$, and $P^* \in \partial D_-$. It results that for $c \geq c_{2^1}$ ∂D_- contains P^* and the increasing rank preimages of P^*, whose limit set on $y = 0$ is $Q^* \cup Q^*_{-1}$. This situation has a new consequence on the Julia set ∂D_- obtained for $\gamma = 0$. Indeed now each of the Fig. 45(a) "bulges" intersects $y = 0$ at two points belonging to the increasing rank preimages of P^*. Then with γ decreasing values, there exists a c-value (say c^1_p) such that as soon as L^a crosses through such a bulge, the inverse bifurcation of Fig. 2 cannot happen. *It results in the impossibility of having islands aggregation to D_{0-}* for $\gamma > 0$.

Figure 51 ($c = 0.78$, $\gamma = 0.01$) shows the formation of islands before attaining $\gamma = 0$. From Figs. 52(a), 52(b) ($c = 0.8$, $\gamma = 0$) it appears that a c increase gives rise to local fractal spikes at the contact of islands inside of fractal hollows (see the Fig. 52(b) enlargement of $\partial D_{0-} \cap \partial D^0_1$ at $x = 0$). With increasing values of c the hollows size decrease, until they vanish, as shown in Fig. 53 ($c = 1$, $\gamma = 0$), and the Fig. 54 ($c = 1.1$, $\gamma = 0$)

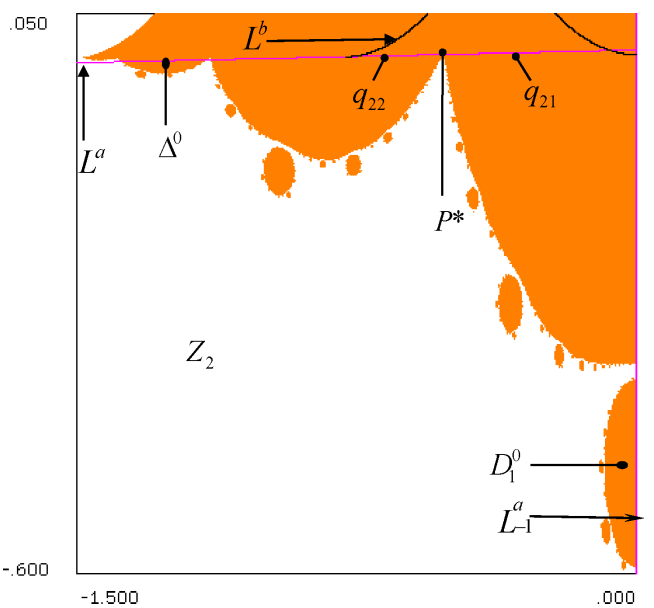

Fig. 51. $c = 0.78$, $\gamma = 0.01$. Formation of islands before attaining $\gamma = 0$.

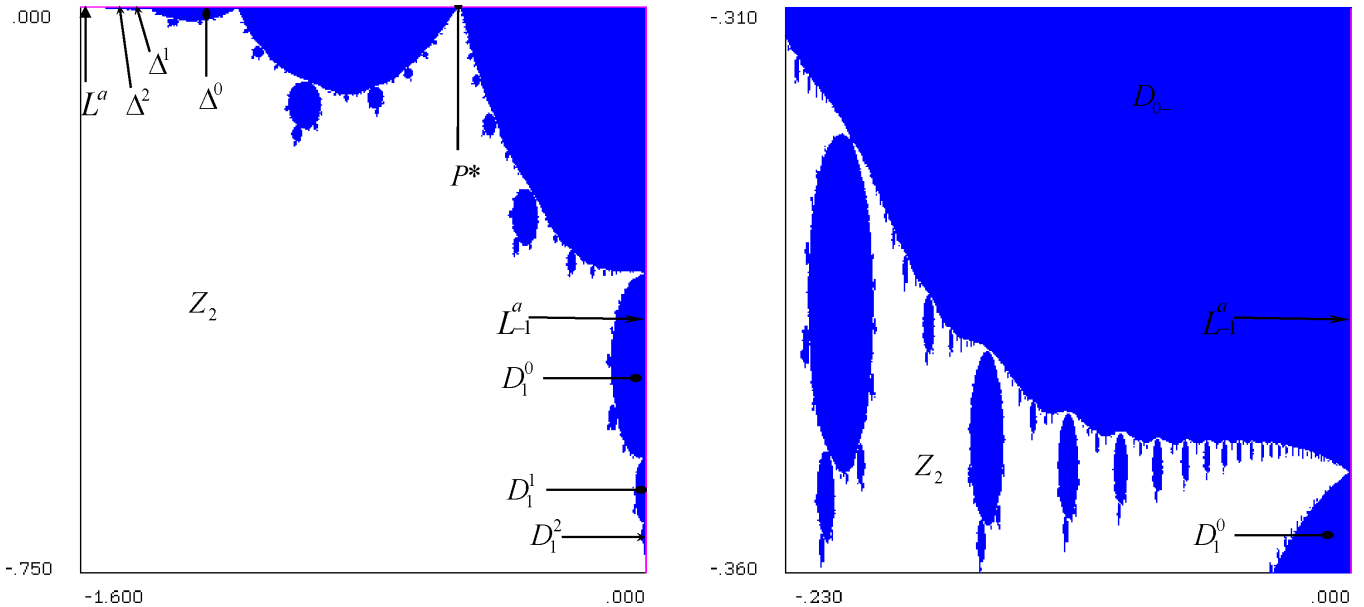

(a) (b)

Fig. 52. (a) $c = 0.8$, $\gamma = 0$. Julia set ∂D_{-}. (b) Enlargement showing local fractal spikes at the contact of islands inside of fractal hollows.

enlargement. For $c = 1$, $\gamma = 0.0008$, Fig. 55 gives a view of the situation before contact with all the islands. When c increases Figs. 56 ($c = 1.24$, $\gamma = 0$), 57 ($c = 1.25$, $\gamma = 0$), 58 ($c = 1.28$, $\gamma = 0$), 59 ($c = 1.3$, $\gamma = 0$), illustrate the modifications of the Julia set J' semi-conjugate of the Julia set J generated by the map $z' = z^2 - c$. For $\gamma > 0$, with decreasing values toward $\gamma = 0$, and for the other intervals bounded by two consecutive flip bifurcations of ω_1, as for the previous intervals, the route toward the Julia set J' is defined from the Fig. 5 bifurcation structure.

7.4. *Interaction of the half plane $y \leq 0$ on the half plane $y > 0$*

Consider the parameter interval ω_1 and $c > c_{2^2}$. When $\gamma = 0$, due to the presence of the stable

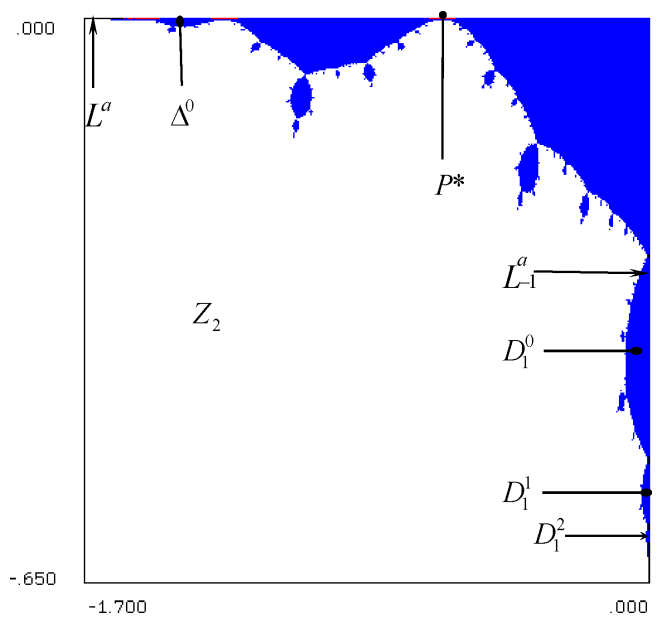

Fig. 53. $c = 1$, $\gamma = 0$.

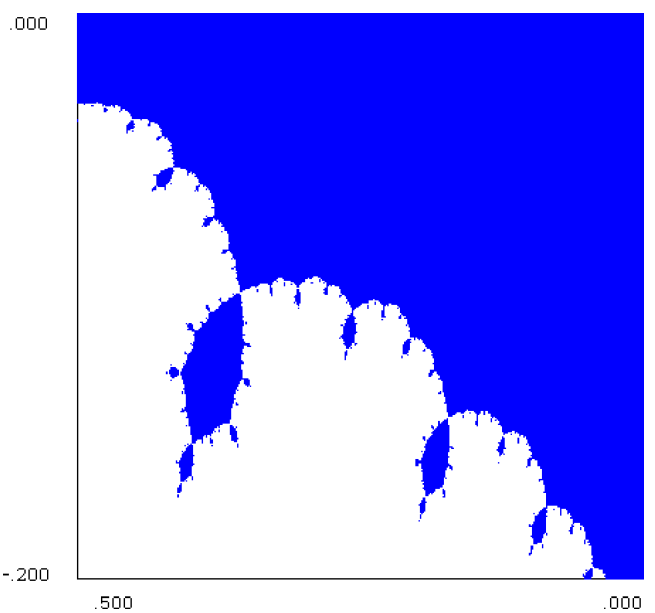

Fig. 54. $c = 1.1$, $\gamma = 0$.

period 2^i cycle $(i = 2, 3, \ldots)$ on the x-axis with a basin overlapping this axis, the number of stable cycles located in the half plane $y > 0$ increases with i. That is, for $\gamma = 0$ the stable cycles of the half plane $y \geq 0$ have a remarkable property, which we have obtained only numerically, as follows:

- For $c_{2^i} < c < c_{2^{i+1}}$, $i \geq 1$, the half plane $y \geq 0$ includes:
  (a) one stable cycle of period 2^{i-1}
  (b) 2^{i-1} stable cycles of period 2^i

The case $i = 1$ is obvious, while the three following examples show a few cases with $i = 2, 3, 4$.

(E1) at $c_{2^2} < c = 1.36 < c_{2^3}$, $\gamma = 0$ we have the following cycles:

$c = 1.36,\ \gamma = 0$	period	x	y	S_1 or ρ	S_2 or φ
Cycle	$2^{i-1} = 2^1$	0.20089	0.7516	$\rho = 0.925$	$\varphi = \pi/2$
Cycle 1	$2^i = 2^2$	−0.07326	0.0000	0.732	−0.856
Cycle 2		−0.71395	0.41048	−0.856	−0.856

and Fig. 60 shows the basins of the stable cycles, the 2-cycle has a green basin, the 2^2-cycle in $(y > 0)$ has a blue basin and the 2^2-cycle on the x-axis a red basin.

(E2) at $c_{2^3} < c = 1.3816 < c_{2^4}$, $\gamma = 0$, we have the following cycles:

$c = 1.3816,\ \gamma = 0$	period	x	y	S_1 or ρ	S_2 or φ
Cycle	$2^{i-1} = 2^2 = 4$	0.49061	0.00134	$\rho = 0.064$	$\varphi = \pi/2$
Cycle 1		−1.38160	0.0000	0.000	−0.004
Cycle 2	$2^i = 2^3$	−1.27854	0.01062	−0.004	−0.004
Cycle 3		−0.75921	0.35478	−0.004	−0.004
Cycle 4		−0.77259	0.37089	−0.004	−0.004

and Fig. 61 shows the basins of the stable cycles, the 2^2-cycle has a blue basin, the four cycles of period $2^3 = 8$ have basins in red, violet, yellow and green.

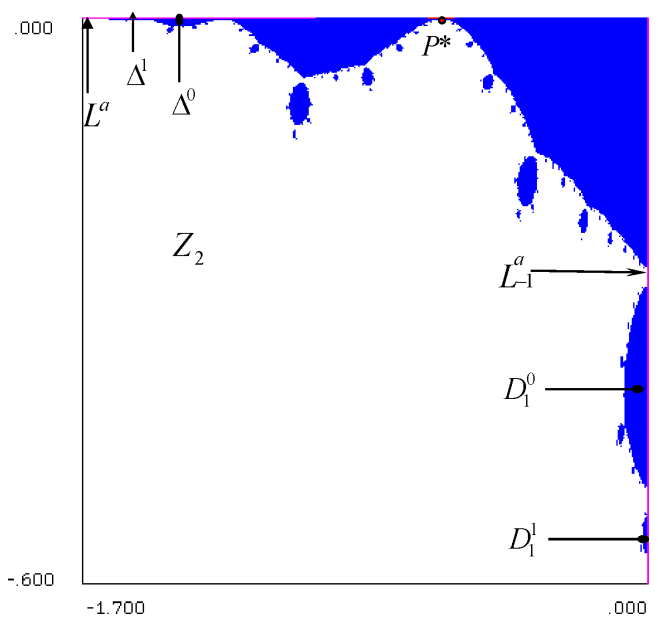

Fig. 55. $c = 1$, $\gamma = 0.0008$.

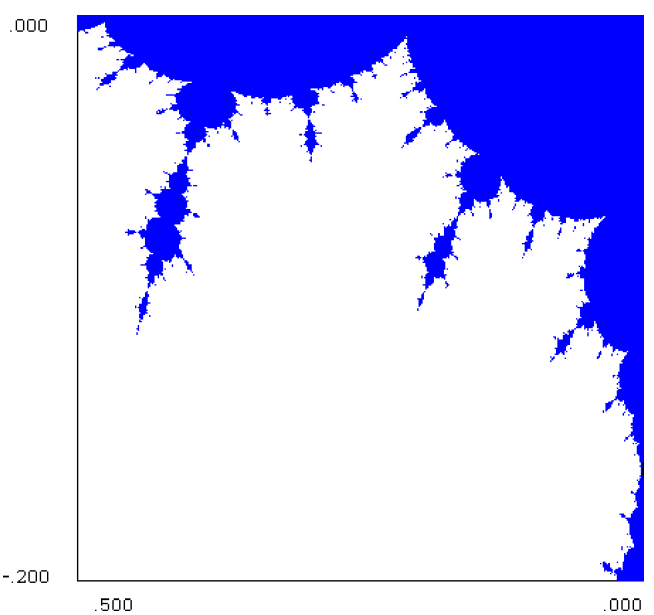

Fig. 56. $c = 1.24$, $\gamma = 0$.

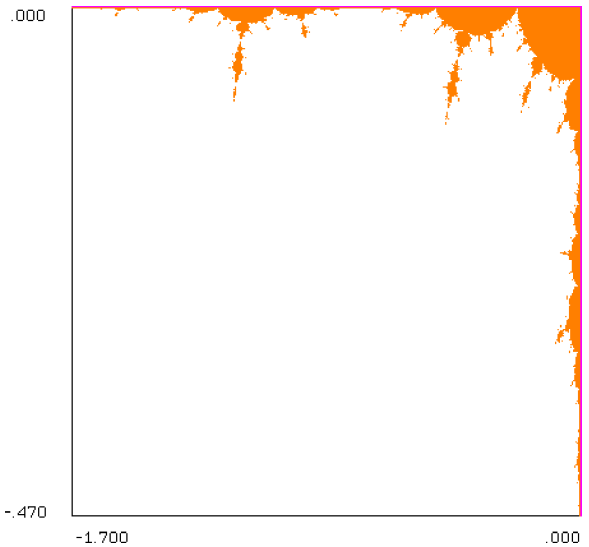

Fig. 57. $c = 1.25$, $\gamma = 0$.

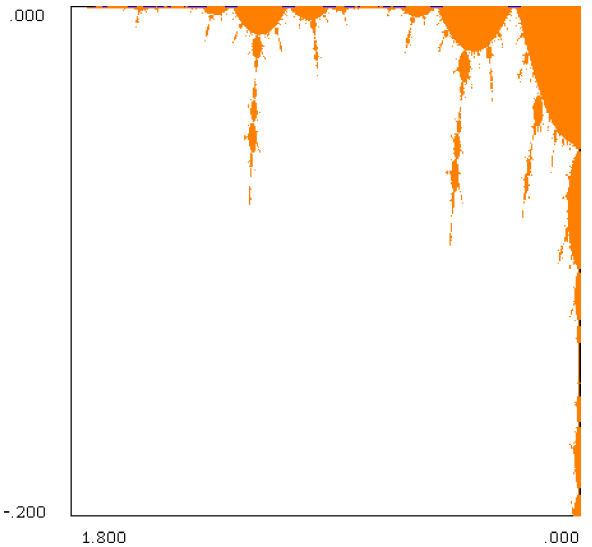

Fig. 58. $c = 1.28$, $\gamma = 0$.

(E3) at $c_{2^4} < c = 1.3975 < c_{2^5}$, $\gamma = 0$, we have the following cycles:

$c = 1.3975,\ \gamma = 0$	period	x	y	S_1 or ρ	S_2 or φ
Cycle	$2^{i-1} = 2^3 = 8$	0.54900	0.00004	$\rho = 0.448$	$\varphi = \pi/2$
Cycle 1		−1.39749	0.00000	0.040	−0.200
Cycle 2		−0.78219	0.32546	−0.200	−0.200
Cycle 3		−0.80460	0.35152	−0.200	−0.200
Cycle 4	$2^i = 2^4$	−1.30175	0.00830	−0.200	−0.200
Cycle 5		−1.38120	0.00027	−0.200	−0.200
Cycle 6		−0.78831	0.33247	−0.200	−0.200
Cycle 7		−0.80228	0.34878	−0.200	−0.200
Cycle 8		−1.30408	0.00873	−0.200	−0.200

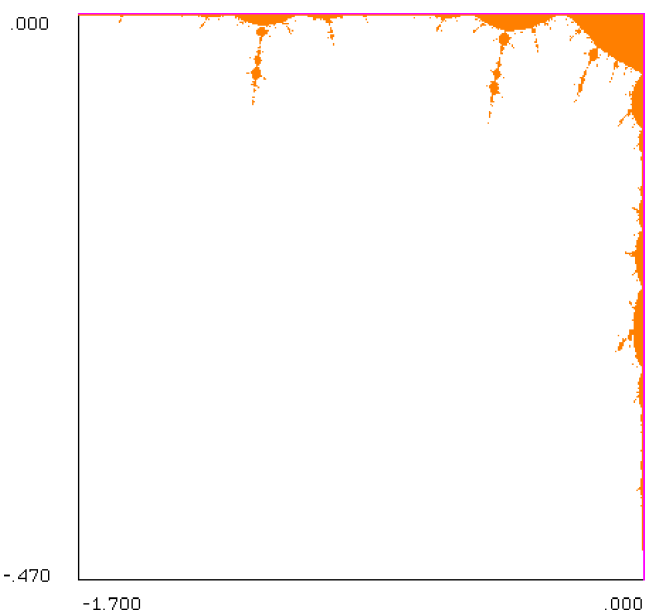

Fig. 59. $c = 1.3$, $\gamma = 0$.

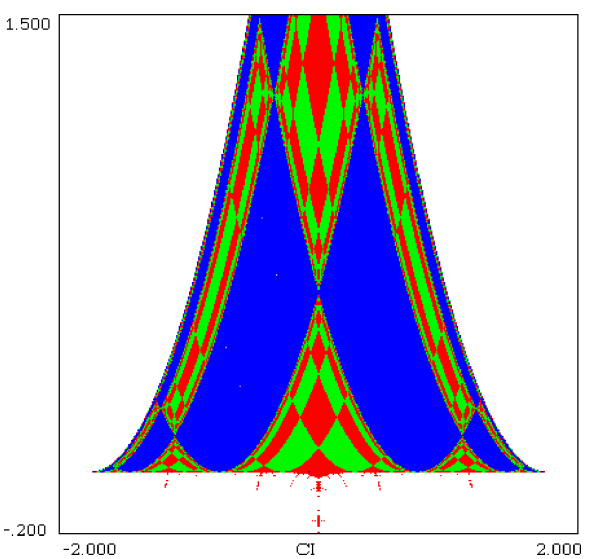

Fig. 60. $c = 1.36$, $\gamma = 0$. The basin of the period 2^i with $i = 1$ is blue colored. The basins of the two cycles with $i = 2$ are green and red colored.

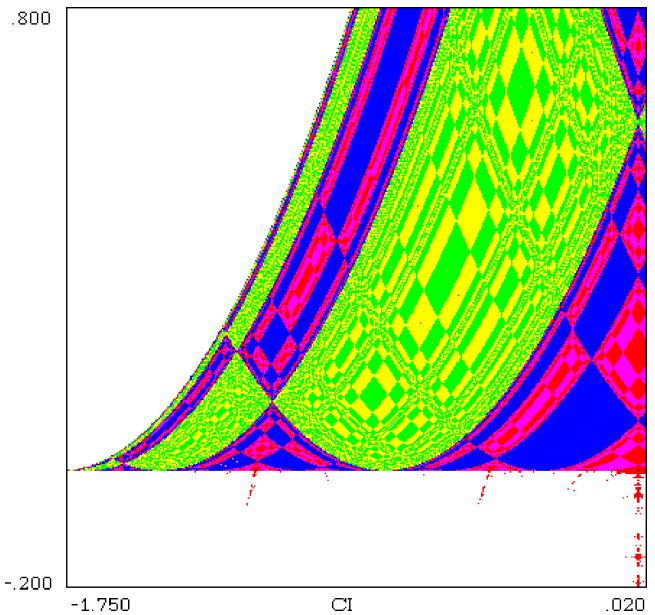

Fig. 61. $c = 1.3616$, $\gamma = 0$. The basin of the period 2^i with $i = 2$ is blue colored. The basins of the four cycles with $i = 3$ are green, yellow, pink and red colored.

and Fig. 62 shows the basins of the nine coexisting stable cycles.

Moreover, we have noticed that:

- One of the 2^{i-1} stable cycles of period 2^i is on the x-axis ($y = 0$) with multiplier S^* related to $y = 0$, and the other $2^{i-1} - 1$ stable cycles in ($y > 0$) of period 2^i have the multipliers $S_1 = S_2 = S^*$.

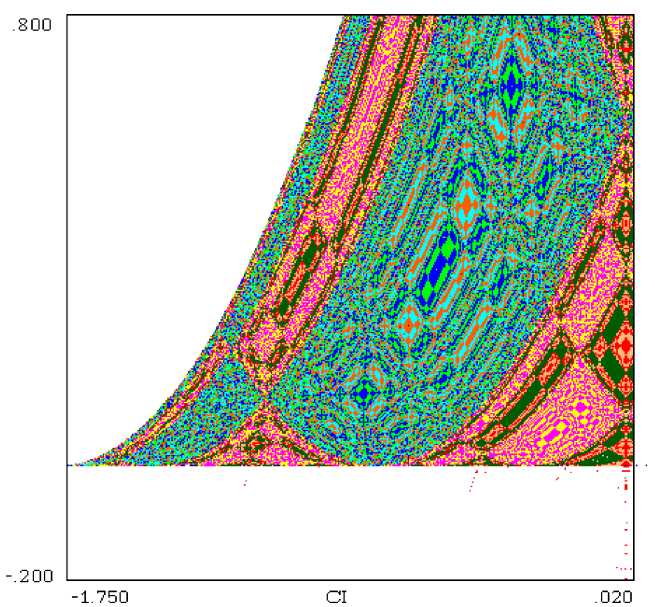

Fig. 62. $c = 1.3975$, $\gamma = 0$. The basin of the period 2^i with $i = 3$ is green colored. The basins of the eight cycles with $i = 4$ correspond to the other eight differently colored areas.

- The unique cycle of period 2^{1-1} is a stable focus, or a stable node either with $S_1 = S_2$ or $S_1 = -S_2$.

8. Toward the Julia Set for $c \in \Delta_1$

Due to the fact that $\overline{T}_{\gamma=0}$ is semiconjugate to T_Z in the invariant half plane ($y \leq 0$), when $\gamma = 0$ the Part I results define completely the properties of the boundary of $J' \equiv \partial D_-$ generated by (2). In the interval $c_{1s} < c < 2$, except the dendrites cases, an attracting, or a neutral ($|S_i| = 1$) period $(k; j)$ cycle exists on the x-axis, $k \neq 2^p$, $p = 0, 1, 2, \ldots$ (i.e. not generated by the period doubling from P^*). This cycle is born from the fold bifurcation $c = c_{(k)_0}$.

With respect to the Julia set obtained for $c \in \omega_1$, now the segment $[Q^*_{-1}, Q^*]$ of the x-axis contains all the unstable cycles generated for $c < c_{(k)_0}$, their increasing rank preimages restricted to $y = 0$, and the limit set of all these points.

Section 4.4 has shown that, in the (c, γ) plane, the set of all the spectra Ξ^n_k, $k = 1, 3, 4, \ldots$, $n = 0, 1, 2, \ldots$, are organized according to the fractal box-within-a-box structure defined in Sec. 2 of Part I. That is, the shape of the Figs. 3 and 9 bifurcation curves is reproduced for other parameter intervals. So the route toward the Julia set J' is here similar to the one described in the previous section.

9. Dendrite Cases for the Julia Set ($\gamma = 0$)

The situations of *dendrites* are defined in Sec. 5.5 of Part I. Such situations are given by the values $c = \hat{c}$ (Sec. 2.4 of Part I, λ becoming now the parameter c), i.e. c^{*j}_k, c^j_{ks}, $\tilde{c}$ and their embedded forms in rank-a boxes, $a > 1$. For such c-values ∂D_- is not the basin boundary of an attracting set on the x-axis, but the boundary of the domain of diverging orbits in the half plane $y < 0$. The dendrites resulting from the limit of Myrberg spectra are, as stated above, those generated for $c = c_{1s}$, $c = c^j_{ks}$, or more generally for the embedded cases $c = c^{j_1,\ldots,j_a}_{(k_1,\ldots,k_a)_s}$.

The situation in the half plane ($y \geq 0$) is not so evident. Let us introduce such particular cases $c = \hat{c}$, associated with a dendrite when $\gamma = 0$, considering the first case $\gamma = \varepsilon > 0$. This is because for $\gamma = \varepsilon > 0$ the map $\overline{T}$ is invariant in the positive half plane (i.e. any point (x, y) with $y > 0$ is mapped again at a point with $y > 0$) and in this half plane there exist some (also many) invariant attracting sets, while for $\gamma = 0$ the map $\overline{T}$ is no longer invariant in the positive half plane, as any

point with $(0, y)$ with $y > 0$ is mapped into a point of the x-axis, which in its turn is invariant, thus the trajectory will stay forever on the x-axis.

For example, consider the case $c = c_{1s} \simeq 1.401155189$ which is the limit of c_{2^i} as $i \to \infty$. As we have seen in Sec. 7.4, at $\gamma = 0$ and $c = c_{2^i}$ in the half plane $y > 0$ we expect the existence of $2^{i-1} - 1$ stable cycles of period 2^i and one stable cycle of period 2^{i-1}. Thus, as $i \to \infty$, it is possible that infinitely many attracting sets exist, but also their periods tend to infinity, which lead to the conjecture that the stable cycles in the half plane $(y > 0)$ are finite in number for any finite i while in the limit the invariant set has a different structure. And this is probably true also for $\gamma = \varepsilon > 0$ when the map $\overline{T}$ is invariant in the positive half plane. In such cases, for (c_{1s}, ε) we have an invariant set on the x-axis and a *different invariant set* in $(y > 0)$, and perhaps with the same "critical" property, as a *critical attractor* $A_{\rm cr}$ (with a Cantor like structure, cf. Part I, Sec. 2.1) that we know to exist on $y = 0$. Then, in the limit, for $(c_{1s}, 0)$ we have an invariant set $A_{\rm cr}$ on $y = 0$ which now *attracts also points from the positive half plane* $(y > 0)$: the vertical segment on the $x = 0$ axis and all its preimages of any rank, which are probably intermingled in a complex way with the existing invariant sets in the half plane $(y > 0)$. Clearly for $(c_{1s}, 0)$ in the half plane $(y < 0)$ we have the points of the dendrite, as described in Sec. 5.5 of Part I, which belongs to the stable set $D(A_{\rm cr})$, set of points of zero measure (in the two-dimensional plane) which are ultimately mapped into the critical attractor on the x-axis. However, the closure of this set is probably such to include the points which are invariant in the positive half plane $(y > 0)$.

This kind of values of c, leading to critical attractors on the x-axis and dendrites in the negative half plane $(y < 0)$ are perhaps more difficult to understand with respect to those for which we have a chaotic interval or cyclical chaotic intervals on the x-axis and dendrites in the negative half plane $(y < 0)$. In fact, let us consider, for example, the case of $\tilde{c} \simeq 1.89291098791$. At this value, on the x-axis we have an invariant chaotic interval $\overline{CC_1}$ where C is the critical point of the Myrberg's map, that is, $C = -c$ (on the x-axis), and C_i is its ith iterate by the one-dimensional Myrberg's map (restriction of $\overline{T}$ on the x-axis). At $c = \tilde{c}$ the third iterate C_3 is merging with the unstable fixed point q_2, i.e. P^* for the map $\overline{T}$. The set $J \cap (y = 0)$ is constituted by $\overline{CC_1}$ and its increasing rank preimages

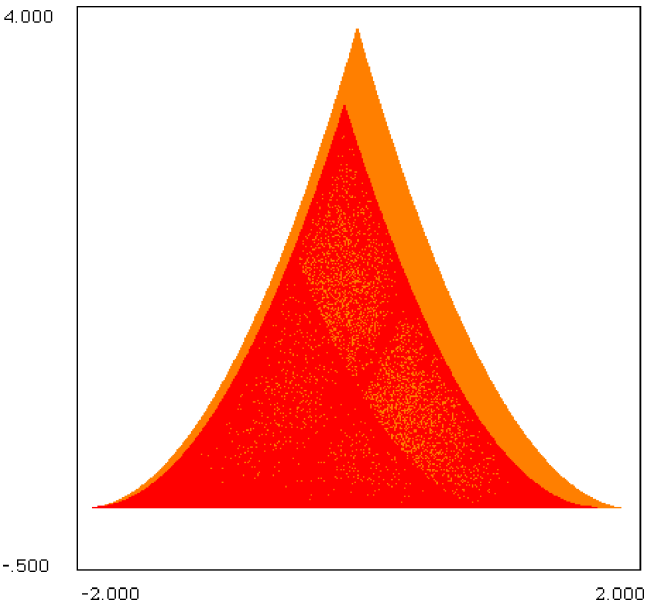

Fig. 63. $c = \tilde{c} \simeq 1.89291098791$, $\gamma = 0$. Chaotic set A^{Ch}. The dendrite part in the region $y < 0$ is not visible.

located on $y = 0$, which gives the closed linear continuum bounded by the fixed point Q^* and its rank-one preimage Q^*_{-1} different from Q^*. Well, let us consider first the case $(\tilde{c}, \gamma = \varepsilon)$ (see Fig. 64 for $\varepsilon = 0.01$). For this set of parameter values we have two disjoint invariant sets, one is the dendrite in the negative half plane $J \cap (y \leq 0)$, whose shape

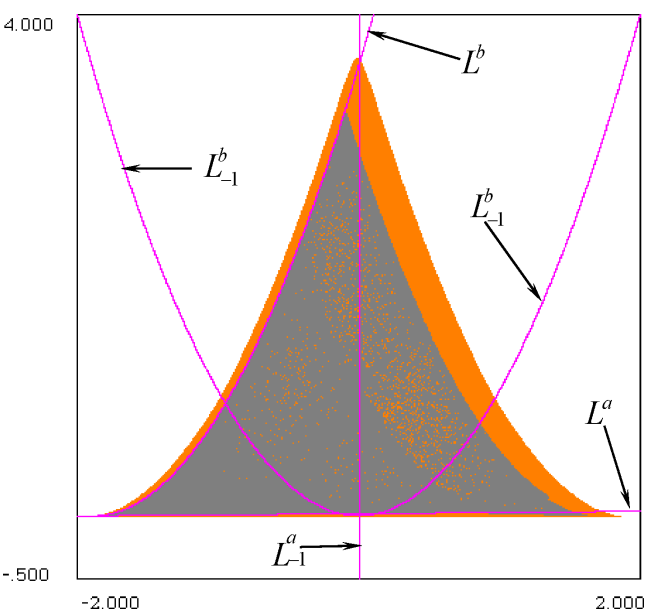

Fig. 64. $c = \tilde{c} \simeq 1.89291098791$, $\gamma = 0.01$. Chaotic area bounded by three critical arcs without any contact with $y = 0$.

has been described in Part I, Sec. 5.5, and the second one, A, belongs to the positive half plane ($y > 0$), and its basin of attraction $D(A)$ as well. In Fig. 64 the invariant set A looks like a chaotic area, bounded by arcs which are images of the critical curves L^a_{-1} and L^b_{-1}. Two segments on L^a and L^b on the boundary of A are shown in Fig. 64. The colored region around it denotes its basin of attraction $D(A)$, and it seems that the x-axis is a limit set of this basin, and thus belongs to its boundary. This is the situation for any $\gamma = \varepsilon > 0$, as $\varepsilon \to 0$.

In the limit, at the parameters $(\tilde{c}, \gamma = 0)$, the portion in the negative half plane ($y < 0$) has the same properties described above. While now the points on the y-axis inside the previous set $D(A)$ are mapped into the x-axis, together with all their preimages of any rank, which are dense in the old area A, it follows that the stable set of the chaotic segment $\overline{CC}_1$ on the x-axis has an explosion. If in the positive half plane ($y > 0$) some attractor B (with an open basin $D(B)$ with positive measure) exists, then $\overline{CC}_1$ is a Milnor attractor: the stable set of $\overline{CC}_1$ is a set with positive measure which is riddled with the basin $D(B)$ in ($y > 0$), and it is the dendrite in the region ($y < 0$). But it is also possible that what is left as invariant in the positive half plane ($y > 0$) is not a basin but a Milnor attractor as invariant set with a stable set of positive measures that is also riddled with the stable set of $\overline{CC}_1$, which means that considering any point in ($y > 0$) whose trajectory is not divergent, then in *any* neighborhood of it, we have points belonging to both sets, i.e. points whose trajectory ends on the x-axis, and also points whose trajectory stays forever in the positive half plane ($y > 0$). A third possibility is that two chaotic sets, disjoint for $\varepsilon > 0$, are merging at $\varepsilon = 0$ (as suggested from Fig. 63). That is, the whole invariant chaotic set is now a set A^{Ch} which is bounded by an arc of the critical set L^a which is now on the x-axis ($y = 0$) (that is, it includes now also the segment $\overline{CC}_1$), an arc of L^b ($y = (x + \tilde{c})^2$, $x \geq -\tilde{c}$), and an arc of its rank-one image L^b_1 intersecting L^b angularly (Fig. 63). Its basin D^c is the set in color in Fig. 63, whose boundary ∂D^c is made up of two symmetric smooth arcs joining in the region $y > 0$, while in the region $y < 0$, the boundary ∂D^c of D^c is made up of the dendrite described in Sec. 5.5 of Part I. In this case, the situation $(\tilde{c}, \gamma = 0)$ is that of the contact of a chaotic area boundary with its basin boundary, here not at a set of isolated points (i.e. not a classical bifurcation, cf. [Gumowski & Mira, 1980; Mira *et al.*, 1996a]), but along a whole segment. For $\gamma < 0$, A^{Ch} is destroyed turning into a strange repeller.

Similarly we can reason for any value of c, leading to chaotic intervals (cyclical or not) and associated with dendrites in the half plane ($y \leq 0$).

As a second example let us consider $c = c_3^{*1} \simeq 1.790327493$. The half plane $y \leq 0$ contains a *dendrite* (cf. Part I, Sec. 5.5) which is the boundary of the domain $D_{\infty -}$ of diverging orbits. In the half plane $y \geq 0$ the map has a basin of points whose trajectory tends to a chaotic set A^{Ch}. This set A^{Ch} now has a contact with $J \cap (y = 0)$, and it includes the period three chaotic segments CH_3^1 for the map restricted to the x-axis (cf. Part I, Sec. 2.1). With respect to the two-dimensional map $\overline{T}$, this invariant chaotic set A^{Ch} has not an open set as basin because it has a contact with its basin boundary in $y \leq 0$, and thus we are at a particular contact bifurcation. The chaotic set A^{Ch} is made up of regions of low density of orbits, and regions of higher densities. It is bounded by an arc of the critical sets made up of L^a ($y = 0$), an arc of L^b ($y = (x + \tilde{c})^2$, $x \geq -\tilde{c}$), and arcs of its rank-n images, $n = 1, \ldots, 5$, L^b_1 intersecting L^b angularly (Fig. 65). The region $y \leq 0$, contains the dendrite. For $\gamma = \varepsilon$, $\varepsilon > 0$ sufficiently small, one has a chaotic area bounded by the above critical arcs, but without any contact with $y = 0$ (Fig. 66).

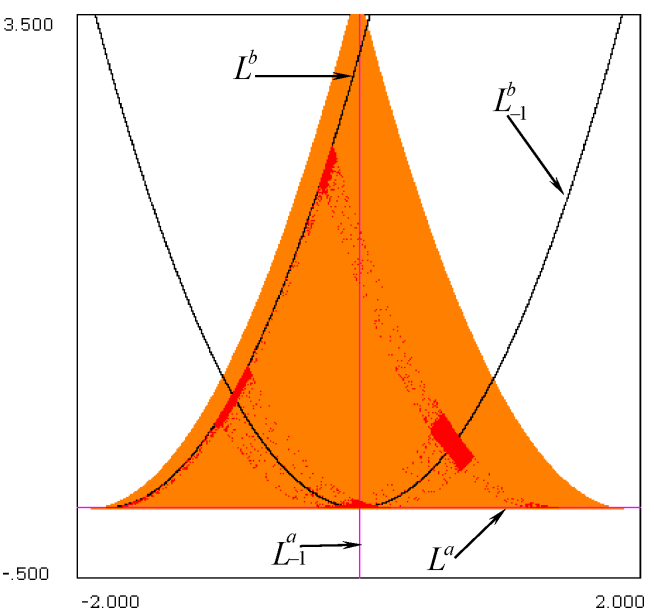

Fig. 65. $c = c = c_3^{*1} \simeq 1.790327493$, $\gamma = 0$. Chaotic set A^{Ch}. The dendrite part in the region $y < 0$ is not visible.

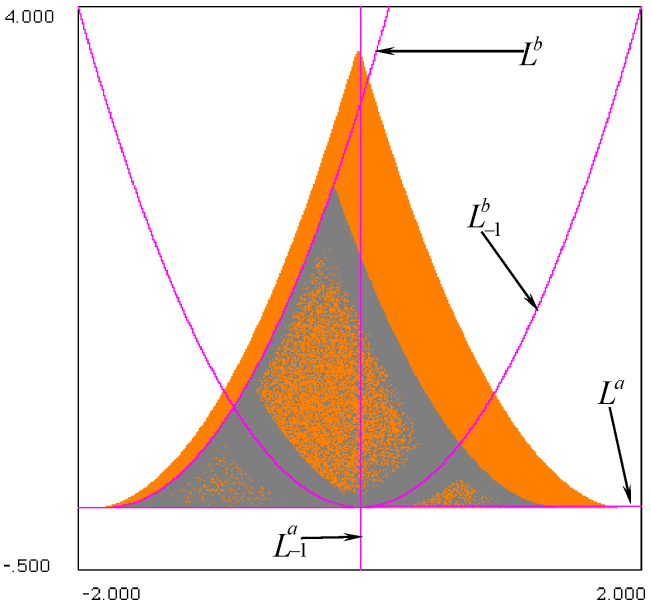

Fig. 66. $c = c = c_3^{*1} \simeq 1.790327493$, $\gamma = 0.001$. Chaotic area bounded by three critical arcs without any contact with $y = 0$.

10. Conclusion

For explaining the different configurations of the Julia sets, generated by the complex map T_Z, $z' = z^2 - c$, c being a real parameter, the method used in this paper belongs to the embedding one. More generally such an approach has the advantage to clarify a particular complicated and multifaceted situation by inserting in it a larger family of equations (here a two-dimensional noninvertible map) depending on one more parameter (here $\gamma \geq 0$ for $\overline{T}$), which restores the initial equation when this new parameter vanishes. In the present case, this enlightenment has been obtained from the sequences of local and global bifurcations generated when γ decreases and tends toward zero. Moreover, it has been shown that the fractal bifurcation organization *box-within-a-box* [Gumowski & Mira, 1975; Mira, 1975], or *embedded boxes* [Guckenheimer, 1980] of the Myrberg's unimodal map, $x' = x^2 - c$, play a fundamental role, not only for the restriction of $\overline{T}$ to $y = 0$, but also in the (c, γ) parameter plane. This occurs for a well defined set of bifurcation curves, which recurs according to this fractal structure, and also when, for a given value of c, the parameter γ decreases reproducing this organization either completely, or in a perturbed form. In this sense, enlightening some sequences of global bifurcations, the paper has given the opportunity of a more complete study of the two-dimensional noninvertible map with respect to previous publications [Agliari *et al.*, 2003, 2004].

At this study stage the paper does not pretend to analyze all the situations generated by the complex map T_Z, because unfortunately the "indirect" (cf. Sec. 1) embedding achieved by $\overline{T}$ does not work with a complex parameter $c = a \pm jb$, $j^2 = -1$. Among other open questions this paper does not explain the striking numerically obtained properties in Sec. 7.4. A theoretical proof of this result would be interesting.

It is worth noting that many different types of imbedding are possible for the paper purpose, but not having the advantages of the "indirect" one adopted for this study. These advantages are induced by the critical line L^a, the slope of which decreases by rotation with center point ($x = -c$, $y = 0$) and tends toward zero if $\gamma \to 0$. This has been at the origin of the understanding of the $\gamma = 0$ case from the phenomena related to the islands, appendices formation, aggregation, and from the follow up of box-within-a-box bifurcations generated on the basin boundary ∂D_- of the attractor located inside $y \leq 0$, until attaining the "full" number of real unstable cycles on this boundary at the parameter limit. It is easy to see that this is not easy from a "direct" embedding consisting of the introduction of a perturbation of the map T_Z, from a parameter ε restoring immediately T_Z when $\varepsilon = 0$, and such that the resulting map does not satisfy the Cauchy Riemann conditions for $\varepsilon \neq 0$, (cf. [Mira, 1987, p. 423]). Indeed in this case, for the maps family so created, the T_Z critical point $(-c; 0)$ turns into a critical close curve tending toward $(c; 0)$ when the embedding parameter $\varepsilon \to 0$, as shown in pp. 444–456 of Mira *et al.* [1996a] for the map

$$x' = x^2 - y^2 + \varepsilon x + c; \quad y' = 2xy - \frac{5\varepsilon y}{2}$$

This approach has not permitted results equivalent to those of the present study.

References

Agliari, A., Gardini, L. & Mira, C. [2003] "On the fractal structure of basin boundaries in two-dimensional noninvertible maps," *Int. J. Bifurcation and Chaos* **13**, 1767–1785.

Agliari, A., Gardini, L. & Mira, C. [2004] "Transition from a smooth basin boundary to a fractal one in a class of two-dimensional endomorphisms," *Proc. European Conf. Iteration Theory* (ECIT 2002) Evora (Portugal) Sept. 2002. Grazer Mathematische Berichte, Nr 346 (2004), pp. 1–18.

Bischi, G. I., Gardini, L. & Mira, C. [2006] "Basin fractalization generated by a two-dimensional family of

($Z_1 - Z_3 - Z_1$) maps," *Int. J. Bifurcation and Chaos* **16**, 647–670.

Fatou, P. [1919] "Mémoire sur les équations fonctionnelles," *Bull. Soc. Math. France* **47**, 161–271.

Fatou, P. [1920] "Mémoire sur les équations fonctionnelles," *Bull. Soc. Math. France* **48**, 33–94, 208–314.

Frouzakis, C. F., Gardini, L., Kevrekidis, Y. G., Millerioux, G. & Mira, C. [1997] "On some properties of invariant sets of two-dimensional noninvertible maps," *Int. J. Bifurcation and Chaos* **7**, 1167–1194.

Guckenheimer, J. [1980] "The bifurcations of quadratic functions," *N.Y. Acad. Sci.* **75**, 343–347.

Gumowski, I. & Mira, C. [1975] "Accumulation de bifurcations dans une récurrence," *Comptes Rendus Acad. Sc. Paris*, Série A **281**, 45–48.

Gumowski, I. & Mira, C. [1980] *Dynamique Chaotique. Transformations Ponctuelles. Transition Ordre Désordre* (Cépadues Editions Toulouse).

Julia, G. [1918] "Mémoire sur l'itération des fonctions rationnelles," *J. Math. Pures Appl.* **4**, 7ème série, 47–245.

Mira, C. [1975] "Accumulations de bifurcations et structures boîtes-emboîtées dans les récurrences et transformations ponctuelles," *Proc. 7th Int. Conf. Nonlinear Oscillations*, Berlin Sept. 1975. Akademic Verlag, Berlin 1977, Band I 2, pp. 81–93.

Mira, C. [1987] *Chaotic Dynamics. From the One-Dimensional Endomorphism to the Two-Dimensional Diffeomorphism* (World Scientific, Singapore).

Mira, C., Fournier-Prunaret, D., Gardini, L., Kawakami, H. & Cathala, J. C. [1994] "Basin bifurcations of two-dimensional noninvertible maps: Fractalization of basins," *Int. J. Bifurcation and Chaos* **4**, 343–381.

Mira, C., Gardini, L., Barugola, A. & Cathala, J. C. [1996a] *Chaotic Dynamics in Two-dimensional Noninvertible Maps*, World Scientific Series on Nonlinear Sciences, Series A, Vol. 20.

Mira, C., Millerioux, G., Carcasses, J. P. & Gardini, L. [1996b] "Plane foliation of two-dimensional noninvertible maps," *Int. J. Bifurcation and Chaos* **6**, 1439–1462.

Mira, C. & Gardini, L. [2009] "From the box-within-a-box bifurcations organization to the Julia set. Part I: Revisited properties of the sets generated by a quadratic complex map with a real parameter," *Int. J. Bifurcation and Chaos* **19**, 281–327.

Myrberg, P. J. [1963] "Iteration von Quadratwurzeloperationen. III," *Ann. Acad. Sci. Fenn.*, Ser. A **336**, 1–10.